2022-09-22

Development of Rapid, Low-cost, and Portable Device to Detect Infectious Diseases

Lee, Yoonjung

UNIVERSITY OF CALGARY

Development of Rapid, Low-cost, and Portable Device to Detect Infectious Diseases

by

Yoonjung Lee

A THESIS

SUBMITTED TO THE FACULTY OF GRADUATE STUDIES

IN PARTIAL FULFILMENT OF THE REQUIREMENTS FOR THE

DEGREE OF MASTER OF SCIENCE

GRADUATE PROGRAM IN MECHANICAL ENGINEERING

CALGARY, ALBERTA

SEPTEMBER, 2022

ABSTRACT

With the spread of COVID-19, which started the global pandemic in 2019 and continues to be prevalent these days, the importance of developing effective diagnostic methods to limit the spread of infectious diseases has emerged. The standard method used to diagnose severe acute respiratory syndrome coronavirus 2 is reverse transcriptase polymerase chain reaction (RT-PCR). Still, its disadvantages include high cost, complex equipment, and long diagnostic time. This study developed two loop-mediated isothermal amplification (LAMP) based diagnostic methods (Saliva-Dry LAMP and Direct Dry-LAMP) which are rapid, sensitive, and near-patient to overcome the limitations of RT-PCR. Saliva-Dry LAMP has the advantages of the LAMP method and requires saliva samples using a customized portable all-in-one box. Direct Dry-LAMP has a more rapid detection time with a heat inactivation step instead of RNA extraction, and the customized device can be executed with batteries and the developed application. The development of these devices reduces the capital cost of instruments significantly, and both methods have shown great performances with excellent positive percent agreement and negative percent agreement compared to each reference RT-PCR. Another convection-based device combined with real-time detection was developed to perform Direct Dry-LAMP. Although this device is still in development, it underscores the growing need for a random-access platform with real-time detection. Overall, Saliva-Dry LAMP and Direct Dry-LAMP can provide rapid and accurate detection of COVID-19 with portable and low-cost devices. With more widespread use, both these methods could play a central role in efficiently limiting the spread of infectious diseases, especially in resource-limited regions.

PREFACE

The research in this thesis was conducted under the supervision of Dr. Keekyoung Kim in the Advanced Biofabrication Laboratory, Department of Mechanical and Manufacturing Engineering, and the collaboration with Noah Toppings and Dr. Dylan R. Pillai in Pillai Lab, Department of Pathology and Laboratory Medicine, at the University of Calgary.

Chapter 2 of this thesis has been published in:

Toppings, N. B., Mohon, A. N., **Lee, Y.**, Kumar, H., Lee, D., Kapoor, R., ... & Pillai, D. R. (2021). A rapid near-patient detection system for SARS-CoV-2 using saliva. *Scientific reports*, *11*(1), 1-9.

ACKNOWLEDGMENTS

First, I would like to express my appreciation to my supervisor, Dr. Keekyoung Kim, for his continuous support and guidance in my study and research at the University of Calgary. Dr. Kim gave me a chance to study in the Advanced Biofabrication Laboratory (ABL) and motivated me not to give up, therefore I was able to complete this journey for my MSc study. Likewise, I would like to thank Dr. Dylan R. Pillai and Noah Toppings for their excellent collaboration and for teaching me other fields that I have never studied. They helped me to have a broad insight into other areas besides my major, and Noah always shared his knowledge and answered all my questions in his field.

Next, I like to thank all members of ABL, Jenny Shin, Hitendra Kumar, Nima Tabatabaei Rezaei, Zhangkang Li, Jeff Shin, and Mahmoud Sakr, for helping me with my research and study and making me continue to improve myself. I would also like to thank Duncan Kennedy, Vianney Nguyen, and Kenny Jeon, who helped me a lot to advance the project during the summer of 2021 as intern students. Furthermore, I would like to thank Dr. Hongseok Jo for giving me a lot of advice at any time for overall research and Dr. Dongwook Kim for teaching the field of electronics in my research. In addition, I would like to thank all my friends in Calgary and South Korea, especially my besties in NEST of UNIST, for always cheering me up and helping me refresh myself for a while away from studying.

Finally, for all my family members, including parents, brother Hojin, sister-in-law Hyeji, and another brother Gyujin, thank you for continuous support throughout my study with delicious meals always!

TABLE OF CONTENTS

LIST OF TABLES

LIST OF FIGURES

LIST OF SYMBOLS AND ABBREVIATIONS

Abbreviation	Definition
+ssRNA	Single-stranded Positive-sense RNA
app	Application
BIP	Backward Inner Primer
CDC	Centers for Disease Control and Prevention
cDNA	Complementary DNA
CHREB	Conjoint Health Research Ethics Board
CRISPR	Clustered Regularly Interspaced Short Palindromic Repeats
CT	Computed Tomography
Ct	Cycle Threshold
DC	Direct Current
EDTA	Ethylenediaminetetraacetic Acid
EGTA	Ethylene Glycol Tetraacetic Acid
ELISA	Enzyme-linked Immunosorbent Assay
FDM	Fused Deposition Modeling
FIP	Forward Inner Primer
HE	Hemagglutinin-esterase Dimer
iNAAT	Isothermal Nucleic Acid Amplification Tests
LAMP	Loop-mediated Isothermal Amplification
LFIA	Lateral Flow Immunoassay
LiFePO4	Lithium-Ion Phosphate

LOD	Limit of Detection
NAAT	Nucleic Acid Amplification Tests
NP	Nasopharyngeal
NPA	Negative Percent Agreement
NTC	No Template Control
PaGeR	Palm Germ-Radar
PLA	Poly-lactic Acid
POC	Point-of-care
POCT	Point-of-care Testing
PPA	Positive Percent Agreement
RAT	Rapid Antigen Test
RdRp	RNA-dependent RNA Polymerase
RFU	Relative Fluorescence Unit
RPA	Recombinase Polymerase Amplification
rRT-PCR	Real-time RT-PCR
RT-LAMP	Reverse Transcription Loop-mediated Isothermal Amplification
RT-PCR	Reverse Transcriptase Polymerase Chain Reaction
SARS-CoV-2	Severe Acute Respiratory Syndrome Coronavirus 2
SHERLOCK	Specific High Sensitivity Enzymatic Reporter UnLOCKing
SLA	Stereolithography
STOPCovid	SHERLOCK Testing in One Pot
UTM	Universal Transport Media

Symbol	Definition	Unit
A	Cross-sectional Area / Heat Transfer Area of Surface	m^2
d	Thickness of Material	m
h	Convective Heat Transfer Coefficient	W/m^2K
k	Thermal Conductivity of Material	W/mK
Q	Heat Transfer	W
T1	Colder Temperature	K
T2	Higher Temperature	K

Chapter 1: Introduction

1.1 Synopsis

COVID-19 is a respiratory infectious disease caused by the severe acute respiratory syndrome coronavirus 2 (SARS-CoV-2) virus that has been prevalent worldwide since December 2019. To control the spread of the virus and minimize ongoing global burdens caused by the COVID-19 pandemic, there is an urgent need to develop effective diagnostic methods. Current diagnostic methods available to detect COVID-19 include nucleic acid amplification testing, serology-based testing, antigen-based testing, computed tomography (CT) scan, and biosensors. In particular, rapid antigen tests (RAT), reverse transcriptase polymerase chain reaction (RT-PCR), and reverse transcription loop-mediated isothermal amplification (RT-LAMP) are the most commonly used. Each has its merits; however, new approaches are continually being developed to overcome the disadvantages of existing methods. Chapter 1 discusses COVID-19 and the SARS-CoV-2 virus before exploring the three most common diagnostic methods in detail. This is followed by a literature review of novel methods or devices which were developed based on general COVID-19 diagnostic approaches. The chapter concludes with a brief description of the research objectives regarding overcoming the limitations of current COVID-19 diagnostic methods.

1.2 Introduction

COVID-19 is a respiratory infectious disease caused by the SARS-CoV-2 that began in Wuhan, China in December 2019 [1]. It has resulted in an ongoing pandemic since March 2020,

with various variants which have developed since and more than 500 million infections officially reported worldwide. BA.5 is the latest coronavirus variant and is causing another wave of infection incidence again globally. The wide spread of COVID-19 necessitates research on vaccination, diagnosis methods, and treatment to prevent the further spread of the virus and potentially reduce the negative impact of an ongoing pandemic.

SARS-CoV-2 is a single-stranded positive-sense RNA (+ssRNA) virus with a large genome, sized at 29.8 kb [2], [3]. Figure 1.1 shows the structure of SARS-CoV-2 [4], which contains sixteen non-structural proteins (nsp1-16) and four structural proteins: nucleoprotein (N) produces the nucleocapsid with the RNA genome, membrane protein (M) is important for generating viruses, an envelope protein (E) forms the viral envelope by adhering to the M protein, and spike glycoprotein (S) catalyzes the viral infection by binding to the host cell receptors [4]–[6]. It also contains Hemagglutinin-esterase dimer (HE), which potentially mediates the attachment and destruction of sialic acid receptors on the host cell surface [4], [7].

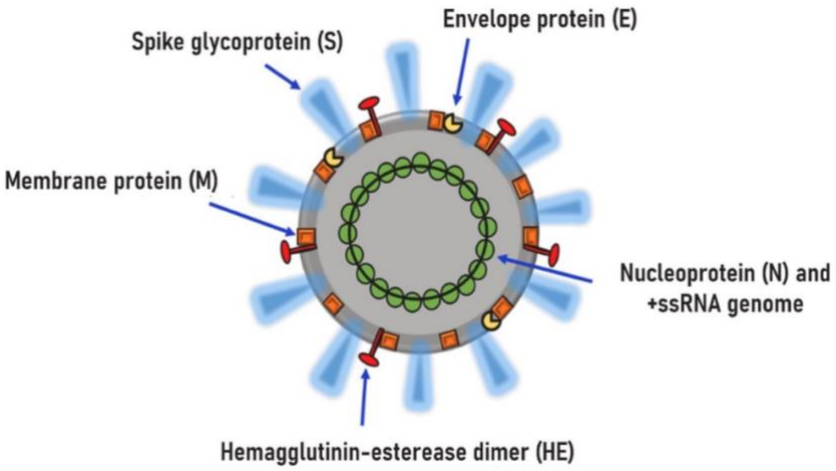

Figure 1.1. Structure of SARS-CoV-2 virus [4].

The most common symptoms of COVID-19 infection include fever, cough, fatigue, and dyspnea [8]. However, severe cases can be fatal, and as of July 2022, more than five million people are officially reported to have died from the SARS-CoV-2 virus. In addition, many cases have been reported that the infectivity of asymptomatic cases was the same as that of symptomatic cases. However, the patients were asymptomatic and showed no signs of the infection in images captured by CT scan [9]. The increase in asymptomatic infections further emphasizes the practical need for an accurate and rapid diagnosis of COVID-19.

General diagnosis methods of COVID-19 can be grouped under three categories, as shown in Figure 1.2. The most sensitive assays and the most preferred method for detection of COVID-19 are nucleic acid amplification tests (NAAT). It includes real-time RT-PCR (rRT-PCR) and clustered regularly interspaced short palindromic repeats (CRISPR) [10]. RT-LAMP is the most frequently used method in isothermal nucleic acid amplification tests (iNAAT) which are designed for point-of-care testing (POCT) diagnosis [11]. Serology-based tests, such as enzyme-linked immunosorbent assay (ELISA) and lateral flow immunoassay (LFIA), are tests for later stages of COVID-19 infection. SARS-CoV-2 antibodies, including immunoglobulin-A (IgA), IgM, and IgG, are produced by the humoral immune system and can be detected by these tests; serology-based tests also help understand how antibodies to SARS-CoV-2 are developed in infected patients [12]. There are additional approaches to detecting COVID-19: rapid antigen-based tests are quicker and less expensive, but they are limited by their low sensitivity; CT scans can also detect signs of infection, although asymptomatic cases present some difficulty; and biosensors are being developed for detecting biomarkers in patient samples [13]. A brief workflow of the diagnostic methods is shown in Figure 1.3.

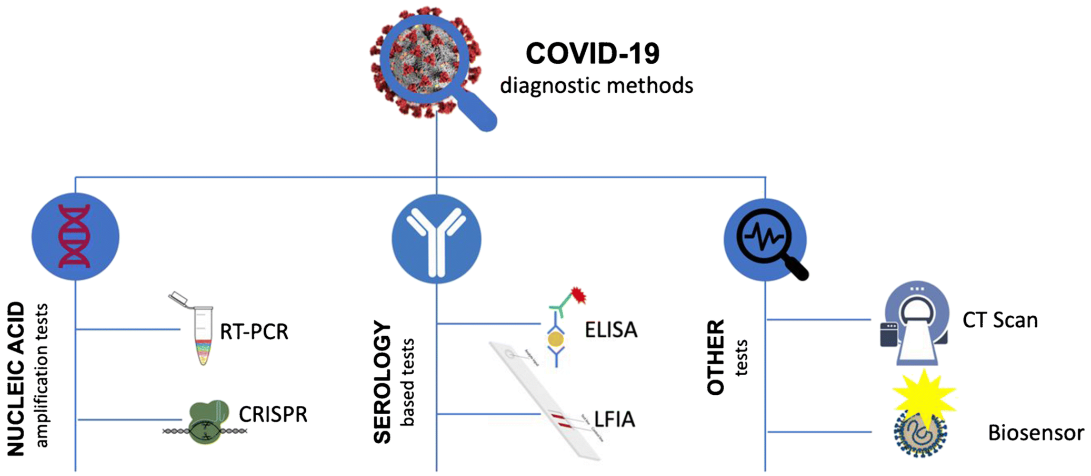

Figure 1.2. General diagnostic methods for COVID-19 [14].

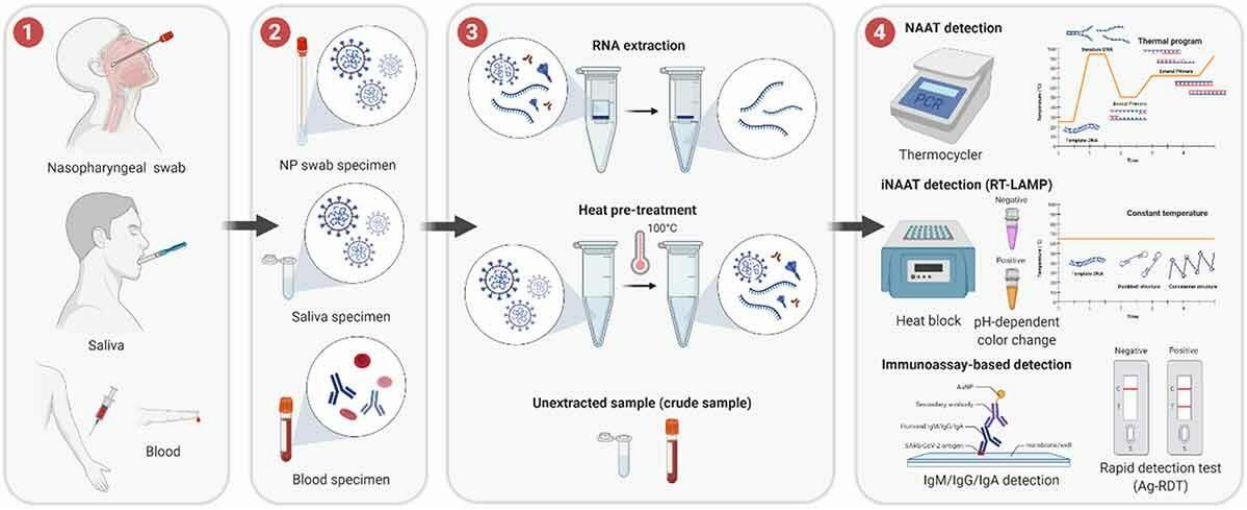

Figure 1.3. Diagnostic workflow of molecular testing for COVID-19 [11].

Herein, RAT, RT-PCR, and RT-LAMP, the most common diagnostic methods currently in practice to detect COVID-19, were specifically elaborated. The principles, advantages, and disadvantages of each method were reviewed. In addition, more novel approaches, both within and beyond general diagnostic methods, are reviewed in each section.

1.3 Rapid Antigen Test (RAT)

RATs are one of the forms of LFIA that can rapidly detect an antigen for POCT, typically in less than 5 to 30 minutes [15]. RAT is the first and most convenient method of COVID-19 detection for the general population because it is low-cost and does not require the help of medical professionals. Khalid *et al.* reviewed a total of 94 studies on the performance of RATs against SARS-CoV-2, published in 2021 and 2020. The sensitivity of the RATs was between 37% and 90%, and the overall pooled sensitivity was 70%. Based on the clinical specimens, RATs showed high sensitivity in nasal swabs (83%), nasopharyngeal (NP) swabs (71%), throat swabs (69%), and saliva swabs (68%). The specificity of the RATs varied from 65% to 100%, with an overall pooled specificity of 98%. Of the 94 studies reviewed, 90 demonstrated over 90% specificity [16].

However, the decisive disadvantage of RAT is that these studies have shown it to be less successful in accurately detecting COVID-19 in asymptomatic patients. The symptomatic group showed higher sensitivity (82%) than the asymptomatic group (68%), although the specificity of RATs was similar in both groups [16]. In addition, Indelicato *et al.* reviewed 11 studies which used RATs granted emergency use authorization by the US Food and Drug Administration (FDA) for asymptomatic patients in the United States; their sensitivity findings ranged from 35.8 to 71%, suggesting the likelihood of false negatives in patients who are still able to spread the virus despite showing no signs or symptoms [17].

1.4 Reverse Transcriptase Polymerase Chain Reaction (RT-PCR)

RT-PCR is the gold standard for molecular diagnosis and is used to detect COVID-19, as well as other viruses. PCR was invented by Kary Mullis at Cetus in 1983 [18]. DNA is detected by original PCR, but the procedure of reverse transcription can detect RNA to convert viral RNA

into complementary DNA (cDNA) [19]. RT-PCR was designed to amplify S, E, N, RNA-dependent RNA polymerase (RdRp) and open reading frames (ORF1a/b) genes [20].

Figure 1.4 shows the underlying principle of RT-PCR. Once RNA is extracted from samples, it is reverse-transcribed into cDNA by reverse transcriptase. Following the reverse transcription stages, cDNA can be amplified with three steps: denaturation, primer annealing, and extension [21]. Denaturation must be completed at high temperatures around 95 ℃ because this allows the target double-stranded DNA to separate into single strands. Next, primer annealing requires temperatures between 50 ℃ and 65 ℃ for the primers to bind to the complementary sequence in the single strands of target DNA. Extension occurs at 72 ℃ when DNA polymerase extends the primer to create two double-stranded DNA from each single-stranded template. After the extension is complete, the three steps are repeated to generate copies of strands of DNA at an exponential rate [22].

RT-PCR cycle threshold (Ct) values represent the number of amplification cycles required for the target gene to exceed a positive threshold level [23]. Generally, for the diagnosis of COVID-19, the test result is considered positive when the Ct value is under 40. However, depending on the country or organization, different Ct values have been used [24], [25]. Sensitivity and efficiency were analytically compared in four commonly used RT-PCR assays by Vogels *et al.* [26].

The total time to get the results using RT-PCR ranges typically from 12 to 24 hours, and this test can be considered a gold standard for diagnosis of COVID-19 due to its rapid detection and high sensitivity [27], [28]. However, RT-PCR also has its disadvantages to overcome. It requires sophisticated equipment and can only be executed by trained professionals. Inaccurate readings resulting in false negatives and false positives are also not uncommon with this method. RT-PCR necessitates access to specific lab equipment, such as a centrifuge, a laminar flow cabinet, and

thermal-cycling equipment, all of which can make this procedure expensive [29], [30]. To overcome these drawbacks, some novel methods based on RT-PCR were developed.

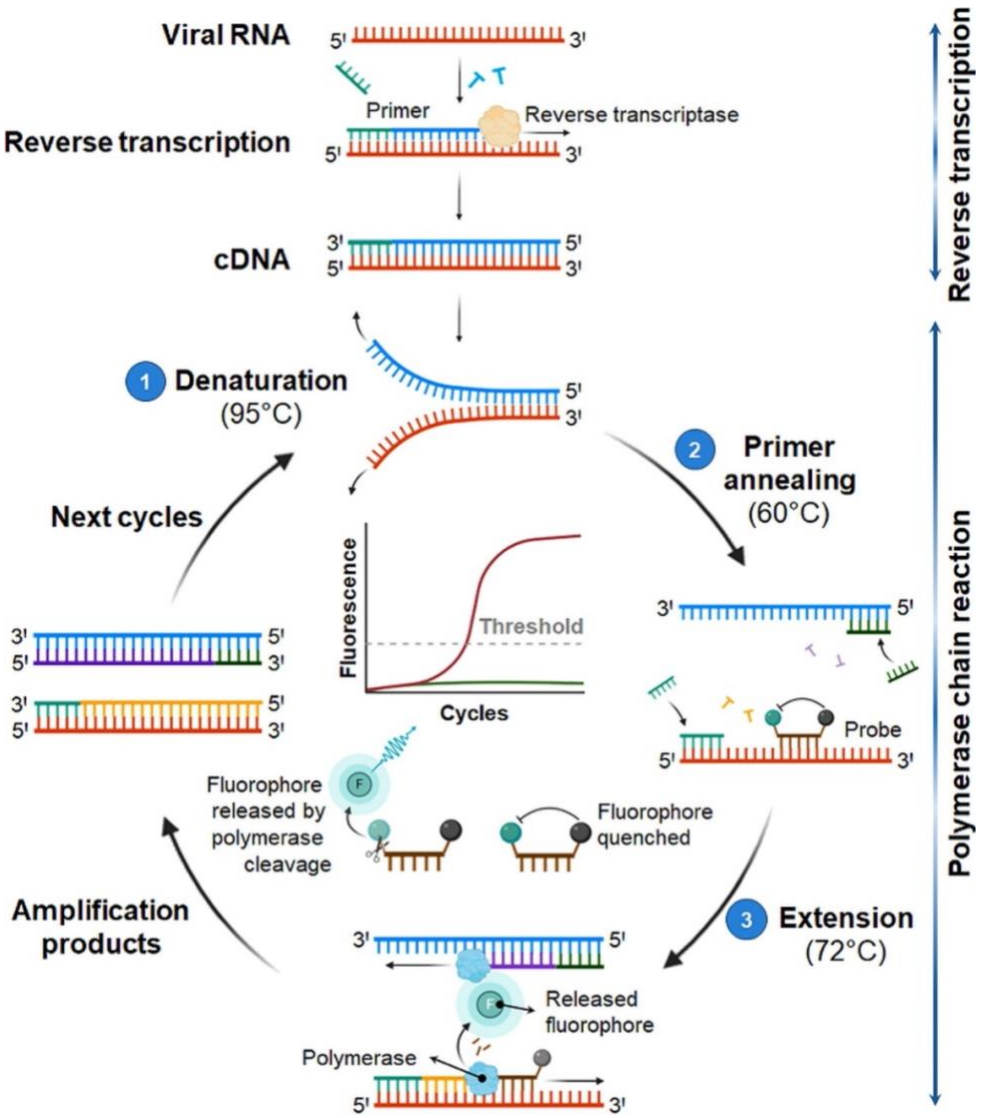

Figure 1.4. Principle of RT-PCR [21].

A multiplex (triplex) rRT-PCR diagnostic method for COVID-19 that can simultaneously target two viral genes (RdRP and E) and one human gene (Rnase P) was developed in 2021 by Tombuloglu *et al.* [31]. For RdRP, E, and Rnase P genes, the average Ct values with standard

deviations (SD) were 28.8 ± 0.51, 27.3 ± 0.51, and 23.6 ± 1.04, respectively; this suggests that three genes can be detected in the same reaction tube. In addition, a total of 91 patient samples can be tested in standard 96-well plates per run, allowing for fewer reactions per sample. Therefore, multiplex rRT-PCR has the potential to be a rapid, reliable, and low-cost detection system with high sensitivity [31].

The CovidNudge point-of-care (POC) rRT-PCR platform was developed to overcome the previously discussed limitations of RT-PCR. The platform has an integrated lab-on-chip device, labelled DnaCatridge, for sample-to-result PCR and a NudgeBox processing unit capable of running an rRT-PCR outside a laboratory environment. Multiplex analysis for seven viral targets and one human gene is provided. The total time to get results ranged from 60 to 90 minutes, the overall sensitivity of the platform compared to standard RT-PCR in local laboratories was 94% and the overall specificity was 100%. These results indicate that the platform can offer rapid, sensitive, and specific POCT diagnosis without requiring any laboratory facilities or pre-processing of samples [32].

Another similar rapid, sensitive, and specific POCT diagnosis, Q-POC™ SARS CoV-2 RT-PCR assay, was introduced by Caffry *et al.* in July 2021, from which results can be obtained in 32 minutes. The overall sensitivity compared with the reference was 97% when the reference test Ct cut-off value was at 35. However, when the reference test Ct cut-off value was 40, the overall sensitivity of Q-POC™ lowered to 80%, underperforming other general RT-PCR tests [33].

Aside from these, several new devices based on RT-PCR overcome the limitations of general RT-PCR and show high sensitivity and specificity. The Visby medical RT-PCR portable device was evaluated by Renzoni *et al.* [34], and a novel rapid total nucleic acid extraction method based on rRT-PCR using the BD MAX open platform was developed and validated by Perng *et al.* [35].

Zowawi *et al.* also assessed the agreement and accuracy of the portable RT-PCR Biomeme SARS-CoV-2 system [36].

1.5 Reverse Transcription Loop-Mediated Isothermal Amplification (RT-LAMP)

RT-PCR is a standard method used to detect SARS-CoV-2, approved by the World Health Organization and the US Centers for Disease Control and Prevention (CDC). However, it is limited by the need for sophisticated equipment, trained personnel, and longer total detection times. RT-LAMP is also a commonly used method for diagnosing COVID-19 that presents potential solutions to these limitations of other diagnostic tests [37]. RT-LAMP has one step of nucleic acid amplification compared to RT-PCR which has a thermal cycle, and occurs at one temperature. The LAMP temperature is typically 60℃ to 65℃ depending on the primer set, and as a result, RT-LAMP has the advantage of a rapid detection time of less than an hour. In addition to RT-LAMP providing results faster than RT-PCR, it provides high sensitivity and specificity. Different pH and temperature ranges are allowed for RT-LAMP, and the reagents for RT-LAMP are stable at room temperature, as well as more affordable than those for RT-PCR [38]. With these various advantages, RT-LAMP can potentially become one of the main diagnostic methods to prevent the spread of COVID-19, but difficulties remain in designing complex primers [39].

RT-LAMP begins with the reverse-transcription process, as shown in Figure 1.5, when backward inner primer (BIP) anneals to the viral RNA to generate cDNA. B3 primer anneals to cDNA to synthesize a new strand of cDNA, and the previous strand is released with a loop at the 5’ end. Forward inner primer (FIP) anneals to the 3’ end of the released cDNA strand, and synthesis of a cDNA strand begins. F3 anneals to the 3’ end of the strand formed by the FIP primer and initiates the synthesis of a new strand. The recently displaced cDNA strand then forms a dumbbell-

shaped structure that contains complementary sequences at each end. This structure is the template for LAMP cycles [40], [41].

New approaches have been developed based on the advantages of RT-LAMP. For example, a Palm Germ-Radar (PaGeR) device that can detect COVID-19 rapidly and simply was developed by Ge *et al.* in March 2022. PaGeR gives rapid test results within an hour, and the costs of the device and the reaction are low. Colorimetric, fluorometric, and lateral dipstick readouts can be performed as detection methods, and one copy/μL of SARS-CoV-2 can be detected. In addition, the accuracy of PaGeR was able to reach 97.2% with 72 clinical samples. PaGeR showed great accuracy with a total of four steps (inactivation, extraction, amplification, and detection), but it has the disadvantage that the extraction step was performed inside of biosafety cabinet without PaGeR [43].

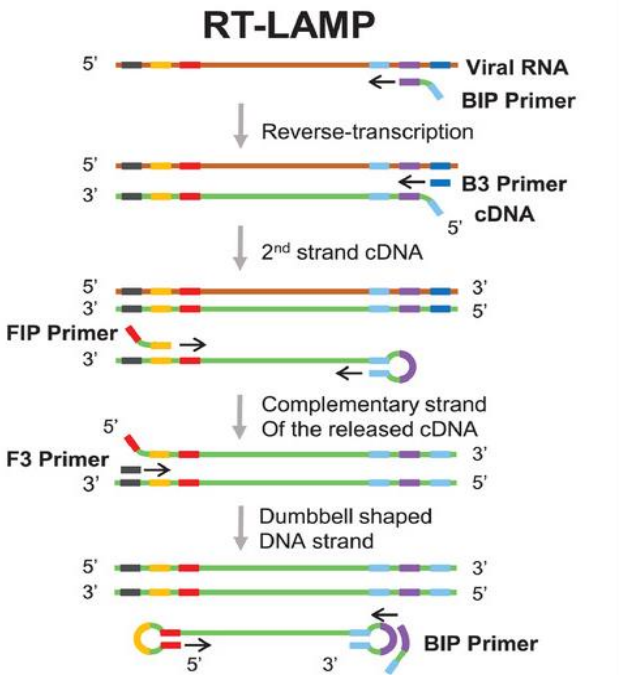

Figure 1.5. Principle of RT-LAMP [42].

iSCAN, the detection module of COVID-19 that combines RT-LAMP and CRISPR-Cas12, is rapid, sensitive, specific, and user-friendly. Combined with lateral flow cells, iSCAN provides efficient POC detection. It has a one-step amplification of RT-LAMP and the specific detection capability of CRISPR-Cas12 for SARS-CoV-2. iSCAN showed 100% agreement with reference RT-PCR when targeting the SARS-CoV-2 E gene in five different patients. However, when an additional 24 clinical samples (21 positives and 3 negatives for SARS-CoV-2) were collected, only 8 of 21 positive samples tested positive with iSCAN. For the N gene, it showed higher sensitivity, around 86%. iSCAN has a limit of detection (LOD) of 10 RNA copies per reaction, compared to the 5 copies per reaction detected by CDC RT-PCR [44]. Another portable and semi-automated device that combines RT-LAMP and CRISPR-CaS12 was developed by Rezaei *et al.* [45]. Various platforms based on RT-LAMP, the variplex™ RT-LAMP [46] and eazyplex® SARS-CoV-2 RT-LAMP [47], were evaluated for rapid detection for SARS-CoV-2 as well.

Penn-RAMP, developed by El-Tholoth *et al.*, combined two isothermal amplification processes, Recombinase Polymerase Amplification (RPA) and LAMP, each occurring at 38℃ and 61℃, respectively [48]. The RPA process includes LAMP F3 and B3 primers in the cap of the tube, and the LAMP process was carried out in the tube without any target. The closed tube was incubated at 38 ℃ for 15-20 minutes, followed by incubation at 61 ℃ for 40 minutes with real-time monitoring. Penn-RAMP showed ten times more sensitivity compared to LAMP and RT-PCR; Penn-RAMP can detect as low as seven copies per reaction, whereas LAMP and RT-PCR detect approximately 70 copies per reaction. Therefore, Penn-RAMP can potentially reduce false negative rates due to its requiring a low viral load from patients.

One-pot RT-LAMP occurs in one tube without an RNA extraction step, and it was developed to detect the N gene of COVID-19 [49]. Specific High Sensitivity Enzymatic Reporter

UnLOCKing (SHERLOCK) combines the LAMP and CRISPR detection methods with SHERLOCK Testing in One Pot (STOPCovid). This simplified test is POCT and can be finished in 70 minutes with lateral flow readout and 40 minutes with fluorescence readout. STOPCovid was clinically validated and provided a LOD of 100 copies per reaction [50].

1.6 Research Objectives

COVID-19 caused an ongoing global pandemic that resulted in the infections and the deaths of millions worldwide in severe cases. Both symptomatic and asymptomatic infections have been shown to be able to transmit the virus to others. Therefore, the importance of accurate and rapid diagnosis for COVID-19 has emerged to prevent the further spread of the virus. RT-PCR has been used as a gold standard to detect SARS-CoV-2 for COVID-19, but this method cannot be utilized outside laboratories. In addition, RT-PCR requires complex equipment and professionally trained healthcare workers. The thermal cycle of the RT-PCR procedure also increases the total virus detection time. RT-LAMP offers an alternative to RT-PCR, overcoming its limitations, for example, by reducing the detection time significantly with one amplification step at one temperature. Sample preparation is simplified in RT-LAMP, and the sensitivity and specificity are comparable with RT-PCR.

Based on the importance of developing rapid, near-patient tests, we aimed to develop a novel detection method for COVID-19 with the following characteristics. The detection process was based on the advantages of RT-LAMP compared to RT-PCR. The diagnostic method should rapidly provide the results with high sensitivity and specificity. Near-patient testing outside the laboratory is needed without sophisticated equipment or cold chains for the experimental setting. A portable device that can operate on batteries even in areas without electricity is needed. The

device and the detection process to detect viruses must also be user-friendly by requiring only minimal training for users. The results need to be interpreted easily, with straightforward results being presented. Considering these characteristics, it is required to develop standalone portable platforms based on RT-LAMP with high accuracy.

In chapter 2, Saliva-Dry LAMP, a rapid near-patient saliva test of COVID-19, as well as a portable, low-cost device capable of using Saliva-Dry LAMP were developed and manufactured. This is to overcome the limitations of existing detection methods, including long detection time, low efficiency due to long sample mixing times, the use of NP samples, high equipment costs, and non-portability of the devices.

Direct Dry-LAMP with additional research objectives while including the advantages of Saliva-Dry LAMP was developed in Chapter 3. SARS-CoV-2 detection using Direct Dry-LAMP attempted to simplify the detection process step and obtain faster results than Saliva-Dry LAMP. The portable, battery-operated device was developed so that Direct Dry-LAMP could also be used in developing countries with minimal power usage. In addition, it was intended to add the ability to analyze the results objectively rather than subjectively with the naked eye.

Lastly, in Chapter 4, a new device was developed to improve the accuracy of the assay. During the isothermal incubation with RT-LAMP assay, a real-time wired/wireless data acquisition can be collected from the fluorescent signal of the samples. A more stable and energy-efficient method was considered compared to the aluminum heating block generally used in LAMP reaction.

Chapter 2: Saliva-Dry LAMP

2.1 Synopsis

The onset of COVID-19 has brought forward the limitations in the detection and understanding of infectious diseases. To overcome the shortcomings of conventional reverse transcription loop-mediated isothermal amplification (RT-PCR) based methods for detecting COVID-19 with nasopharyngeal (NP) samples, a low-cost and portable device to perform rapid, near-patient, and saliva-based detection (Saliva-Dry LAMP) was developed.

2.2 Introduction

NP swabs have been used as a standard for the detection of COVID-19, but saliva has been shown that it is more acceptable for rapid point-of-care testing (POCT) in resource-limited environments while still maintaining high sensitivity [51], [52]. Saliva samples can be collected by patients themselves, reducing the intervention of healthcare workers, thereby reducing the exposure of viruses to healthcare workers in hospitals. In addition, the demand for personal protective equipment (PPE) can be minimized [52]. Therefore, we developed Saliva-Dry LAMP, a rapid, near-patient, and saliva-based detection method, to overcome the limitations of existing NP sample detection methods to detect SARS-CoV-2. A portable and low-cost device to run Saliva-Dry LAMP tests was manufactured. The device combines the three essential steps in the sequence of Saliva-Dry LAMP assay: a heating block for the isothermal incubation, excitation LEDs for visual fluorescent examination, and a centrifuge for RNA extraction. It reduces the capital equipment cost using 3D printing, and the total procedure can be finished in 105 minutes. The Saliva-Dry LAMP assisted by the developed device achieved a limit of detection comparable

to commercially available assays. Saliva-Dry LAMP showed excellent positive and negative agreement compared to two different reference standard RT-PCR tests. Overall, Saliva-Dry LAMP can provide rapid and accurate detection of COVID-19 with a portable and low-cost device. These characteristics lend Saliva-Dry LAMP a high potential for becoming a key player in our approach to limiting the spread of infectious diseases.

2.3 Device Development

A customized device was developed for the execution of each step for Saliva-Dry LAMP: centrifugation, isothermal incubation, and naked-eye fluorescent detection. The developed device consists of three components, including a centrifuge, a heating block, and a transilluminator (470 nm light emitting diode, LED, arrays). The design was modeled using Solidworks™ 2020 (Dassault Systems, Waltham, MA, USA). All housing parts/fixtures were fabricated using a fused deposition modeling (FDM) 3D printer (Anycubic Technology Co., Shenzhen, China) with poly-lactic acid (PLA) filament which is biodegradable unless specified. The centrifuge rotor was fabricated using polycarbonate filament for better heat insulation. The transilluminator consists of two LED arrays – a 6 × 8 LED array mounted inside the developed device and a pair of 2 × 8 LED arrays mounted on the sides of the cap to provide illumination from the sides. A second cap was placed on the transilluminator with an acrylic sheet window to block the wavelengths emitted by the LEDs, but not the intercalating dye. The aluminum heating block was machined to house both 2 mL and 1.5 mL microcentrifuge tubes. The temperature of the heating block was maintained at 61 °C using two heating elements and three thermocouple sensors. The centrifuge was made with a direct current (DC) powered brushless motor (T-motor F40 Pro3 2600 kV, Nanchang, China) mounted on an aluminum bracket. The centrifuge rotor was mounted on the brushless motor and

achieved 8000 RCF. All components were controlled by an ESP32 microprocessor. The device was operated through the user interface using an LCD display and push buttons. A DC power supply of 21–23V was used to power the device. 3D modeling and photographs of the fabricated device are shown in Figure 2.1. The specifications of the developed device is summarized in Table 2.1.

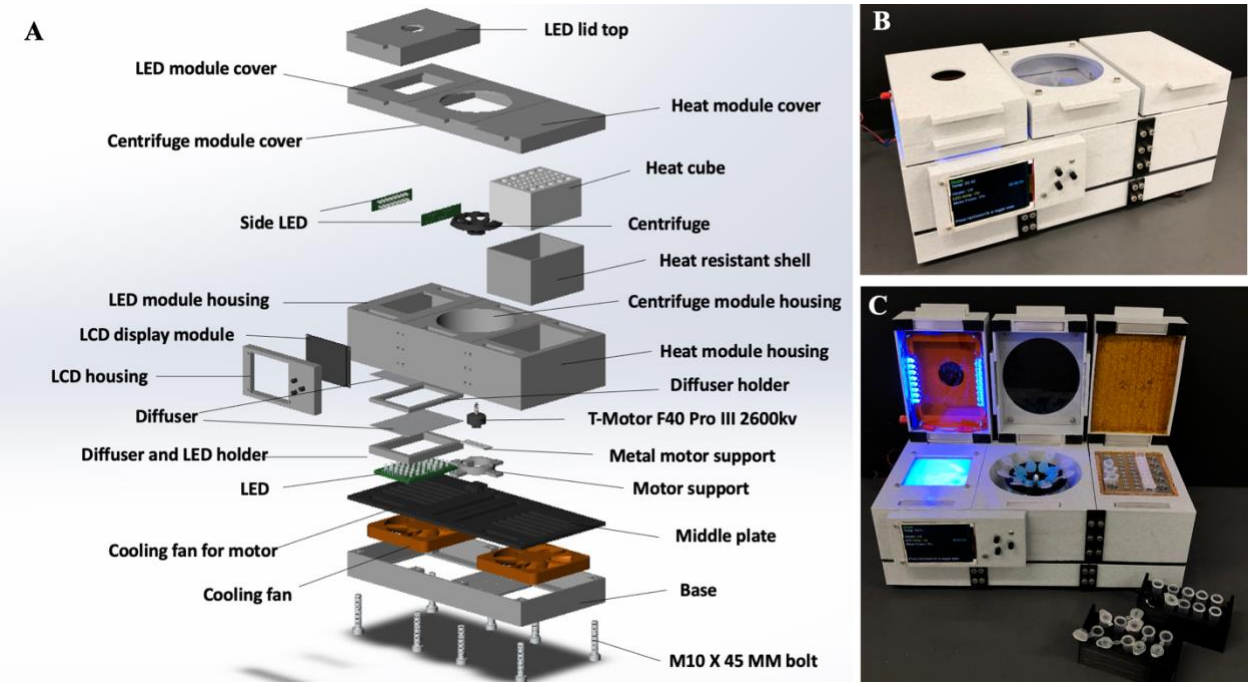

Figure 2.1. (A) Exploded view of the developed device. (B) and (C) Photographs of the fabricated device [55].

Table 2.1. Specifications of the developed device.

Specification	Parameter value
Centrifuge	2600kV, 8000 RCF
Aluminum heating block	61 ℃
Cartridge heater	12V, 40W
Thermistor	100KΩ, accuracy ± 1%
LED	470 nm
LCD	3.2 inch, 320*240 (Pixel)
ESP32	2.4 GHz, 38 Pin, Micro USB

2.4 Experimental Methods

The workflow of Saliva-Dry LAMP on commercially available instruments and the developed device is shown in Figure 2.2; it includes RNA extraction, isothermal incubation, and fluorescent detection. The following steps were performed for RNA extraction. Saliva was diluted in UTM (approximately 25% saliva, 75% UTM, 140 µL total) to prevent spin columns from being clogged with undiluted saliva and mixed with a concentrated preparation of lysis buffer (560 µL) described by Zainabadi *et al.* [53]. It was then spiked with 2 µL of 50,000 pfu/µL MS2 bacteriophage (Zeptometrix, Buffalo, NY). The tube was shaken by hand and incubated at 61 ℃ for 5 minutes. The lysate was applied to a spin column (Omega Bio-Tek Inc., Norcross, USA) and rotated at a maximum speed of 11,300 RPM for 110 seconds at a mySPIN™ 12 (Thermo Fisher Scientific Inc., Waltham, USA). The flow-through was discarded. Wash 1 (500 µL) was applied to the column and the column was centrifuged again (110 s, 11,300 RPM) and the flow-through was discarded. Next, wash 2 (500 µL) was applied to the column and the column was centrifuged (170 s, 11,300 RPM). Columns were then transferred to new collection tubes. RNA was eluted with a final spin (110 s, 11,300 RPM) after elution buffer (50 µL) was added. The RNA extraction

process through the developed device had the same conditions as above, except that the centrifugation time was 50 seconds shorter because of faster ramping.

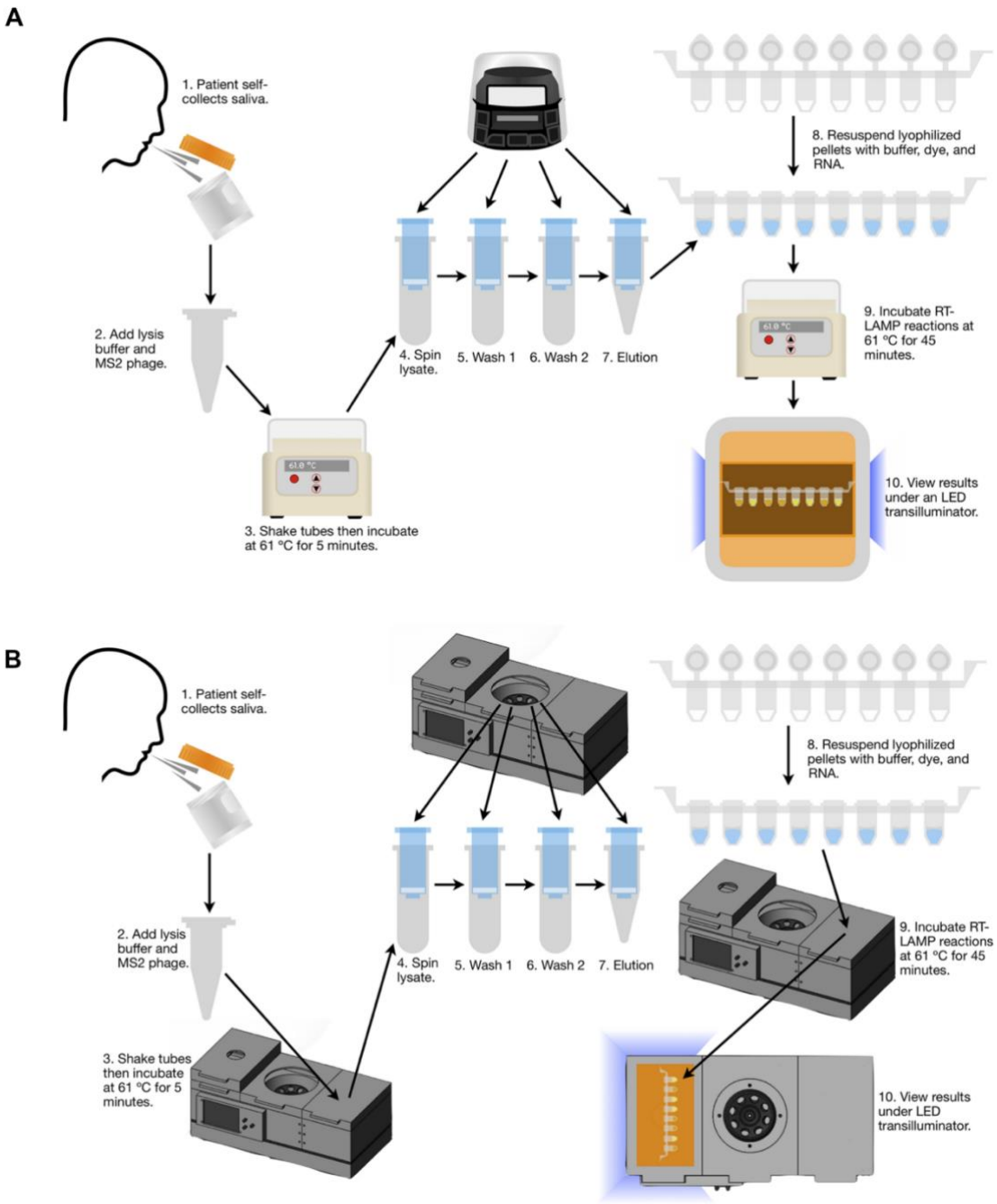

Figure 2.2. Workflow of Saliva-Dry LAMP on (A) commercially available instruments and (B) the developed device [55].

Saliva samples were collected from anonymized individuals in Alberta between May and September 2020 without any clinical information. Saliva and NP swabs were collected in universal transport media (UTM) (COPAN Diagnostics Inc., Murrieta, USA). Human participants were included in this study, and all clinical practices were conducted in accordance with all relevant guidelines and regulations. All participants' prior consent was obtained and approved by Conjoint Health Research Ethics Board (CHREB) at the University of Calgary (REB20-0402/0444).

Lyophilized RT-LAMP reactions for SARS-CoV-2 detection prepared by Pro-Lab Diagnostics Inc. (Richmond Hill, ON, Canada) used patented dual-target primers [54] and the GspSSD2.0 Isothermal Mastermix (ISO-004) (OptiGene Ltd., Horsham, UK). These pellets were dissolved in 10 μL resuspension buffer R1 (Pro-Lab Diagnostics Inc.) and 0.5 μL of dye mix comprised of 5.95 mM hydroxynapthol blue trisodium salt and 69.5 X GelGreen®(Biotium, Fremont, USA) and 14.5 μL of extracted RNA was subsequently added. 30 μL of mineral oil was then added on top of the mixed reaction. An IncuBlock™ Mini Dry Bath (Thomas Scientific, Swedesboro, NJ, USA) was used for reaction incubation (45 minutes, 61 °C), and the results were visualized under an LED transilluminator (MaestroGen Inc., Hsinchu City, China). The lyophilized RT-LAMP reagents for the amplification of SARS-CoV-2 on the developed device were obtained from Illucidx Inc. (Calgary, Alberta, Canada). Lastly, 25 μL of extracted RNA was mixed, and 30 μL of mineral oil was added on top.

Separate lyophilized RT-LAMP reactions prepared by Pro-Lab Diagnostics Inc. using the primers from Benzine *et al.* [56] were used for MS2 external amplification controls performed in parallel. Lyophilized reactions were dissolved with 15 μL of resuspension buffer R1, 0.5 μL dye mix and 4.5 μL elution buffer. The reactions contained 5 μL of extracted RNA and were run

simultaneously with SARS-CoV-2 reactions with identical procedures. They were used with both the developed device and commercially available instruments.

2.4.1 Saliva-Dry LAMP Clinical Validation

For clinical validation of Saliva-Dry LAMP, two different reference standard RT-PCR tests were used. For the first RT-PCR test, the US CDC N2-gene assay [57] and the Alberta Precision Labs E-gene assay [58] were performed with RNA extracted from saliva samples. For the E-gene assay, 5 μL of extracted RNA, 2.5 μL of TaqMan Fast Virus One-Step RT-PCR Master Mix, 0.4 μL each of forward and reverse primers (800 nM final concentration), 0.2 μL of probe (200 nM final concentration), and 1.5 μL of nuclease-free water are mixed. CFX96 (Bio-Rad Laboratories Inc., Hercules, CA, USA) performed reactions with the following thermocycling parameters: 50 °C for 5 minutes, 95 °C for 20 seconds, and then 45 cycles of 95 °C for 3 seconds and 60 °C for 30 seconds. The CDC N2 assay was performed in the same way as described below, except that it was performed on a CFX96 instrument.

Paired saliva and NP swabs were collected in the second reference RT-PCR, the US CDC N1/N2/RNase P RT-PCR test performed according to CDC-006-00019, Revision: 01 [57]. For this test, a viral RNA mini kit (QIAamp, QIAGEN, Hilden, Germany) was used to extract 140 μL of NP swab UTM, which was finally eluted in 50 μL of AE buffer. For the RT-PCR, 5 μL of extracted RNA, 5 μL of TaqPath™ 1-Step RT-qPCR Master Mix (ThermoFisher Scientific, Waltham, MA, USA), 1.5 μL of combined primer/probe mix, and 8.5 μL of nuclease-free water were mixed. A Real-Time PCR Instrument (Applied Biosystems™ 7500 Fast Dx, ThermoFisher Scientific, Waltham, MA, USA) was utilized for the run of reactions using the following thermocycling profile: 25 °C for 2 minutes, 50 °C for 15 minutes, 95 °C for 2 minutes, and then 45 cycles of

95 °C for 3 seconds, 55 °C for 30 seconds. Completely different sets of samples were used for each of the two comparator tests (saliva versus saliva and saliva versus NP swab).

2.4.2 Saliva-Dry LAMP Limit of Detection Studies

For the determination of the limit of detection (LOD) on commercially available instruments and the developed device, a diluted sample from an NP swab quantified by a PCR system (QX200™ Droplet Digital™, Bio-Rad Laboratories, Hercules, CA, USA) was used. This sample was diluted two-fold to have a range of 1 to 0.25 copies/μL. The selected saliva: UTM ratio was 1:3 based on two factors. First, 3 mL of UTM was contained in the standard UTM collection tubes; second, the average volume of the collected saliva was approximately 1 mL. This is supported by Lagerlöf and Dawes [59].

2.5 Results

The visual results of Saliva-Dry LAMP are shown in Figure 2.3. Bright green colour indicates a positive reaction, whereas an orange colour represents a negative reaction. To maximize the sensitivity, the intermediate reaction where a colour between orange and bright green appears was also labelled as a positive reaction. The throughput for commercially available instruments is ten samples per batch and eight samples per batch for the developed device. The total time required to perform Saliva-Dry LAMP is approximately 105 minutes.

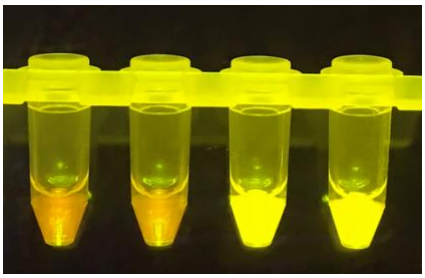

Figure 2.3. Visual results of Saliva-Dry LAMP reactions [55].

Table 2.2 shows the results of clinical validation conducted on 63 unique clinical saliva samples using commercially available instruments and lyophilized RT-LAMP reactions from Pro-Lab Diagnostics Inc. compared to CDC N2-gene and E-gene RT-PCR as a reference method. Positive percent agreement (PPA) and negative percent agreement (NPA) were calculated, and a PPA of 93.33% and an NPA of 100.00% were achieved for Saliva-Dry LAMP. Two samples were indicated as positive by both RT-PCR and negative by Saliva-Dry LAMP. One sample was considered negative because it was barely positive by E-gene RT-PCR and negative by N2-gene RT-PCR.

The clinical validation using commercially available instruments and lyophilized RT-LAMP reactions from Pro-Lab Diagnostics Inc. was conducted on 60 unique clinical saliva samples. PPA and NPA were calculated compared to the CDC reference RT-PCR which was run on the corresponding NP swabs. Saliva-Dry LAMP achieved a PPA of 100% and an NPA of 96.7% and shown in Table 2.3.

Table 2.2. Saliva-Dry LAMP clinical validation for saliva on commercially available instruments compared to reference RT-PCR (E gene and N2 gene) [55], [57], [58].

		RT-PCR (E and N2 gene)	
		Positive	Negative
Saliva-Dry LAMP	Positive	28	0
	Negative	2	33
Total		30	33
Positive percent agreement (PPA)		**93.33% (28/30)**	
Negative percent agreement (NPA)		**100.00% (33/33)**	

Table 2.3. Saliva-Dry LAMP clinical validation for saliva and NP swab on commercially available instruments compared to reference RT-PCR (N1 and N2 gene) [55], [57].

		RT-PCR (N1 and N2 gene)	
		Positive	Negative
Saliva-Dry LAMP	Positive	30	1
	Negative	0	29
Total		30	30
PPA		**100.00% (30/30)**	
NPA		**96.70% (29/30)**	

Table 2.4 shows the LOD determined by the developed device and commercially available instruments for Saliva-Dry LAMP. A sample from an NP swab was diluted to have a range of 1 to 0.25 copies/µL. A single experiment that was conducted with four replications at each concentration using a contrived saliva sample containing SARS-CoV-2 is shown in the table. All replicates with 1.0 copies/μL of both the developed device and commercially available instruments tested positive. However, the confirmation of LOD was conducted using 20 replicates at 0.5 copies/μL on commercially available instruments and failed as only 14 replicates were positive. The LOD confirmation at one copy/μL on commercially available instruments was retried, and the

results were successfully achieved with 19 positives out of 20 replicates. Therefore, LOD for Saliva-Dry LAMP can be determined to be one copy/μL for both commercially available instruments and the developed device.

Table 2.4. Limit of detection comparison of the developed device and commercially available instruments for Saliva-Dry LAMP [55].

Sample concentration (copies/µL)	Positive reactions	
	Developed device	Commercially available instruments
1.0	4/4	4/4
0.5	3/4	4/4
0.25	2/4	0/4

The development of the device reduced the capital cost of the device significantly compared to commercially available instruments. The capital cost of commercially available instruments to execute Saliva-Dry LAMP is CAD 2534.95, shown in Table 2.5, with more than half of the cost being due to the centrifuge. The capital cost of the developed device, when calculated with major components, was CAD 495.75, as shown in Table 2.6.

Table 2.5. Capital cost of commercially available instruments for Saliva-Dry LAMP [55].

Instrument	**Cost Per Unit (CAD)**
mySPIN™ 12 Mini Centrifuge	$1582.20 (Bento Bioworks Ltd. Bento Lab)
IncuBlock™ Mini Dry Bath	$252.00 (Lucira Health Inc.)
2 X Aluminum blocks (for 0.2 mL and 2 mL tubes)	$174 (Lucira Health Inc.)
Ultra Slim LED Transilluminator	$526.75 [60] [59]
Total Capital Cost	**$2534.95**

Table 2.6. The capital cost of the developed device for Saliva-Dry LAMP [55].

Instrument	Cost Per Unit (CAD)
Fan	$56.19
Cable	$46.38
Heat block & machining	$130.29
Motor	$38.43
Other	$224.46
Total Capital Cost	**$495.75**

2.6 Discussion and Challenges

Saliva-Dry LAMP is a rapid, near-patient, and saliva test to detect SARS-CoV-2 that was developed to meet a growing need for effective, convenient diagnostic methods. It is a LAMP-based method that can give rapid results (~105 min) compared to RT-PCR. The results are visual and can be easily interpreted even by users who have not received professional training. Saliva samples were used successfully in the experimental procedures due to their acceptable high sensitivity, similar to the standard NP swab, as well as other advantages such as being less invasive for the patient. Furthermore, self-collection of saliva samples minimizes the need for healthcare workers, and subsequently, PPE supplies, and symptoms, such as sneezing and coughing, are reduced. The results of clinical validations for Saliva-Dry LAMP showed excellent PPA and NPA compared to reference RT-PCR. The lowest agreement was a PPA of 93.33% compared to CDC N2-gene and E-gene RT-PCR. The LOD of Saliva-Dry LAMP was determined as 1.0 copies/ μL for both the developed device and commercially available instruments. The developed device is a portable all-in-one device which can execute Saliva-Dry LAMP. The developed device showed excellent performance in detecting SARS-CoV-2 compared to commercially available instruments

while significantly reducing capital costs. It means that the developed device with Saliva-Dry LAMP can be a portable, sensitive, and low-cost device that could play a crucial role in limiting the spread of viral infections. Rapid detection time, near-patient method, ease of use, and low costs are the primary advantages of Saliva-Dry LAMP.

Nevertheless, Saliva-Dry LAMP and the developed device have their limitations as well. First, Saliva-Dry LAMP relies on visually distinguishing a color change for results, and results may be subjective depending on the user in calling positive or negative reactions depending on the color. Subjectivity of readings may increase especially for intermediate reactions which resemble both positive and negative colors. Second, a cold chain is still required to run Saliva-Dry LAMP because the positive controls, dye, and resuspension buffer used are not stable at room temperature. Third, RNA extraction is included in the procedure of Saliva-Dry LAMP. Standard laboratory RNA extraction is a time-consuming process, and the silica spin column-based RNA extraction used for Saliva-Dry LAMP also takes around 30 minutes. The procedure of RNA extraction can increase the total detection time and the risk of laboratory contamination. Lastly, clinical validation experiments done in this study used commercially available instruments rather than the developed device, making it more difficult to fully demonstrate the performance of the developed device. The developed device is not battery-driven; therefore, electricity is needed, and its size is considerably smaller as a result.

2.7 Summary

Saliva-Dry LAMP is a newly developed diagnostic method for COVID-19, which is rapid, near-patient, and saliva-based. It shows the advantages of overcoming the limitations of the conventional diagnostic method, RT-PCR. The customized device is low-cost, portable and all-in-

one to execute Saliva-Dry LAMP. Clinical validation for Saliva-Dry LAMP was done with commercially available instruments compared to two different references RT-PCR and showed excellent PPA and NPA. The LOD experiments for both the developed device and commercially available instruments showed the same result of 1.0 copies/ μL. Despite the advantages, there are still limitations of Saliva-Dry LAMP. Visual results are analyzed subjectively, the cold chain and RNA extraction process are still required, the clinical validation of the developed device was not confirmed, and the developed device is not battery-driven.

Chapter 3: Direct Dry-LAMP

3.1 Synopsis

The RNA extraction procedure in general diagnostic methods to detect severe acute respiratory syndrome coronavirus 2 (SARS-CoV-2) has limitations, and the heat inactivation step can replace RNA extraction with the advantage of decreased time and cost. To overcome the limitations of Saliva-Dry LAMP presented in Chapter 2, Direct Dry-LAMP is another rapid, sensitive, and near-patient method for COVID-19 that was developed alongside a customized, portable, and low-cost device. This device combines the three essential steps in the sequence of Direct Dry-LAMP assay: one heating block for heat inactivation, another heating block for isothermal incubation, and excitation LEDs for visual fluorescent examination. The total procedure of Direct Dry-LAMP can be finished in 50 minutes. Direct Dry-LAMP showed excellent positive and negative agreement for clinical validation experiments. The developed device is portable and battery-driven, which can be useful in resource-limited regions, and it reduces the capital equipment cost while also giving an objective interpretation.

3.2 Introduction

SARS-CoV-2 can be transmitted through various routes, including environmentally. Decontamination of immediate surroundings can prevent the transmission of infectious substances, and it helps workers reuse potentially contaminated medical, personal protective equipment (PPE), and laboratory equipment safely. Heat inactivation is a general method for decontamination, particularly for viruses, and has also been used for SARS-CoV-2 [61]. The existing COVID-19 diagnostic method usually includes the RNA extraction process, which has the disadvantages of

increasing the overall diagnostic time and contamination in the laboratory due to the process used for RNA extraction. Reverse transcriptase polymerase chain reaction (RT-PCR), which is extraction-free but has a heat inactivation step to detect SARS-CoV-2, was described by Smyrlaki *et al.*, and it was demonstrated that the extraction-free RT-PCR could be a viable option to detect SARS-CoV-2 due to its simpler procedures. As the RNA extraction process was omitted, both the total time and the cost of performing RT-PCR decreased [62]. It has been proven that SARS-CoV-2 can be completely inactivated after being heated at 95 ℃ for 1 minute or 5 minutes [63], and the other experiment also showed that SARS-CoV-2 was inactivated 3 minutes after the heat was applied at 95 ℃ [64]. However, viral RNA quantity could decrease after inactivation at 95 ℃, but the Ct value was found to increase less than when the virus was heated at 80 ℃ for 30 minutes [63], [64].

To overcome the limitations of Saliva-Dry LAMP developed in Chapter 2, Direct Dry-LAMP was developed with a heat inactivation step rather than with RNA extraction. In addition, a customized device for Direct Dry-LAMP beyond the limitations of the device for Saliva-Dry LAMP was developed, and it can be operated with a battery while allowing for objective interpretation of the results through the application (app) developed.

3.3 Device Development

A customized device was developed for the execution of each step for Direct Dry-LAMP – heat inactivation, isothermal incubation, and naked-eye fluorescent detection, and a 3D design modeled using Solidworks™ 2020 (Dassault Systems, Waltham, MA, USA). The photographs of the developed device are shown in Figure 3.1. The developed device consists of three components – one heating block maintained at 95 ℃, another heating block maintained at 61 ℃, and a

transilluminator (470 nm light emitting diode, LED, arrays). All housing parts/fixtures were fabricated using a FDM 3D printer(Anycubic Technology Co., Shenzhen, China) with polylactic acid (PLA) filament. The transilluminator consists of two 14 × 2 LED arrays mounted on the sides of the part where the samples are placed to provide illumination from the sides. A cap was placed on the transilluminator with an acrylic sheet window to block the wavelengths emitted by the LEDs but not the intercalating dye.

Two aluminum blocks were purchased from a local store. One aluminum heating block was machined to house four 1.5 mL tubes. The temperature of the heating block was maintained at 95 °C using two heating elements and three thermocouple sensors. Another aluminum heating block maintained at 61 °C using two heating elements and three thermocouple sensors was machined to house a total of eight 0.125 mL tubes. Heating lids were added to the lid of each heating block to prevent the evaporation and condensation of the buffer without mineral oil added on the top, as shown in Figure 3.2. Epoxy putty was added to the wall of the heating blocks to fill out the empty space due to the conical shape of the tubes.

All components were controlled by an ESP32 microprocessor. The device is operated through the user interface using an LCD display and push buttons or the developed app. A DC power supply of 21–23V was used to power the device. In addition, two 12.8V, 30Ah rechargeable Lithium-Ion Phosphate (LiFePO4) batteries (Eco-Worthy, Los Angeles, CA, USA) were connected in series, which can have a total of 25.6V 30A, and the batteries can operate the developed device for approximately 32 hours. For charging one 12.8V 30Ah LiFePO4 battery, the power supply provides a voltage of 14.6V and a current which is 1/10 to 1/5 of the capacity. The charging time varies depending on the current provided. A battery monitor (SUPNOVA, Shenzhen,

China) was used to monitor the remaining capacity percentage of batteries. The specifications of the developed device is summarized in Table 3.1.

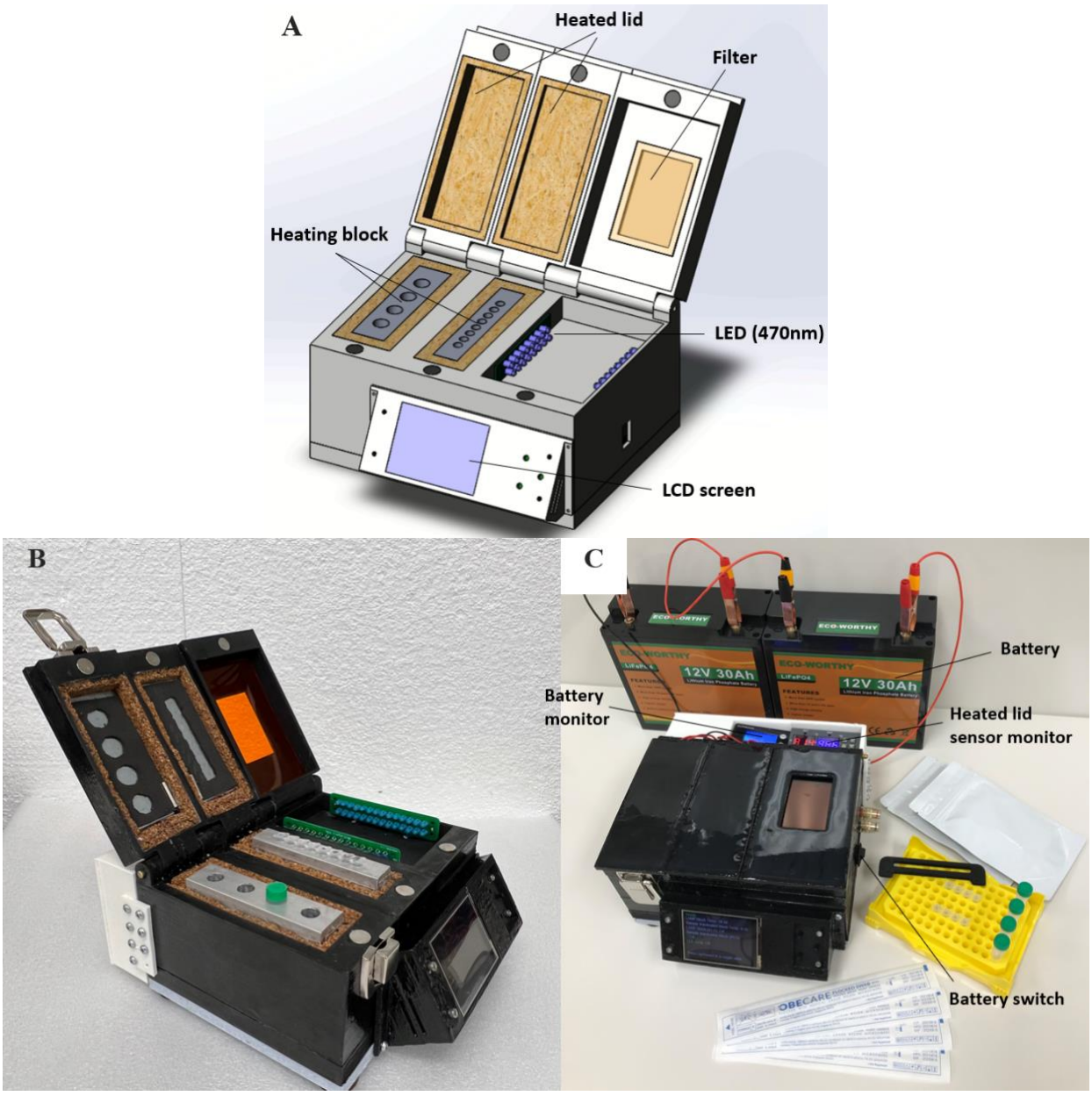

Figure 3.1. (A) 3D modeling of the developed device for 3D printing. (B) and (C) Photographs of the fabricated device.

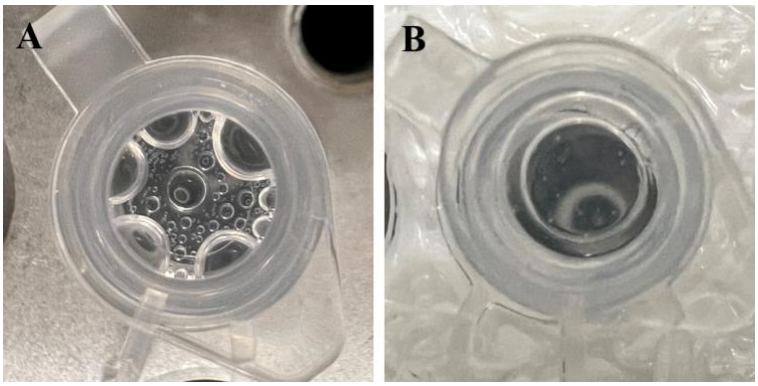

Figure 3.2. Evaporation and condensation difference when the tube is maintained at 61 ℃ for 40 minutes (A) without the heating lid and (B) with the heating lid.

Table 3.1. Specifications of the developed device.

Specification	Parameter value
Aluminum heating block (Heat inactivation)	95 ℃
Aluminum heating block (LAMP)	61 ℃
Cartridge heater	12V, 40W
Thermistor	100KΩ, accuracy ± 1%
LED	470 nm
LCD	2.8 inch, 320*240 (Pixel)
ESP32	2.4 GHz, 38 Pin, Micro USB
LiFePO4 Battery	12V, 30Ah
Battery monitor	DC8-100V, accuracy ± 1%
Heater Plate (Heated lid)	12V, 7W

3.4 Experimental Methods

Nasopharyngeal (NP) swab samples were collected from individuals at various testing sites in Calgary, Alberta, Canada, in January 2022. This research was conducted under relevant guidelines and regulations, including human participants. All individuals' prior consent was

obtained and approved by CHREB at the University of Calgary (REB20-0402/0444). NP swabs were collected in 3 mL universal transport media (UTM). After the samples were partially consumed for testing at the Khan Lab at the University of Calgary, the leftover swab samples were stored at 4 ℃ for one night to check whether the samples were necessary for retesting.

SARS-CoV-2 lyophilized reaction and control lyophilized reaction were prepared by Biolyph LLC., using patented-dual target primers [54] and primers from Singelton *et al.* [65], respectively. The lyophilized reverse transcription loop-mediated isothermal amplification (RT-LAMP) reactions contained 0.5 µL of lyophilized CFI dye mix comprised of 5.95 mM hydroxynaphthol blue trisodium salt and 69.5 X GelGreen® (Biotium, Fremont, CA, USA).

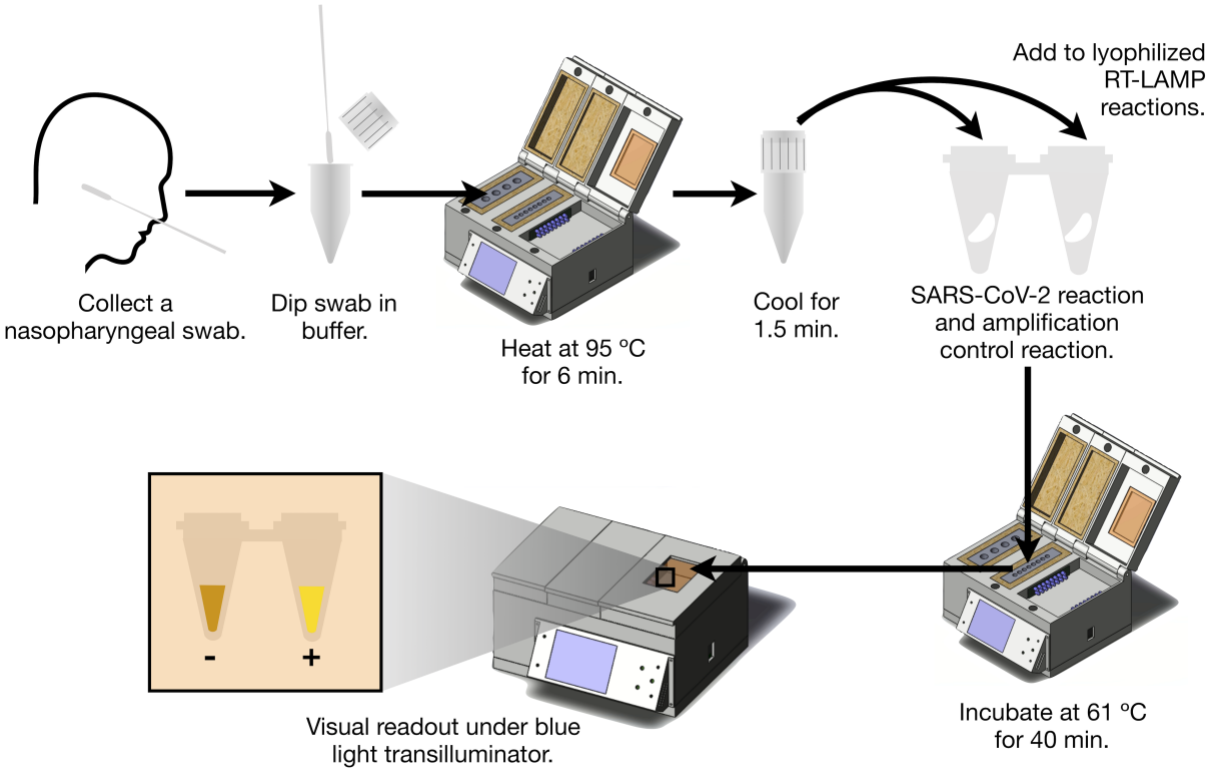

Figure 3.3. Workflow of Direct Dry-LAMP with the developed device (Figure made by Dr. Pillai Lab).

The workflow of Direct Dry-LAMP included heat inactivation, isothermal incubation, and fluorescent detection, as shown in Figure 3.3. First, a swab was dipped in the collected UTM swab samples from the Khan lab and then into 500 µL of TEEG buffer comprised of 10 mM Tris, 1 mM ethylene glycol tetraacetic acid (EGTA), and 1mM ethylenediaminetetraacetic acid (EDTA) in pH 8.0. TEEG buffer is optimal for stabilizing the SARS-CoV-2 RNA before and during heat inactivation, as well as ideal for not interfering with downstream amplification (RT-LAMP). For Direct Dry-LAMP, samples were heat-inactivated at 95 ℃ for 6 minutes. After 6 minutes, tubes were cooled down for at least 1.5 minutes, but not more than 30 minutes. A total of 25 μL of cooled samples were added to a strip of SARS-CoV-2 lyophilized reaction (Biolyph LLC., Chaska, MN, USA) and a strip of control lyophilized reaction (Biolyph LLC., Chaska, MN, USA), and then incubated at 61 ℃ for 40 minutes. Lastly, the results can be interpreted under a blue light LED transilluminator with an amber filter. For commercially available instruments to perform Direct Dry-LAMP, an advanced mini block heater with a heated lid (VWR International, Radnor, PA, USA) and an LED transilluminator (MaestroGen Inc., Hsinchu City, China) were utilized.

3.4.1 Direct Dry-LAMP Clinical Validation

The performance of Direct Dry-LAMP on the developed device and commercially available instruments were compared to a reference standard RT-PCR test and the RT-PCR test used at the clinical testing lab. The US CDC nCoV-19 RT-PCR test (N1/N2/RNase P) was performed with swab-diluted samples as a reference. The E-gene RT-PCR assay using E-gene primers/probe from Corman *et al.* [66] was performed with undiluted fresh samples in Khan lab. It was used to check the discrepancy of the results and compared with Direct Dry-LAMP. RNA extraction for US CDC RT-PCR was done using the QIAmp viral RNA mini kit (QIAGEN, Hilden, Germany) following

kit instructions for centrifugation. Finally, 140 µL of UTM sample was inputted, with 50 µL of sample eluted. The workflow of Direct Dry-LAMP clinical validation is shown in Figure 3.4.

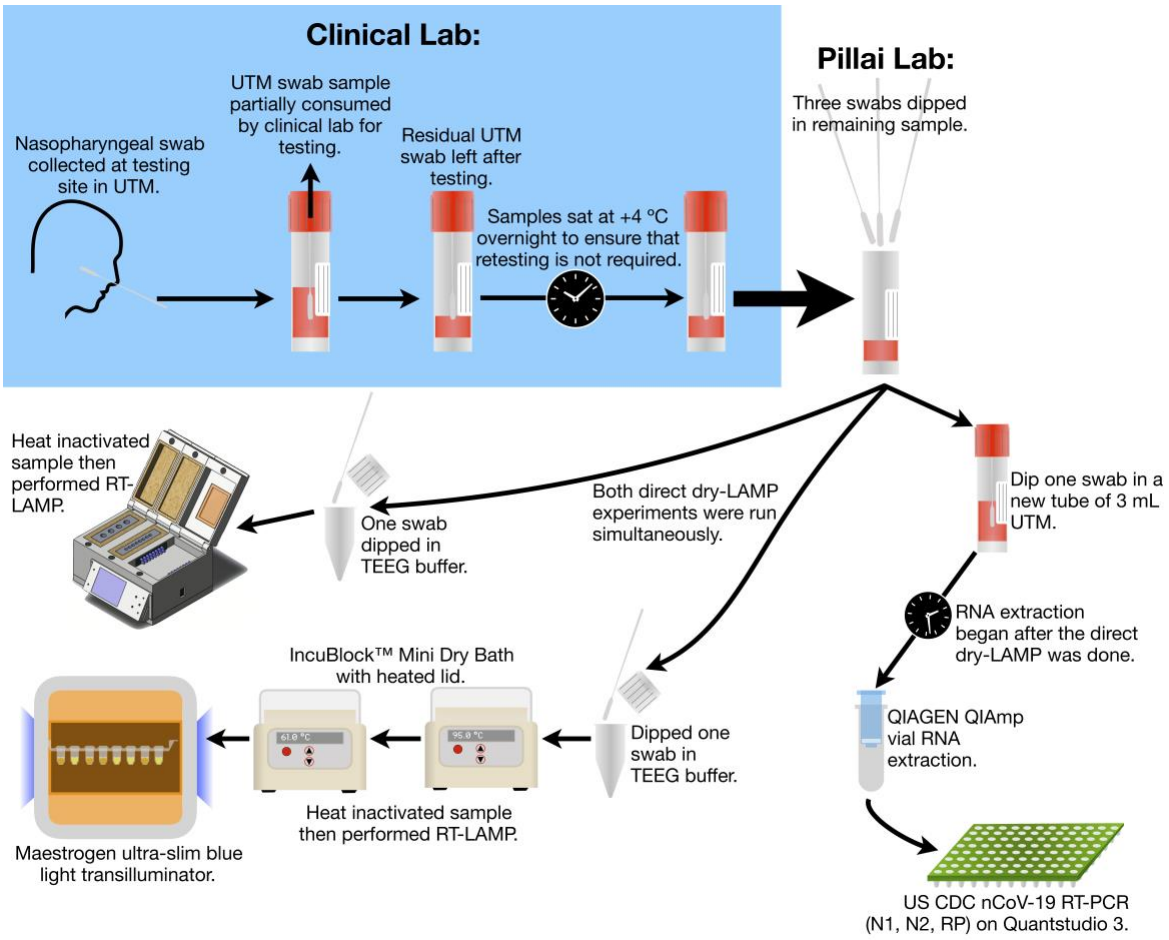

Figure 3.4. Direct Dry-LAMP clinical validation workflow (Figure made by Dr. Pillai Lab).

3.4.2 Direct Dry-LAMP Limit of Detection (LOD) Studies

Direct Dry-LAMP LOD experiments were done with contrived samples using ddPCR quantified PBNP7 frozen stock diluted in fresh SARS-CoV-2 negative NP swabs. Lyophilized RT-LAMP reactions that were from the January 2022 lot (BioLyph LLC, Chaska, MN, USA), and the liquid RT-LAMP reactions were used. The liquid RT-LAMP reactions were prepared as previously

described by Mohon *et al.* [54], except that the CFI dye was used instead. Amplification control reactions were used throughout the LOD experiments. The sample was diluted serially two-fold in the sample matrix to have a range of 40 to 1.25 copies/μL.

3.4.3 Heating Temperature Test and Development of Application

Heating temperature measurements were conducted to determine how well the aluminum heating block was maintained at 61 ℃ after being heated, and the test can show how temperature maintenance affects the performance of the LAMP reaction. A multimeter (KAIWEETS, Shenzhen, China) with K-type thermocouple included was used, and the measurement uncertainty for the temperature was $\pm$1 ℃. Three out of eight holes were tested for the developed device, and the corresponding holes were tested in VWR® advanced mini block heater with heated lid. The temperature was recorded every 10 seconds for 40 minutes. Considering that the temperature measured with the multimeter was always 2 ℃ lower than the temperature of the VWR® advanced mini block heater, 2 ℃ was added to all the measured temperatures. The average of the temperature difference from 61 ℃ for all temperatures after 1 minute was calculated. One minute was the time that the temperature of the aluminum heating block could reach around 61 ℃ generally.

A smartphone application (app) named ‘Biobox’ was developed in the Advanced Biofabrication Laboratory to control the developed device wirelessly and interpret the visual results objectively. Patient information and the results stored in this Biobox can be stored in Microsoft Excel.

3.5 Results

The visual results of Direct Dry-LAMP are shown in Figure 3.5, positive reactions and negative reactions are indicated by a bright green color and an orange color, respectively. The

method to read the intermediate reaction is the same as that of Saliva-Dry LAMP described in Chapter 2. The total time required to get results for Direct Dry-LAMP is around 50 minutes with a throughput of 4 samples. For the visual results in Figure 3.5, the same negative samples were used in SARS-CoV-2 lyophilized reaction (1st row) and control lyophilized reaction (2nd row). Results under the developed device and commercially available instruments are compared, and there seems to be no difference in visual quality that represents the results.

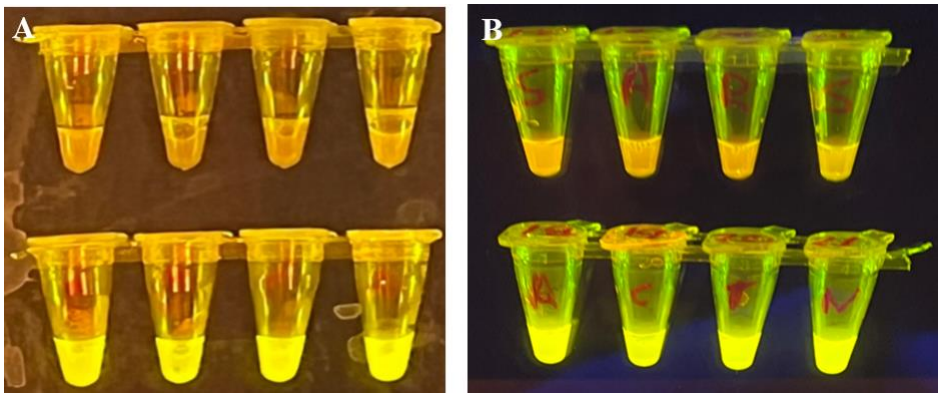

Figure 3.5. Visual results of Direct Dry-LAMP (A) on the developed device and (B) on commercially available instruments.

Table 3.2 shows the result of clinical validation of Direct Dry-LAMP conducted on 62 unique clinical diluted samples using the developed device compared to US CDC RT-PCR (N1/N2/RNase P) as a reference method. Positive percent agreement (PPA) and negative percent agreement (NPA) were calculated, and a PPA of 90.91% (30/33) and an NPA of 96.55% (28/29) were achieved for Direct Dry-LAMP on the developed device. The clinical validation of Direct Dry-LAMP using commercially available instruments was conducted on 26 unique swab-diluted samples. PPA and NPA were calculated compared to the US CDC reference RT-PCR (N1/N2/RNase P) which was run on the corresponding swab-diluted samples. Direct Dry-LAMP

on commercially available instruments achieved a PPA of 90.91% (10/11) and an NPA of 93.33% (14/15), as shown in Table 3.3. Table 3.4 shows the clinical validation of Direct Dry-LAMP on the developed device using 62 diluted samples compared to E-gene RT-PCR using corresponding undiluted samples, and a PPA of 90.63% (29/32) and an NPA of 93.33% (28/30) were achieved for Direct Dry-LAMP on the developed device. The clinical validation of Direct Dry-LAMP on the developed device compared to commercially available instruments using 26 diluted samples is shown in Table 3.5. A PPA of 90.91% (10/11) and an NPA of 93.33% (14/15) were achieved.

Table 3.2. Direct Dry-LAMP clinical validation using the developed device compared to CDC RT-PCR (N1/N2/RNase P)

		US CDC RT-PCR on swab-diluted sample		Total
		Positive	Negative	
Direct-LAMP on the developed device	Positive	30	1	31
	Negative	3	28	31
Total		33	29	62
Positive percent agreement (PPA)		**90.91% (30/33)**		
Negative percent agreement (NPA)		**96.55% (28/29)**		

Table 3.3. Direct Dry-LAMP clinical validation using commercially available instruments compared to CDC RT-PCR (N1/N2/RNase P)

		US CDC RT-PCR on swab-diluted sample		Total
		Positive	Negative	
Direct-LAMP on commercial instruments	Positive	10	1	11
	Negative	1	14	15
Total		11	15	26
PPA		**90.91% (10/11)**		
NPA		**93.33% (14/15)**		

Table 3.4. Direct Dry-LAMP clinical validation using the developed device compared to E-gene RT-PCR

		E-gene RT-PCR on undiluted sample (HTL)		Total
		Positive	Negative	
Direct-LAMP on the developed device	Positive	29	2	31
	Negative	3	28	31
Total		32	30	62
PPA		**90.63% (29/32)**		
NPA		**93.33% (28/30)**		

Table 3.5. Direct Dry-LAMP clinical validation using the developed device compared to Direct Dry-LAMP using commercially available instruments

		Direct LAMP on Commercially Available Instruments		Total
		Positive	Negative	
Direct-LAMP on the developed device	Positive	10	1	11
	Negative	1	14	15
Total		11	15	26
PPA		**90.91% (10/11)**		
NPA		**93.33% (14/15)**		

Table 3.6. Estimated viral RNA degradation and dilution resulting from diluting samples with a flocked swab refrigerated for 1 day compared to E-gene RT-PCR

US CDC RT-PCR Target	**N1**	**N2**	**Rnase P**
Different in cycle threshold values ± s.d.	**5.14 ± 2.04**	**5.51 ± 1.46**	**5.33 ± 1.64**

Diluting samples with a flocked swab made viral RNA degradation, and diluted samples showed higher Ct values. Ct values for diluted samples from US CDC RT-PCR were compared to

Ct values of E-gene RT-PCR, and Table 3.6 shows the Ct value difference in N1, N2, and RNase P genes.

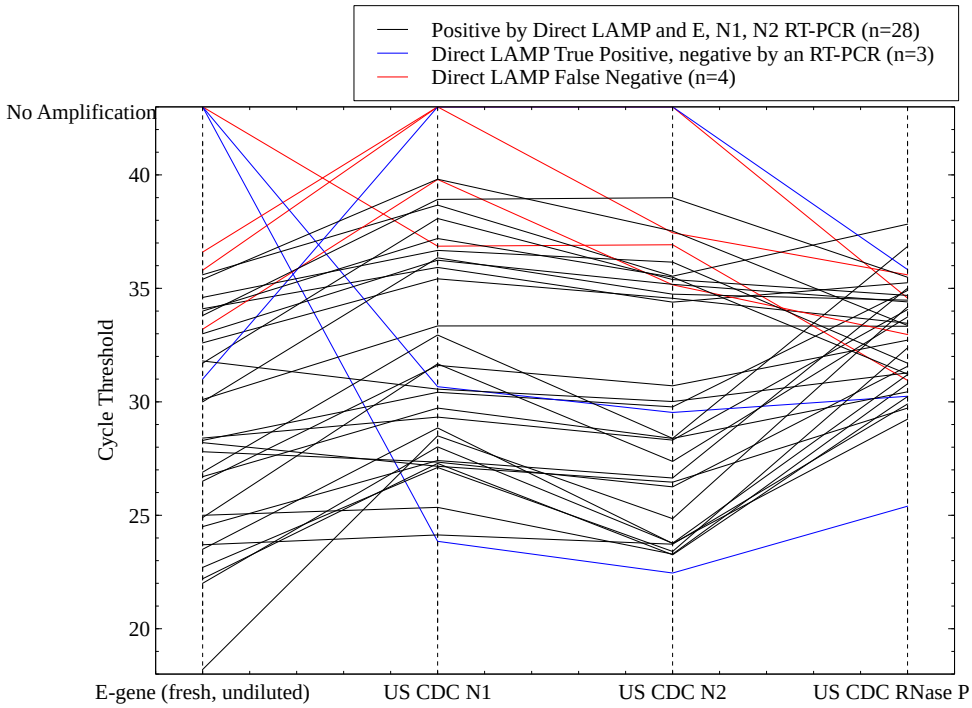

Figure 3.6. Cycle threshold value distribution of positive samples for SARS-CoV-2 by RT-PCR tested by Direct-LAMP on the developed device.

To confirm the clinical validation of Direct Dry-LAMP analytically, Ct values of 35 positive SARS-CoV-2 samples, which were tested on the developed device, were distributed in Figure 3.6. Four samples were indicated as negative by Direct Dry-LAMP on the developed device. However, only one out of those four samples was indicated positive by both US CDC RT-PCR and E-gene RT-PCR. The other sample was indicated positive by US CDC RT-PCR but negative by E-gene RT-PCR. The remaining two samples were indicated positive by E-gene RT-PCR but negative by US CDC RT-PCR. In addition, three samples were indicated positive by Direct Dry-LAMP, but

one sample was indicated negative by US CDC RT-PCR, and the last two samples were indicated negative by E-gene RT-PCR. This Ct value analysis can influence the interpretation of the clinical validation of Direct Dry-LAMP.

Direct Dry-LAMP LOD experiments were carried out using the developed device and commercially available instruments for Direct Dry-LAMP, as shown in Table 3.7. The sample was diluted serially two-fold to have a range of 40 to 1.25 copies/μL. Liquid RT-LAMP reactions and lyophilized RT-LAMP reactions were used. A single experiment was conducted with four replications at each concentration. With lyophilized RT-LAMP chemistry, all replicates with 10 copies/μL of the developed device tested positive, and all replicates with 2.5 copies/μL of commercially available instruments tested positive. With liquid RT-LAMP chemistry, all replicates with 40 copies/μL of the developed device tested positive, and all replicates with 20 copies/μL of commercially available instruments tested positive. Liquid and lyophilized reactions received 12 µL and 25 µL of the sample, respectively, and the LOD of Direct Dry-LAMP in terms of copies/µL and copies/reaction is shown in Table 3.8.

Table 3.7. Direct Dry-LAMP LOD experiments on the developed device and commercially available instruments

	Liquid RT-LAMP Chemistry		Lyophilized RT-LAMP Chemistry	
Copies/µL	Developed device	Commercially Available Instruments	Developed device	Commercially Available Instruments
40	**4/4**	4/4	Not tested	Not tested
20	2/4	**4/4**	4/4	4/4
10	3/4	3/4	**4/4**	4/4
5	Not tested	Not tested	2/4	4/4
2.5			Not tested	**4/4**
1.25				2/4

Table 3.8. LOD of Direct Dry-LAMP in terms of copies/µL and copies/reaction

	Liquid RT-LAMP Chemistry		Lyophilized RT-LAMP Chemistry	
	Developed device	Commercially Available Instruments	Developed device	Commercially Available Instruments
Copies/µL	40	20	10	2.5
Copies/Reaction	480	240	250	62.5

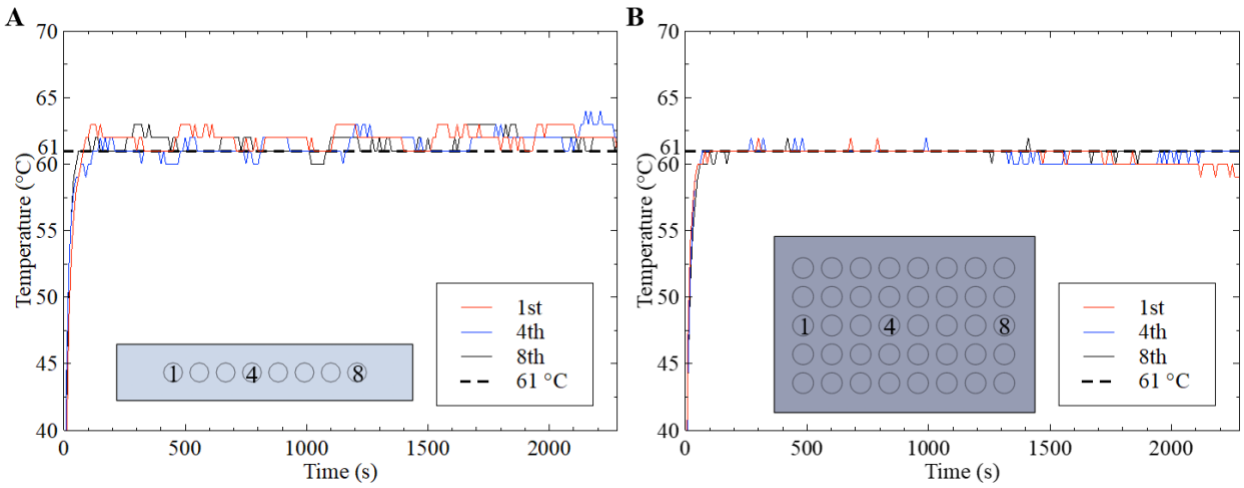

Figure 3.7. The heating temperature of LAMP reaction (A) on the developed device and (B) on the commercial aluminum heating block (VWR® advanced mini block heater with heated lid).

The 1st, 4th, and 8th holes of the aluminum heating block in the developed device were selected to measure the temperature during the LAMP reaction. For the VWR® advanced mini block heater, the corresponding holes in the middle row were chosen. Figure 3.7 shows the temperature during the LAMP reaction in the developed device and commercial heating block graphically. The average of the temperature difference from 61 ℃ for all temperatures after 1 minute was calculated and the results for each are as follows: 0.969 ℃, 0.668 ℃, and 0.664 ℃ for

the 1st, 4th, and 8th hole of the developed device, respectively; and 0.309 ℃, 0.305 ℃, and 0.058 ℃ for 1st, 4th, and 8th hole of the commercial aluminum heating block, respectively. Standard deviations for all holes were calculated, which were 0.672, 0.694, 0.662, and 0.517, 0.460, and 0.234, respectively.

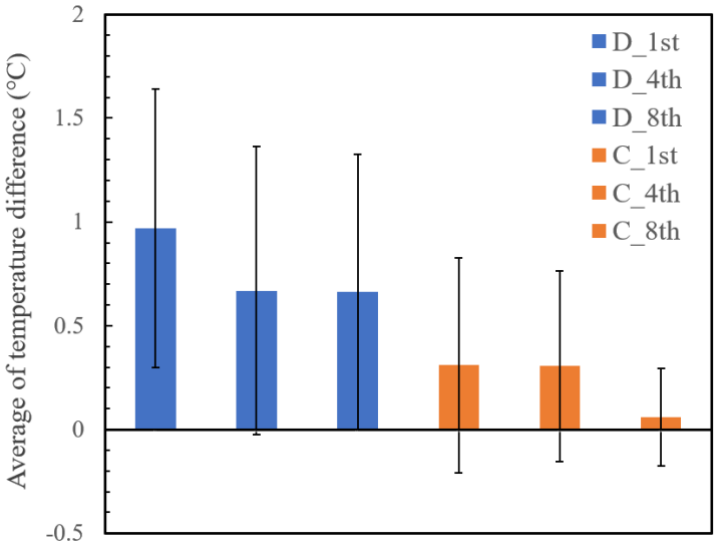

Figure 3.8. Average of the temperature difference from 61 ℃ (D: developed device, C: commercial aluminum block).

Figure 3.9 shows all seven steps detailing the 'Biobox' app configuration. After the ESP32 microprocessor was connected with the smartphone by the app using a Bluetooth function, the developed device was successfully controlled by the app. To analyze the result of the sample, patient number and tube number can be written, and the app presents the results between positive, negative, and undetermined based on the color. Patient information, tube number, and the test results were successfully stored in Microsoft Excel.

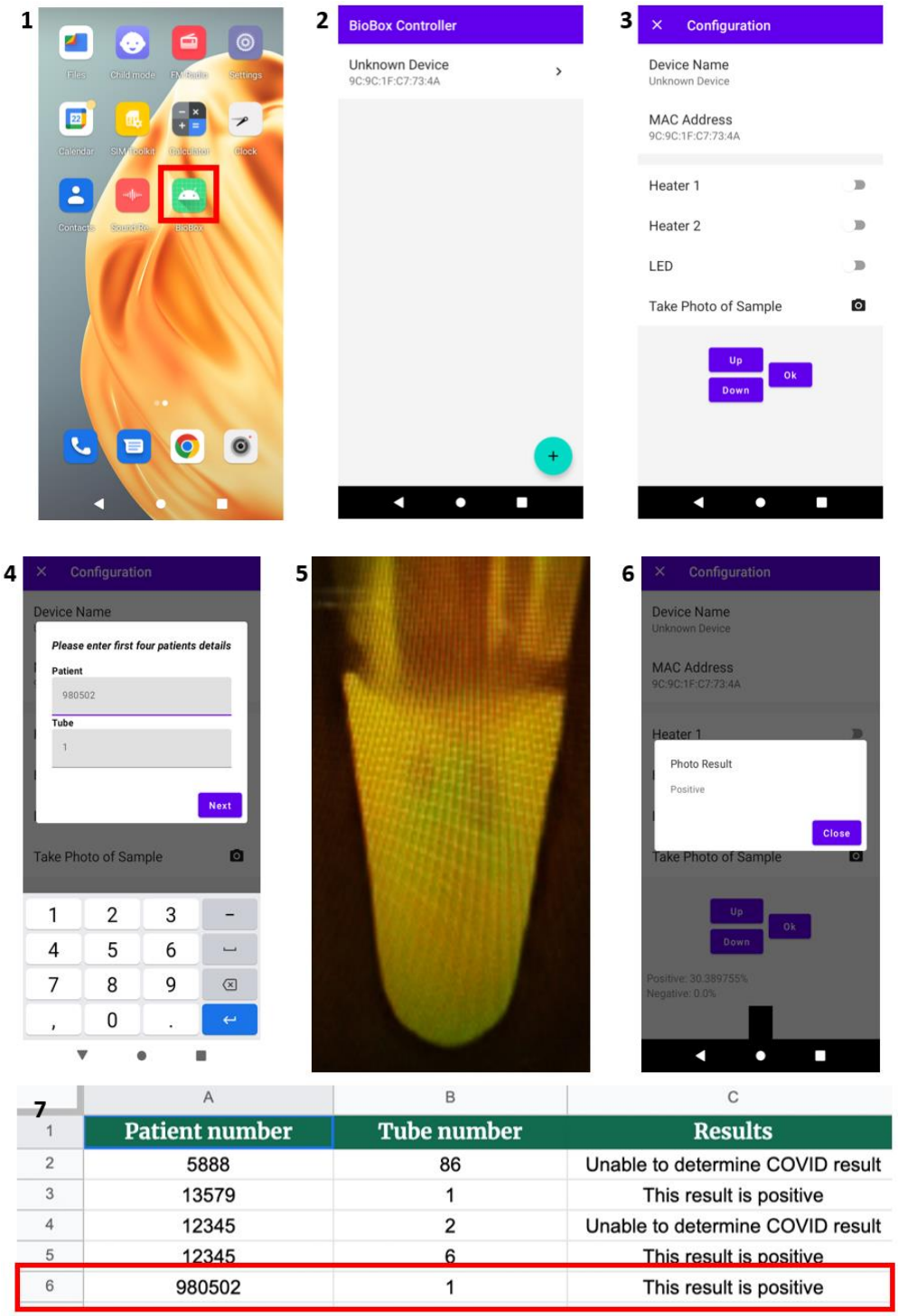

	A	B	C
1	Patient number	Tube number	Results
2	5888	86	Unable to determine COVID result
3	13579	1	This result is positive
4	12345	2	Unable to determine COVID result
5	12345	6	This result is positive
6	980502	1	This result is positive

Figure 3.9. Configuration of ‘Biobox’ app with steps 1 to 7.

Table 3.9 and Table 3.10 shows the capital cost of commercially available instruments and the developed device for Direct Dry-LAMP, respectively. The development of the device

significantly reduced the capital cost of the device compared to commercially available instruments, from CAD 2092.96 to CAD 686.42. As per Table 3.8, the price of batteries accounts for more than half of the total cost of the developed device.

Table 3.9. The capital cost of commercially available instruments for Direct Dry-LAMP.

Instrument	Cost Per Unit (CAD)
VWR® Advanced Mini Block Heater with Heated Lid	$629.05
VWR® Advanced Mini Block Heater with Heated Lid	$629.05
Mini Block for 40 x 0.2 mL Tubes	$118.52
Mini Block for 15 x 1.5 mL Tubes	$133.91
Maestrogen Blue Light Transilluminator | UltraSlim	$582.43
Total Capital Cost	**$2092.96**

Table 3.10. The capital cost of the developed device for Direct Dry-LAMP.

Instrument	Cost Per Unit (CAD)
Battery	$417.9
Lid temperature controller	$24.13
Heat block	$26.75
3D printer filament	$59.9
Others	$157.74
Total Capital Cost	**$686.42**

3.6 Discussion and Challenges

Direct Dry-LAMP is a new diagnostic method for COVID-19 which is rapid, sensitive, and near-patient. It eliminates the procedure of RNA extraction, thereby reducing the total detection time, while minimizing laboratory contamination. With heat inactivation step at 95 ℃ for 5

minutes, the total procedure of Direct Dry-LAMP is much simpler than that of Saliva-Dry LAMP and the rapid results can be obtained in 50 minutes. The visual results can be easily interpreted by users and the developed app can interpret the results objectively. Direct Dry-LAMP on the developed device and commercially available instruments got excellent PPA and NPA compared to US CDC RT-PCR, and the results were compared with E-gene RT-PCR as well. As shown and described in the graph of Ct value distribution of RT-PCR (Figure 3.6), there were three false negatives from US CDC RT-PCR used as a reference, which means that we can expect better performance of Direct Dry-LAMP than the analyzed data. The LOD of Direct Dry-LAMP on commercially available instruments (2.5 copies/μL) was better than that of the developed device (10 copies/μL), and it can be explained with the performance of LAMP reaction. The commercial aluminum block, VWR® advanced mini block heater, also showed better performance with less variance in temperature than the aluminum heating block in the developed device.

The customized developed device is a portable all-in-one device for Direct Dry-LAMP, and the capital cost of instruments (CAD 686.42) is much less than commercially available instruments (CAD 2092.96). Two LiFePO4 batteries were utilized to operate the developed device for approximately 32 hours without any malfunction. Batteries can be recharged easily using power supply. This suggests that the developed device for Direct Dry-LAMP can be used in resource-limited regions. The device can be further developed to detect various other respiratory infectious diseases.

There are a few limitations of Direct Dry-LAMP and the developed device. First, the performance of the aluminum block in the developed device affected the performance of the LAMP reaction, eventually affecting the LOD. Second, the battery used is not small, it adds substantial weight (total 6.53 kg), and is expensive such that the battery accounts for more than

half of the total cost of the developed device. Third, the result interpretation from the developed app can be error-prone and takes much longer than analyzing the results with the naked eye because only one tube can be analyzed at a time. Further research is necessary to increase the performance and accuracy by machine learning and image processing. Lastly, real-time detection is not available with the developed device.

3.7 Summary

Direct Dry-LAMP overcame the limitations of Saliva-Dry LAMP by eliminating the RNA extraction process and adding the heat inactivation step. As a result, Direct Dry-LAMP showed simpler preparation and much more rapid detection time compared to Saliva-Dry LAMP. The customized device is a portable, all-in-one device to execute Direct Dry-LAMP while reducing the capital cost of equipment significantly. Clinical validation for Direct Dry-LAMP using the developed device and commercially-available instruments showed excellent PPA and NPA. The developed device can be executed using chargeable batteries and also the app was developed to control the device and interpret the results objectively. The LOD of Direct Dry-LAMP on commercially available instruments was better than that of the developed device.

Chapter 4: Convection-based device for Direct Dry-LAMP

4.1 Synopsis

Conventional loop-mediated isothermal amplification (LAMP) based devices used to detect COVID-19 typically use an aluminum heating block for the LAMP reaction. Herein, the device using a convection system for LAMP reaction was developed for energy efficiency and the convection system was combined with real-time detection. The flow simulation was conducted to ensure that the convection-based device was suitable for the LAMP reaction with stable temperature maintenance. Heating temperature measurements and LAMP reactions were performed to test the performance of the developed device, which was able to give real-time detection results, but limitations exist due to the early stage of the development.

4.2 Introduction

Direct Dry-LAMP, as described in Chapter 3, is a rapid and near-patient diagnostic method for COVID-19, as well as a battery-powered device, making it possible for the procedure to be carried out in resource-limited regions. The corresponding developed device also detailed in Chapter 3 can be utilized by two Lithium-Ion Phosphate batteries, which provide the machine a large capacity for power. Convection heat transfer through the aluminum heating block, rather than conduction heat transfer, was considered alternatively for energy efficiency. The difference in heat transfer between conduction and convection was calculated and compared for theoretical proof. The conduction heat transfer is calculated with the equation as follows:

$$Q = \frac{kA(T2 - T1)}{d} \tag{4.1}$$

Q is the amount of heat transferred through the material, k is the thermal conductivity of the material, A is a cross-sectional area, T2 is the higher temperature, T1 is the colder temperature, and d is the thickness of the material. For aluminum, thermal conductivity is 237 W/mK; the aluminum heating block used for Direct Dry-LAMP in Chapter 3 determined its thickness and cross-sectional area to be 0.0508 m and 0.00158064 m^2, respectively. The alumninum block then must be heated from a room temperature of 25 ℃ to 61 ℃ to reach the appropriate temperature of the LAMP reaction; therefore, T2 is 334.15 K and T1 is 298.15 K. Inputting these measurements into equation 4.1 provides a final Q value of 433.4256 W.

Compared to conduction heat transfer, convection heat transfer can be calculated with the equation below.

$$Q = hA(T2 - T1) \tag{4.2}$$

In this equation, Q is convection heat transfer, h is the convective heat transfer coefficient of the process, A is the heat transfer area of the surface, T2 is the higher temperature, and T1 is the colder temperature. For forced convection of air, h is between 10 to 1000 W/m^2K, but for the purposes of the computation, it is assumed to be 25 W/m^2K. For better accuracy, we used the area of the location where the convection system is installed in the developed device, referenced in Chapter 4, which measured out to 0.0057552 m^2. As with conduction heat transfer, T2 is 334.15 K and T1 is 298.15 K. Based on these numbers, convection heat transfer through the air is 5.17968 W. The results show that convection heat transfer has a lower Q value than conduction heat transfer. Therefore, we can expect that less time is required to heat the former system to 61 ℃, rendering it the more energy-efficient choice.

4.3 Device Development

A convection-based device to run Direct Dry-LAMP was developed. The overall design of the developed device using Solidworks™ 2020 (Dassault Systems, Waltham, USA) is shown in Figure 4.1 (A). Its most significant difference from the device described in Chapter 3 is it combines the use of isothermal incubation and fluorescent detection. This developed device consists of two components – one heating block maintained at 95 ℃ for heat inactivation and the convection-based system with a transilluminator (470 nm light emitting diode, LED, arrays) as shown in Figure 4.1 (B). The real photograph of the developed device is shown in Figure 4.1 (C). For the fabrication of the heating block for heat inactivation, an aluminum heating block was machined to house four 1.5 mL tubes. The temperature of the heating block was maintained at 95 °C using two heating elements and three thermocouple sensors. For the convection-based system with real-time detection, a PTC Electric Fan Heater (24V 150W) and ESP32-CAM were used. A CANADUINO® 120° wide-angle camera module OV2640 for ESP32-CAM was used to widen the angle of view seen by the camera.

Real-time detection can be achieved through a smartphone with the assigned address for the internet. The air was maintained at 61 ℃ using one thermocouple sensor. All housing parts and fixtures were fabricated using an FDM 3D printer (Anycubic C, Commerce, USA) with polycarbonate filament unless specified. The transilluminator (470 nm light emitting diode, LED, arrays) consisted of two 14 × 2 LED arrays and was mounted on the sides of the convection-based system. An acrylic sheet window to block the wavelengths emitted by the LEDs, but not the intercalating dye, was placed on the top of the camera. Heating lids were added to the lid of each part, heat inactivation part and convection-based part. All components were controlled by an ESP32 microprocessor. The device is operated through the user interface using an LCD display

and push buttons. A DC power supply of 21–23V was used to power the device; 23V 6A is ideal. The specifications of the developed device is summarized in Table 4.1.

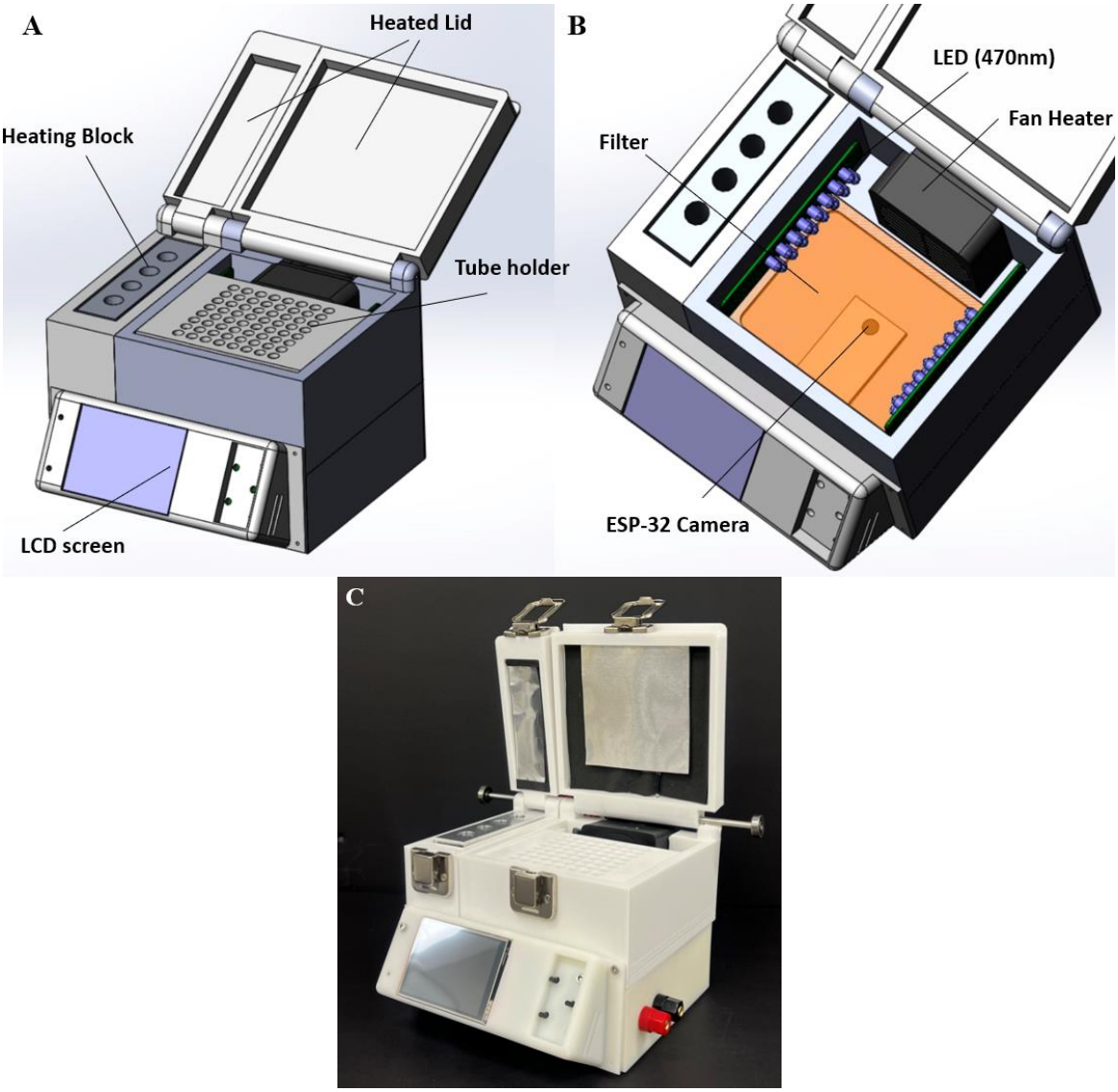

Figure 4.1. (A) The overall design of the developed device. (B) Convection system with real-time detection of the developed device. (C) Photographs of the fabricated device.

Table 4.1. Specifications of the convection-based device.

Specification	Parameter value
Aluminum heating block (Heat inactivation)	95 °C
Fan heater	24V, 150W
Cartridge heater	12V, 40W
Thermistor	100KΩ, accuracy ± 1%
LED	470 nm
LCD	2.8 inch, 320*240 (Pixel)
ESP32	2.4 GHz, 38 Pin, Micro USB
ESP32-CAM	2MP Camera
Heater Plate (Heated lid)	12V, 7W

4.4 Experimental Methods

The flow simulation was done with Solidworks™ 2016 (Dassault Systems, Waltham, USA) first to get more theoretical data, carried out at a total physical time of 600 seconds. An environment pressure of 101325 Pa and gravity of -9.81 m/s^2 in the y direction were applied. Only the convection-based part of the device was included in the flow simulation, and the dimensions are the same as the developed device. All tubes and the tube holder were eliminated in the flow simulation for simplification. The fan contributed an angular velocity of 250 rad/s and a volume heat source with a heat operation rate of 150 W was used. If the average temperature of the fluid (air) rose above 61 ℃, the heat source was rigged to turn off automatically, and if it dipped below 61 ℃, the heat source was set to turn on again. The specified materials include polycarbonate and nichrome solid material. The average temperature of the fluid (air) was calculated numerically, and the simulation of the average temperature of fluid was shown with a cut plot through the right surface. Iso-surface simulation with the range of 60 to 62 ℃ was obtained. Another two flow simulations were conducted to see how the average temperature of water in the tube changed inside an aluminum heating block maintained at 61 ℃ and surrounded by an air temperature of 61 ℃.

The simulation with the aluminum block was carried out for a total physical time of 600 seconds, and the simulation with the tube around the air was done for a total physical time of 1000 seconds.

For the performance test of the developed device, heating temperature measurements were conducted to check how well the temperature of 25 μL of water in each tube was maintained at 61 ℃. A multimeter (KAIWEETS, Shenzhen, China) with K-type thermocouple included was used, and the measurement uncertainty for the temperature was $\pm$1 ℃. Three holes were tested for the developed device. The temperature was recorded every 10 seconds for 40 minutes, and 2 ℃ was added to all the measured temperatures for the same reasoning presented in Chapter 3. The average temperature difference from 61 ℃ for all temperatures after 10 minutes was calculated. On average, the temperature of the tubes could reach around 61 ℃ for approximately 10 minutes.

To check the performance of the developed device, the liquid RT-LAMP reactions were prepared as previously described by Mohon *et al.* [54], except that the CFI dye was used instead. Liquid amplification control reactions were used with liquid SARS-CoV-2 reactions. For liquid SARS-CoV-2 reactions, water as a no template control (NTC) and Twist Biosciences synthetic RNA positive control were used. For liquid amplification control reactions, water as an NTC and previously extracted and frozen human total nucleic acid from NP swab were used. The liquid RT-LAMP reactions were incubated in the convection-based device for 50 minutes, and the results were interpreted using a blue light LED transilluminator. The results through the ESP32-CAM, which uses an amber filter, were captured with a smartphone every 1 minute. The same experiment was repeated simultaneously in CFX96 (Bio-Rad Laboratories Inc., Hercules, USA), and a LED transilluminator (MaestroGen Inc., Hsinchu City, China) was used to see the results. Each of the readings was compared between the developed device and CFX96 in the LED transilluminator (MaestroGen Inc., Hsinchu City, China).

4.5 Results

Figure 4.2 (A) shows that the average temperature of the fluid (air) continues to increase and reaches 60.501 ℃ after 117.298 s of physical time. Then, the heat source continues to turn on and off, and the average temperature of the air is maintained at about 61 ℃. Figure 4.2 (B) shows the temperature distribution after heating up to 61 ℃ when looking across the right plane, and it shows that the farther away from the heat source, the lower the temperature. Figure 4.2 (C) of the isometric view shows only the air temperature from 60 to 62 ℃, which is important for the LAMP reaction.

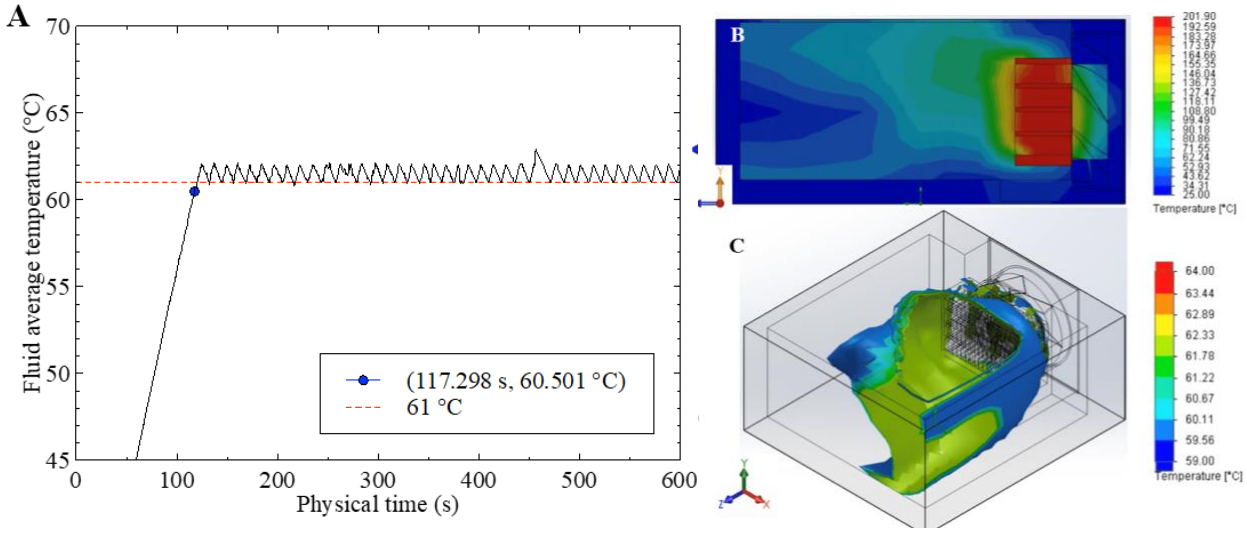

Figure 4.2. (A) The average temperature of the fluid (air) in flow simulation of the convection-based device in the graph and (B) with a cut plot through the right surface (C) Iso-surface simulation, which has the range of 60 to 62 ℃ with an isometric view.

Figure 4.3 (A) shows how the average temperature of water changed when the tube was in the 61 ℃ aluminum heating block at a physical time of 0 seconds, 60 seconds, 150 seconds, and

300 seconds, visually. The space between the tube and the aluminum heating block is air, and the water temperature in the tube rises after the air initially reaches 61 ℃. Figure 4.3 (B) shows the average temperature of the fluid (water) in the tube contained within the 61 ℃ aluminum heating block took 355.908 seconds of physical time to reach 60.506 ℃.

Figure 4.4 (A) shows how the average temperature of water changed when the tube was surrounded by 61 ℃ air at a physical time of 0 seconds, 100 seconds, 200 seconds, and 500 seconds, visually. When the tube was surrounded by 61 ℃ air, it required 615 seconds of physical time for the water temperature to reach 60.504 ℃, as shown in Figure 4.4 (B).

As seen by the camera, three spots from the tube holder were selected to measure the temperature during the LAMP reaction. Figure 4.5 (A) shows the temperature in the developed device during this reaction, which dropped sharply when the fan and the heat source were operated to maintain 61 ℃. The average temperature difference from 61 ℃ for all temperatures after 10 minutes was calculated and the results for each are as follows: 1.195 ℃, 0.775 ℃, and 1.237 ℃ for the first, second, and third spots of the developed device, with standard deviations of 0.816, 0.767, 1.633, respectively (Figure 4.5 B).

The results of the LAMP reaction were taken with an ESP32-CAM after 1 minute and 50 minutes before being captured by a smartphone. The first row is a negative, positive, negative, and positive sample with a strip of control lyophilized reaction. The second row is a negative, positive, negative, and positive sample with a strip of SARS-CoV-2 lyophilized reaction. As shown in Figure 4.6, the results from the SARS-CoV-2 lyophilized reaction can be easily interpreted, but the results with the control lyophilized reaction were unclear and difficult to interpret.

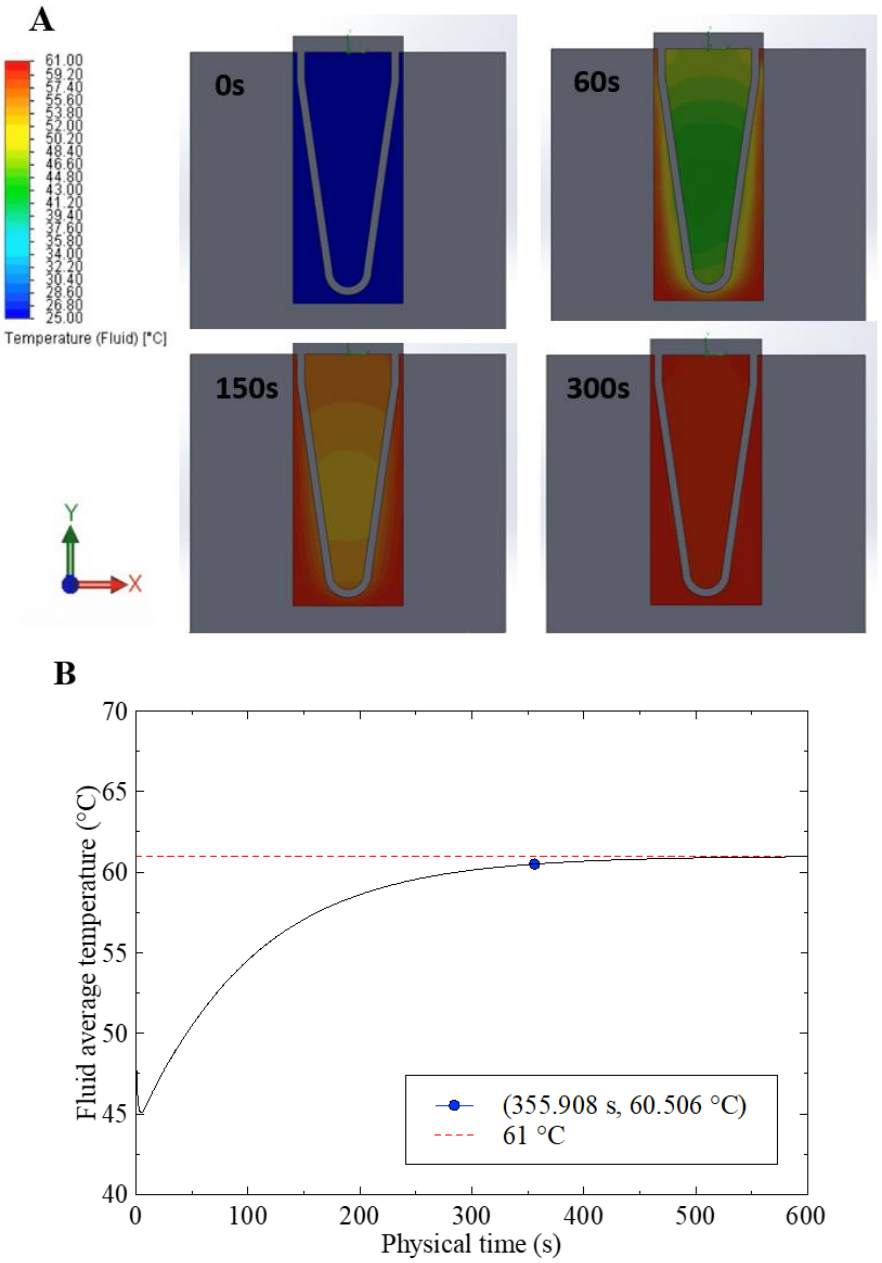

Figure 4.3. (A) Visual simulation of the average temperature of flow in the tube in 61 ℃ aluminum heating block at a physical time of 0 s, 60 s, 150 s, and 300 s with a front view. (B) The average temperature of water in the tube in the 61 ℃ aluminum heating block.

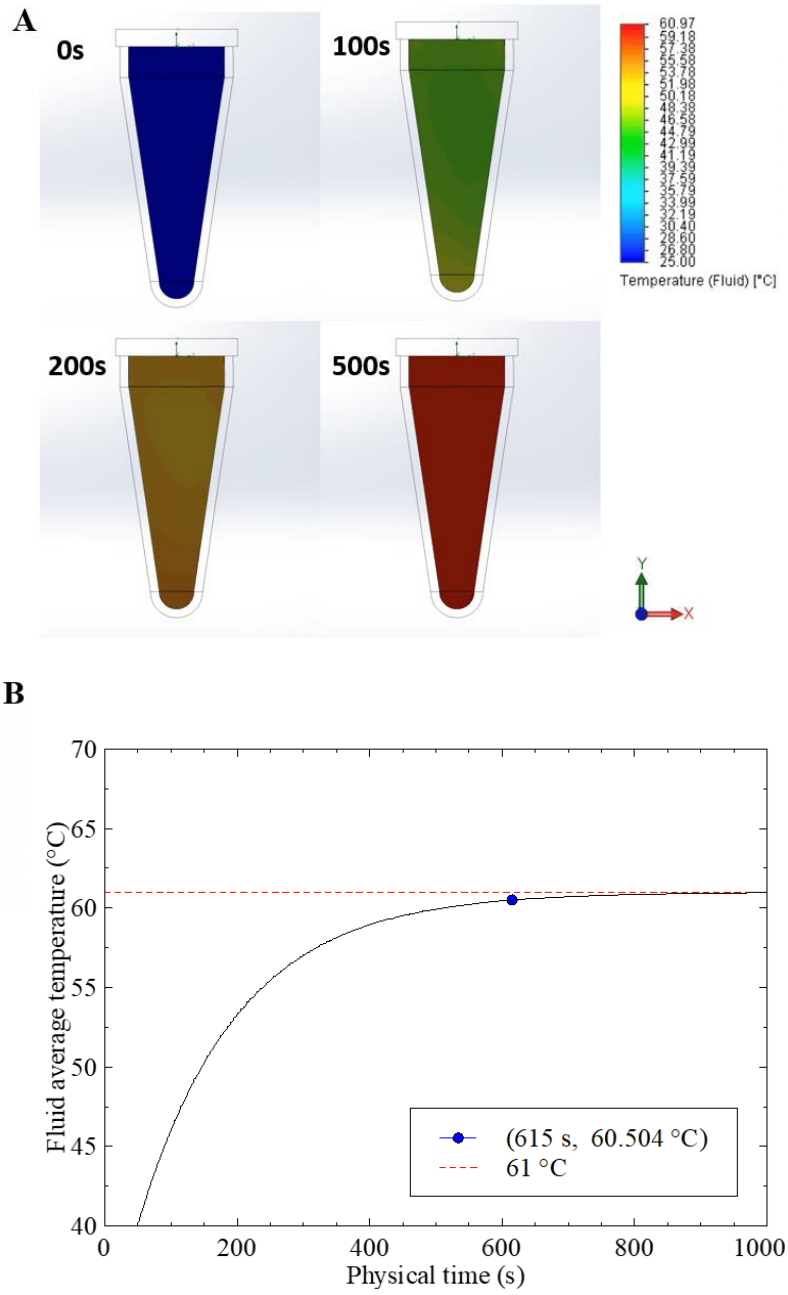

Figure 4.4. (A) Visual simulation of the average temperature of flow in the tube surrounded by 61 ℃ air at a physical time of 0 s, 100 s, 200 s, and 500 s with a front view. (B) The average temperature of water in the tube surrounded by 61 ℃ air.

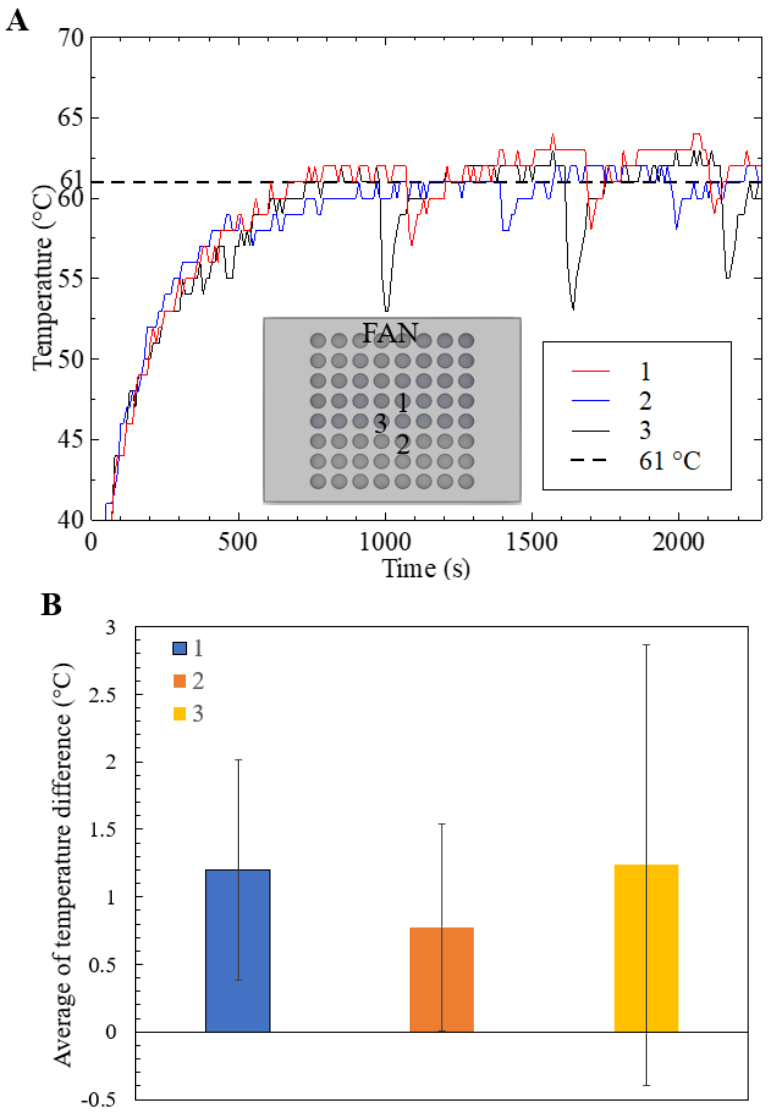

Figure 4.5. (A) The heating temperature of LAMP reaction on the convection-based developed device. (B) Average of the temperature difference from 61 ℃.

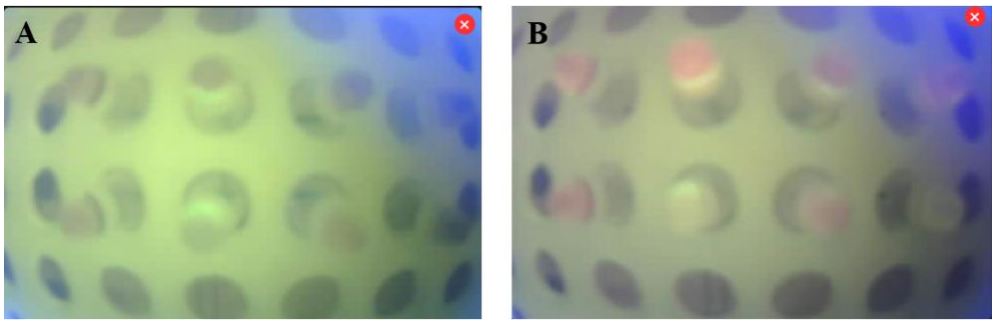

Figure 4.6. Visual results of LAMP reaction taken with ESP32-CAM camera after (A) 1 minute and (B) 50 minutes from the developed device.

The results using CFX96 were taken with the developed device; Figure 4.7 (A) shows that the correct results can be visually interpreted. The comparison of the LAMP reaction between CFX96 and the developed device was done using the commercial LED transilluminator, as shown in Figure 4.7 (B). The strip in the first row and first column shows the results of the SARS-CoV-2 lyophilized reaction done by CFX96, and the second column in the first row shows the results of the control lyophilized reaction done by CFX96. The first column in the second row and the second column in the second row show the results of the developed device using SARS-CoV-2 lyophilized reaction and control lyophilized reaction, respectively. The relative fluorescence unit (RFU) graph according to the cycle from CFX96 is shown in Figure 4.7 (C), and the fluorescent using control lyophilized reaction was amplified approximately ten cycles after the fluorescent amplification of the SARS-CoV-2 lyophilized reaction.

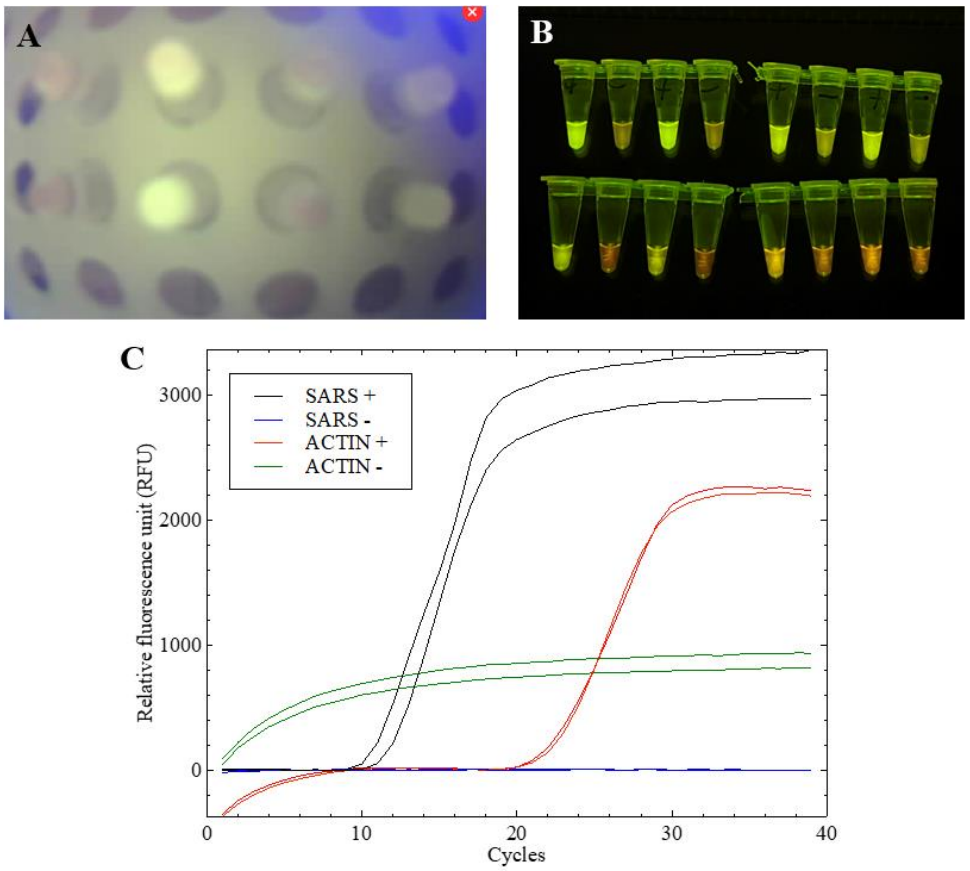

Figure 4.7. (A) Visual results of LAMP reaction from CFX96 taken with ESP32-CAM after 50 minutes under the developed device. (B) Comparison of LAMP reaction between CFX96 (1st row) and the developed device (2nd row) under commercial LED transilluminator. (C) RFU graph from CFX96.

4.6 Discussion and Challenges

The developed device for executing Direct Dry-LAMP used a convection-based system, rather than a conventional conduction-based, as well as an aluminum heating block for LAMP reaction. Theoretical calculation and simulation confirmed that the average temperature of the air could reach 61 ℃ quickly, and the temperature can remain stable. This can help to use power when operating the device efficiently. However, the average temperature calculation of the air in the

simulation included air near a heat source that has a high temperature and a low temperature of air that was not affected by the heat source. A temperature was unable to be taken from a specific location to control the heat source subsequently, therefore, it is expected that the actual result may vary from the simulation findings. The results of LAMP reaction using the developed device enabled real-time detection with a smartphone through a camera installed in the equipment.

Development of this device with a convection-based system is at stage 1 and has several limitations which need to be addressed more. First, the results of the flow simulation which showed the average temperature of water in the tube inside an aluminum heating block and surrounded by air may differ from the actual results. The simulation used the tube fully filled with water, but in actual experiments, there was a mixture of fluids, and the tube was not completely filled as well. Second, the insulation function of the developed device needs improvement to maintain stable air temperature optimally. Polycarbonate is a material that can give some degree of thermal insulation, but it is necessary to add another insulation material inside of the developed device for better performance. Third, LAMP reactions showed poor results with the developed device. The reason was shown in the heating temperature measurements, which demonstrated some drop-down points of the temperature during the LAMP reactions. This is because the heat source and the fan are set to turn on together when the temperature of the internal air needs to be adjusted, and the fan that emits cold wind affects the temperature of the air first before the temperature of the heat source rises. This limitation is expected to be solved by setting the heat source to turn on before the fan. Fourth, there was difficulty obtaining accurate measurements of the air temperature inside of the device because the heat source was controlled by relying on a single sensor. This drawback necessitates several more sensitive and accurate sensors to measure the temperature of the air.

Lastly, the quality of the visual results of more samples simultaneously can be further improved by using a higher-resolution camera that is also placed farther from the tubes.

4.7 Summary

The convection-base device for Direct Dry-LAMP was developed for energy efficiency beyond the aluminum heating block, which was generally used to proceed with LAMP. Real-time detection was combined with the developed device. In theory, convective heat transfer was calculated to be more energy efficient than conductive heat transfer, and flow simulation showed how fast the temperature of the air increased and maintained at 61 ℃. LAMP reactions were done with the developed device and compared to commercially available instruments. The results of LAMP reactions using the developed device were taken with the installed camera. Since the convection-based device is in its early stages of development, it has still shown many limitations.

Chapter 5: Conclusion

5.1 Concluding Remarks

Saliva-Dry LAMP, a rapid, near-patient, and saliva-based diagnostic method for COVID-19, was developed with a low-cost and portable all-in-one device to overcome the shortcomings of conventional RT-PCR-based detection method using nasopharyngeal samples. This method showed excellent positive and negative agreement compared to two different reference standard RT-PCR tests with a rapid detection time. The LOD of the developed device for Saliva-Dry LAMP was comparable to the LOD of similar commercially available instruments. There are limitations of Saliva-Dry LAMP as well, which include subjectively analyzed visual results, the requirement of the cold chain, and the reliance on the RNA extraction process. The developed device was not used for clinical validation experiments and is still not battery driven.

To overcome the limitations of Saliva-Dry LAMP, Direct Dry-LAMP was developed to replace RNA extraction as the heat inactivation step. It significantly reduced the total detection time with an excellent positive and negative agreement in clinical validation experiments. The portable and battery-driven device for Direct Dry-LAMP was also developed. As this developed device was built to use batteries, it has the potential to be especially valuable in resource-limited regions. The developed device reduces the capital equipment cost compared to commercially available instruments and gives objective interpretation with the developed app. However, the LOD experiments of Direct Dry-LAMP showed better results on commercially available instruments than the developed device because of the performance of the aluminum block. In addition, the developed app needs further research to increase the accuracy of analysis of visual results. Real-time detection was not available with the developed device.

A convection-based device to perform Direct Dry-LAMP was later developed, and the convection system was combined with real-time detection. Convection heat transfer is theoretically more energy efficient than conduction heat transfer. The flow simulation was done to see how fast the convection system increased the air temperature and how consistently it maintained the increased temperature. LAMP reactions were performed with the developed convection-based device, but there were several limitations because the development of the device is still currently in early stages.

Overall, Saliva-Dry LAMP and Direct Dry-LAMP are rapid, near-patient alternative diagnostic methods for the detection of SARS-CoV-2 offering simpler steps, ease of use, and accurate results. The portable and low-cost devices were customized for each method. For example, its use of a battery would allow it to be operated in resource-limited regions, it can give objective interpretation with the developed app, and be combined with real-time detection as well. When the temperature of the LAMP reaction and the wavelength of the transilluminator are changed, these methods and devices have the potential to be used to diagnose other infectious diseases. Therefore, these two diagnostic methods could become a key player in effectively and accurately detecting infections to limit the spread of diseases like COVID-19.

5.2 Significance of Contributions

The development of rapid diagnostic methods for COVID-19 with high accuracy results has emerged as a decisive way to limit the disease. Currently, the standard diagnostic method is RT-PCR, but there are limitations such as long detection time and sophisticated equipment. These limitations were addressed in this study, leading to the development of new LAMP-based

diagnostic methods (Saliva-Dry LAMP and Direct Dry-LAMP). The contribution and the novelty of the research in this thesis are as follows:

1. Low-cost and portable all-in-one devices were developed for each method.
2. Both Saliva Dry-LAMP and Direct Dry-LAMP showed rapid detection time compared to reference RT-PCR.
3. Clinical validation and LOD experiment were done to confirm the performance of each method and the developed devices.
4. More rapid detection time was obtained in Direct Dry-LAMP with heat inactivation step without RNA extraction step.
5. The developed device for Direct Dry-LAMP can be executed with chargeable batteries and a developed app.
6. Developed app can interpret the results of infection objectively.
7. Energy efficient convection-based LAMP device was developed through the verification of flow simulation.
8. Real-time detection was combined with a convection-based LAMP device.

5.3 Future works

Workflows developed to diagnose COVID-19 (Saliva-Dry LAMP and Direct Dry-LAMP) included a process that users can easily follow with minimal training and have shown rapid and accurate diagnostic results. These diagnostic methods using customized devices could become the primary method of diagnosing infectious diseases in countries with insufficient resources, along with the following two developments. First, app development should proceed further so that more accurate results can be objectively analyzed. Second, the device should be able to operate for a

prolonged period using batteries by consuming power efficiently. This advantage benefits using multiplex testing for other infectious diseases, especially for countries vulnerable to COVID-19. Multiplex testing can be performed when different colours of LEDs are simultaneously present in the transilluminator. Finally, research on the convection-based device for the LAMP reaction can promote further advances in random access systems. The convection-based LAMP system theoretically would require minimal time to heat up to a specific temperature. As explored in this study, these two developed diagnostic systems have demonstrated the potential to provide efficient and accurate results by preventing the spread of not only COVID-19 but also other infectious diseases which may arise in the future.

Bibliography

[1] F. Ndaïrou, I. Area, J. J. Nieto, and D. F. M. Torres, "Mathematical modeling of COVID-19 transmission dynamics with a case study of Wuhan," *Chaos Solitons Fractals*, vol. 135, p. 109846, Jun. 2020, doi: 10.1016/j.chaos.2020.109846.

[2] M. A. Cristina Huergo and N. T. Kim Thanh, "Current advances in the detection of COVID-19 and evaluation of the humoral response," *Analyst*, vol. 146, no. 2, pp. 382–402, 2021, doi: 10.1039/D0AN01686A.

[3] D. C. Dinesh *et al.*, "Structural basis of RNA recognition by the SARS-CoV-2 nucleocapsid phosphoprotein," *PLOS Pathog.*, vol. 16, no. 12, p. e1009100, Dec. 2020, doi: 10.1371/journal.ppat.1009100.

[4] M. Yüce, E. Filiztekin, and K. G. Özkaya, "COVID-19 diagnosis —A review of current methods," *Biosens. Bioelectron.*, vol. 172, p. 112752, Jan. 2021, doi: 10.1016/j.bios.2020.112752.

[5] M.-Y. Wang, R. Zhao, L.-J. Gao, X.-F. Gao, D.-P. Wang, and J.-M. Cao, "SARS-CoV-2: Structure, Biology, and Structure-Based Therapeutics Development," *Front. Cell. Infect. Microbiol.*, vol. 10, 2020, Accessed: Jul. 14, 2022. [Online]. Available: https://www.frontiersin.org/articles/10.3389/fcimb.2020.587269

[6] J. Zhang, T. Xiao, Y. Cai, and B. Chen, "Structure of SARS-CoV-2 spike protein," *Curr. Opin. Virol.*, vol. 50, pp. 173–182, Oct. 2021, doi: 10.1016/j.coviro.2021.08.010.

[7] S. Rosales-Mendoza, V. A. Márquez-Escobar, O. González-Ortega, R. Nieto-Gómez, and J. I. Arévalo-Villalobos, "What Does Plant-Based Vaccine Technology Offer to the Fight against COVID-19?," *Vaccines*, vol. 8, no. 2, Art. no. 2, Jun. 2020, doi: 10.3390/vaccines8020183.

[8] Y. Alimohamadi, M. Sepandi, M. Taghdir, and H. Hosamirudsari, "Determine the most common clinical symptoms in COVID-19 patients: a systematic review and meta-analysis," *J. Prev. Med. Hyg.*, vol. 61, no. 3, Art. no. 3, Aug. 2020, doi: 10.15167/2421-4248/jpmh2020.61.3.1530.

[9] Z. Gao *et al.*, "A systematic review of asymptomatic infections with COVID-19," *J. Microbiol. Immunol. Infect.*, vol. 54, no. 1, pp. 12–16, Feb. 2021, doi: 10.1016/j.jmii.2020.05.001.

[10] P. Rai, B. K. Kumar, V. K. Deekshit, I. Karunasagar, and I. Karunasagar, “Detection technologies and recent developments in the diagnosis of COVID-19 infection,” *Appl. Microbiol. Biotechnol.*, vol. 105, no. 2, pp. 441–455, Jan. 2021, doi: 10.1007/s00253-020-11061-5.

[11] L. M. Bui *et al.*, “Recent findings and applications of biomedical engineering for COVID-19 diagnosis: a critical review,” *Bioengineered*, vol. 12, no. 1, pp. 8594–8613, Jan. 2021, doi: 10.1080/21655979.2021.1987821.

[12] C. H. Chau, J. D. Strope, and W. D. Figg, “COVID-19 Clinical Diagnostics and Testing Technology,” *Pharmacother. J. Hum. Pharmacol. Drug Ther.*, vol. 40, no. 8, pp. 857–868, 2020, doi: 10.1002/phar.2439.

[13] I. El Jaddaoui *et al.*, “A review on current diagnostic techniques for COVID-19,” *Expert Rev. Mol. Diagn.*, vol. 21, no. 2, pp. 141–160, Feb. 2021, doi: 10.1080/14737159.2021.1886927.

[14] B. Giri, S. Pandey, R. Shrestha, K. Pokharel, F. S. Ligler, and B. B. Neupane, “Review of analytical performance of COVID-19 detection methods,” *Anal. Bioanal. Chem.*, vol. 413, no. 1, pp. 35–48, Jan. 2021, doi: 10.1007/s00216-020-02889-x.

[15] R. T. Aruleba *et al.*, “COVID-19 Diagnosis: A Review of Rapid Antigen, RT-PCR and Artificial Intelligence Methods,” *Bioengineering*, vol. 9, no. 4, Art. no. 4, Apr. 2022, doi: 10.3390/bioengineering9040153.

[16] M. F. Khalid *et al.*, “Performance of Rapid Antigen Tests for COVID-19 Diagnosis: A Systematic Review and Meta-Analysis,” *Diagnostics*, vol. 12, no. 1, Art. no. 1, Jan. 2022, doi: 10.3390/diagnostics12010110.

[17] A. M. Indelicato, Z. H. Mohamed, M. J. Dewan, and C. P. Morley, “Rapid Antigen Test Sensitivity for Asymptomatic COVID-19 Screening,” *Primer Peer-Rev. Rep. Med. Educ. Res.*, vol. 6, p. 18, Jun. 2022, doi: 10.22454/PRiMER.2022.276354.

[18] K. Mullis, F. Faloona, S. Scharf, R. Saiki, G. Horn, and H. Erlich, “Specific Enzymatic Amplification of DNA In Vitro: The Polymerase Chain Reaction,” *Cold Spring Harb. Symp. Quant. Biol.*, vol. 51, pp. 263–273, Jan. 1986, doi: 10.1101/SQB.1986.051.01.032.

[19] O. Filchakova, D. Dossym, A. Ilyas, T. Kuanysheva, A. Abdizhamil, and R. Bukasov, “Review of COVID-19 testing and diagnostic methods,” *Talanta*, vol. 244, p. 123409, Jul. 2022, doi: 10.1016/j.talanta.2022.123409.

[20] E. Sheikhzadeh, S. Eissa, A. Ismail, and M. Zourob, “Diagnostic techniques for COVID-19 and new developments,” *Talanta*, vol. 220, p. 121392, Dec. 2020, doi: 10.1016/j.talanta.2020.121392.

[21] A. Afzal, “Molecular diagnostic technologies for COVID-19: Limitations and challenges,” *J. Adv. Res.*, vol. 26, pp. 149–159, Nov. 2020, doi: 10.1016/j.jare.2020.08.002.

[22] J. Singh, N. Birbian, S. Sinha, and A. Goswami, “A critical review on PCR, its types and applications,” *Int. J. Adv. Res. Biol. Sci.*, vol. 1, no. 7, pp. 65–80, Oct. 2014.

[23] S. N. Rao, D. Manissero, V. R. Steele, and J. Pareja, “A Systematic Review of the Clinical Utility of Cycle Threshold Values in the Context of COVID-19,” *Infect. Dis. Ther.*, vol. 9, no. 3, pp. 573–586, Sep. 2020, doi: 10.1007/s40121-020-00324-3.

[24] N. Shoaib *et al.*, “Factors associated with cycle threshold values (Ct-values) of SARS-CoV2-rRT-PCR,” *Mol. Biol. Rep.*, vol. 49, no. 5, pp. 4101–4106, May 2022, doi: 10.1007/s11033-022-07360-x.

[25] W. F. Sule and D. O. Oluwayelu, “Real-time RT-PCR for COVID-19 diagnosis: challenges and prospects,” *Pan Afr. Med. J.*, vol. 35, no. Suppl 2, p. 121, Jul. 2020, doi: 10.11604/pamj.supp.2020.35.24258.

[26] C. B. F. Vogels *et al.*, “Analytical sensitivity and efficiency comparisons of SARS-CoV-2 RT–qPCR primer–probe sets,” *Nat. Microbiol.*, vol. 5, no. 10, Art. no. 10, Oct. 2020, doi: 10.1038/s41564-020-0761-6.

[27] H. A. Gietema *et al.*, “CT in relation to RT-PCR in diagnosing COVID-19 in The Netherlands: A prospective study,” *PLOS ONE*, vol. 15, no. 7, p. e0235844, Jul. 2020, doi: 10.1371/journal.pone.0235844.

[28] A. Tahamtan and A. Ardebili, “Real-time RT-PCR in COVID-19 detection: issues affecting the results,” *Expert Rev. Mol. Diagn.*, vol. 20, no. 5, pp. 453–454, May 2020, doi: 10.1080/14737159.2020.1757437.

[29] M. Pradhan *et al.*, “COVID-19: clinical presentation and detection methods,” *J. Immunoassay Immunochem.*, vol. 43, no. 1, p. 1951291, Jan. 2022, doi: 10.1080/15321819.2021.1951291.

[30] M. Teymouri *et al.*, “Recent advances and challenges of RT-PCR tests for the diagnosis of COVID-19,” *Pathol. - Res. Pract.*, vol. 221, p. 153443, May 2021, doi: 10.1016/j.prp.2021.153443.

[31] H. Tombuloglu, H. Sabit, E. Al-Suhaimi, R. A. Jindan, and K. R. Alkharsah, “Development of multiplex real-time RT-PCR assay for the detection of SARS-CoV-2,” *PLOS ONE*, vol. 16, no. 4, p. e0250942, Apr. 2021, doi: 10.1371/journal.pone.0250942.

[32] M. M. Gibani *et al.*, “Assessing a novel, lab-free, point-of-care test for SARS-CoV-2 (CovidNudge): a diagnostic accuracy study,” *Lancet Microbe*, vol. 1, no. 7, pp. e300–e307, Nov. 2020, doi: 10.1016/S2666-5247(20)30121-X.

[33] J. Caffry *et al.*, “The QuantuMDx Q-POC™ SARS-CoV-2 RT-PCR assay for rapid detection of COVID-19 at point-of-care: preliminary evaluation of a novel technology.” medRxiv, p. 2021.07.12.21260119, Jul. 14, 2021. doi: 10.1101/2021.07.12.21260119.

[34] A. Renzoni *et al.*, “Analytical Evaluation of Visby Medical RT-PCR Portable Device for Rapid Detection of SARS-CoV-2,” *Diagnostics*, vol. 11, no. 5, Art. no. 5, May 2021, doi: 10.3390/diagnostics11050813.

[35] C.-L. Perng *et al.*, “Novel rapid identification of Severe Acute Respiratory Syndrome Coronavirus 2 (SARS-CoV-2) by real-time RT-PCR using BD Max Open System in Taiwan,” *PeerJ*, vol. 8, p. e9318, Jun. 2020, doi: 10.7717/peerj.9318.

[36] H. M. Zowawi *et al.*, “Portable RT-PCR System: a Rapid and Scalable Diagnostic Tool for COVID-19 Testing,” *J. Clin. Microbiol.*, vol. 59, no. 5, pp. e03004-20, Apr. 2021, doi: 10.1128/JCM.03004-20.

[37] D. Thompson and Y. Lei, “Mini review: Recent progress in RT-LAMP enabled COVID-19 detection,” *Sens. Actuators Rep.*, vol. 2, no. 1, p. 100017, Nov. 2020, doi: 10.1016/j.snr.2020.100017.

[38] L. E. Lamb, S. N. Bartolone, E. Ward, and M. B. Chancellor, “Rapid Detection of Novel Coronavirus (COVID-19) by Reverse Transcription-Loop-Mediated Isothermal Amplification.” medRxiv, p. 2020.02.19.20025155, Feb. 24, 2020. doi: 10.1101/2020.02.19.20025155.

[39] R. Augustine *et al.*, “Loop-Mediated Isothermal Amplification (LAMP): A Rapid, Sensitive, Specific, and Cost-Effective Point-of-Care Test for Coronaviruses in the Context of COVID-19 Pandemic,” *Biology*, vol. 9, no. 8, Art. no. 8, Aug. 2020, doi: 10.3390/biology9080182.

[40] J. Abduljalil, “Laboratory diagnosis of SARS-CoV-2: available approaches and limitations,” *New Microbes New Infect.*, vol. 36, p. 100713, Jun. 2020, doi: 10.1016/j.nmni.2020.100713.

[41] M. Parida, S. Sannarangaiah, P. K. Dash, P. V. L. Rao, and K. Morita, "Loop mediated isothermal amplification (LAMP): a new generation of innovative gene amplification technique; perspectives in clinical diagnosis of infectious diseases," *Rev. Med. Virol.*, vol. 18, no. 6, pp. 407–421, 2008, doi: 10.1002/rmv.593.

[42] M. Xu *et al.*, "COVID-19 diagnostic testing: Technology perspective," *Clin. Transl. Med.*, vol. 10, no. 4, p. e158, 2020, doi: 10.1002/ctm2.158.

[43] A. Ge *et al.*, "A Palm Germ-Radar (PaGeR) for rapid and simple COVID-19 detection by reverse transcription loop-mediated isothermal amplification (RT-LAMP)," *Biosens. Bioelectron.*, vol. 200, p. 113925, Mar. 2022, doi: 10.1016/j.bios.2021.113925.

[44] Z. Ali *et al.*, "iSCAN: An RT-LAMP-coupled CRISPR-Cas12 module for rapid, sensitive detection of SARS-CoV-2," *Virus Res.*, vol. 288, p. 198129, Oct. 2020, doi: 10.1016/j.virusres.2020.198129.

[45] M. Rezaei *et al.*, "A Portable RT-LAMP/CRISPR Machine for Rapid COVID-19 Screening," *Biosensors*, vol. 11, no. 10, Art. no. 10, Oct. 2021, doi: 10.3390/bios11100369.

[46] J. Rödel *et al.*, "Use of the variplex™ SARS-CoV-2 RT-LAMP as a rapid molecular assay to complement RT-PCR for COVID-19 diagnosis," *J. Clin. Virol.*, vol. 132, p. 104616, Nov. 2020, doi: 10.1016/j.jcv.2020.104616.

[47] R. Egerer, B. Edel, B. Löffler, A. Henke, and J. Rödel, "Performance of the RT-LAMP-based eazyplex® SARS-CoV-2 as a novel rapid diagnostic test," *J. Clin. Virol.*, vol. 138, p. 104817, May 2021, doi: 10.1016/j.jcv.2021.104817.

[48] M. El-Tholoth, H. H. Bau, and J. Song, "A Single and Two-Stage, Closed-Tube, Molecular Test for the 2019 Novel Coronavirus (COVID-19) at Home, Clinic, and Points of Entry," *ChemRxiv*, p. 10.26434/chemrxiv.11860137.v1, Feb. 2020, doi: 10.26434/chemrxiv.11860137.v1.

[49] D. Wang, "One-pot Detection of COVID-19 with Real-time Reverse-transcription Loop-mediated Isothermal Amplification (RT-LAMP) Assay and Visual RT-LAMP Assay." bioRxiv, p. 2020.04.21.052530, Apr. 22, 2020. doi: 10.1101/2020.04.21.052530.

[50] J. Joung *et al.*, "Point-of-care testing for COVID-19 using SHERLOCK diagnostics." medRxiv, p. 2020.05.04.20091231, May 08, 2020. doi: 10.1101/2020.05.04.20091231.

[51] B. M. Berenger *et al.*, "Saliva collected in universal transport media is an effective, simple and high-volume amenable method to detect SARS-CoV-2," *Clin. Microbiol. Infect.*, vol. 27, no. 4, pp. 656–657, Apr. 2021, doi: 10.1016/j.cmi.2020.10.035.

[52] A. L. Wyllie *et al.*, “Saliva or Nasopharyngeal Swab Specimens for Detection of SARS-CoV-2,” *N. Engl. J. Med.*, vol. 383, no. 13, pp. 1283–1286, Sep. 2020, doi: 10.1056/NEJMc2016359.

[53] K. Zainabadi *et al.*, “A novel method for extracting nucleic acids from dried blood spots for ultrasensitive detection of low-density Plasmodium falciparum and Plasmodium vivax infections,” *Malar. J.*, vol. 16, no. 1, p. 377, Sep. 2017, doi: 10.1186/s12936-017-2025-3.

[54] A. N. Mohon *et al.*, “Optimization and clinical validation of dual-target RT-LAMP for SARS-CoV-2,” *J. Virol. Methods*, vol. 286, p. 113972, Dec. 2020, doi: 10.1016/j.jviromet.2020.113972.

[55] N. B. Toppings *et al.*, “A rapid near-patient detection system for SARS-CoV-2 using saliva,” *Sci. Rep.*, vol. 11, no. 1, Art. no. 1, Jun. 2021, doi: 10.1038/s41598-021-92677-z.

[56] J. W. Benzine *et al.*, “Molecular Diagnostic Field Test for Point-of-Care Detection of Ebola Virus Directly From Blood,” *J. Infect. Dis.*, vol. 214, no. suppl_3, pp. S234–S242, Oct. 2016, doi: 10.1093/infdis/jiw330.

[57] Centers for Disease Control and Prevention, “CDC 2019-Novel Coronavirus (2019-nCoV) Real-Time RT-PCR Diagnostic Panel,” 2020, Accessed: Jul. 25, 2022. [Online]. Available: https://pesquisa.bvsalud.org/global-literature-on-novel-coronavirus-2019-ncov/resource/pt/grc-739806

[58] K. Pabbaraju *et al.*, “Development and validation of RT-PCR assays for testing for SARS-CoV-2,” *Off. J. Assoc. Med. Microbiol. Infect. Dis. Can.*, vol. 6, no. 1, pp. 16–22, May 2021, doi: 10.3138/jammi-2020-0026.

[59] F. Lagerlof and C. Dawes, “The Volume of Saliva in the Mouth Before and After Swallowing,” *J. Dent. Res.*, vol. 63, no. 5, pp. 618–621, May 1984, doi: 10.1177/00220345840630050201.

[60] L. Bokelmann *et al.*, “Point-of-care bulk testing for SARS-CoV-2 by combining hybridization capture with improved colorimetric LAMP,” *Nat. Commun.*, vol. 12, no. 1, Art. no. 1, Mar. 2021, doi: 10.1038/s41467-021-21627-0.

[61] A. Gamble, R. J. Fischer, D. H. Morris, C. K. Yinda, V. J. Munster, and J. O. Lloyd-Smith, “Heat-Treated Virus Inactivation Rate Depends Strongly on Treatment Procedure: Illustration with SARS-CoV-2,” *Appl. Environ. Microbiol.*, vol. 87, no. 19, pp. e00314-21, Sep. 2021, doi: 10.1128/AEM.00314-21.

[62] I. Smyrlaki *et al.*, “Massive and rapid COVID-19 testing is feasible by extraction-free SARS-CoV-2 RT-PCR,” *Nat. Commun.*, vol. 11, no. 1, Art. no. 1, Sep. 2020, doi: 10.1038/s41467-020-18611-5.

[63] J. Burton *et al.*, “The effect of heat-treatment on SARS-CoV-2 viability and detection,” *J. Virol. Methods*, vol. 290, p. 114087, Apr. 2021, doi: 10.1016/j.jviromet.2021.114087.

[64] C. Batéjat, Q. Grassin, J.-C. Manuguerra, and I. Leclercq, “Heat inactivation of the severe acute respiratory syndrome coronavirus 2,” *J. Biosaf. Biosecurity*, vol. 3, no. 1, pp. 1–3, Jun. 2021, doi: 10.1016/j.jobb.2020.12.001.

[65] J. Singleton *et al.*, “Electricity-Free Amplification and Detection for Molecular Point-of-Care Diagnosis of HIV-1,” *PLOS ONE*, vol. 9, no. 11, p. e113693, Nov. 2014, doi: 10.1371/journal.pone.0113693.

[66] V. M. Corman *et al.*, “Detection of 2019 novel coronavirus (2019-nCoV) by real-time RT-PCR,” *Eurosurveillance*, vol. 25, no. 3, p. 2000045, Jan. 2020, doi: 10.2807/1560-7917.ES.2020.25.3.2000045.

APPENDIX A. Arduino Code For Convection-based Device

The Arduino code to execute the convection-based device in Chapter 4 is shown as follows:

```
// Include servo software
#include <ESP32_Servo.h>

// Include Adafruit Graphics Library (to be used with ST7735 display)
#include <Adafruit_GFX.h> // Core graphics library
#include <Fonts/FreeSans9pt7b.h>
#include <Adafruit_ILI9341.h>
#include <SPI.h>

#include <WebServer.h>
#include <ESPmDNS.h>

#include <biobox_ble.h>

// Wifi AP Setup
const char *ssid = "ESP32_ABL_NET";
const char *password = "password";

// Define pin designations
#define HEATER_PIN 13 //Heating Block
#define HEATER_PIN2 12 //Convection
#define LED_ARRAY_PIN 22
#define LID_PIN 14 //heatingblock
#define LID_PIN2 27 //Convection
#define SERVO_PIN 25
#define TEMP1_SENSOR_PIN 39
#define TEMP2_SENSOR_PIN 36
#define TEMP3_SENSOR_PIN 35
#define TEMP4_SENSOR_PIN 34 // Air sensor
#define TEMP5_SENSOR_PIN 32 //HeatingBlock Lid
#define TEMP6_SENSOR_PIN 33 //Convection Lid
#define TFT_DC 2
#define TFT_RST -1
#define TFT_CS 5
#define UP_PIN 17
#define DOWN_PIN 16
#define OK_PIN 15

#define N_BIOBOX 1
#define Y_BIOBOX 2

/**
 * Data Structs & Enums
```

```
 */
struct StatusMessage
{
   String message;
   short colour;
};

struct IoState
{
   bool heaterEnabled;
   bool heaterActive;
   bool heaterEnabled2;
   bool heaterActive2;
   bool heaterEnabled3;
   bool heaterActive3;
   bool heaterEnabled4;
   bool heaterActive4;
   bool ledArrayEnabled;
   int motorPower;
   double currentTemp;
   unsigned long lastTempCheck;
   double currentTemp2;
   unsigned long lastTempCheck2;
   double currentTemp3;
   unsigned long lastTempCheck3;
   double currentTemp4;
   unsigned long lastTempCheck4;
};

struct Timer
{
   unsigned long currentTime;
   unsigned long lastTimerTick;
   unsigned long motorTimer;
   unsigned long ledArrayTimer;
   unsigned long heaterTimer;
   unsigned long heaterTimer2;
   unsigned long heaterTimer3;
   unsigned long heaterTimer4;
};

struct ButtonsPressed
{
   bool wasUpPressed;
   bool wasDownPressed;
   bool wasOkPressed;
   unsigned long lastInterruptTime;
};

enum Controls
{
   Heater = 0,
   LedArray = 1,
   Motor = 2,
   Heater2 = 3,
   Heater3 = 4,
```

```
    Heater4 = 5
};

/**
 * Globals
 */
struct StatusMessage tftStatus = {
    "Initializing...",
    0x057F};

struct IoState ioState;
struct ButtonsPressed buttonsPressed;
struct Timer timer;
unsigned long screenRefresh = 0;

/*
 * MotorController
 */
class MotorController
{
private:
    Servo servo;
    int power = 0;
    int ms = 1500;
    int pin;
    void ease();
    unsigned long lastIncrementTime;

public:
    MotorController(int pin);
    ~MotorController();
    void setPower(int power);
    int getPower();
    void run();
};

MotorController::MotorController(int pin)
{
    this->pin = pin;
    servo.attach(pin);
    servo.writeMicroseconds(ms);
}

MotorController::~MotorController()
{
}

int MotorController::getPower()
{
    return power;
}

void MotorController::setPower(int power)
{
    this->power = constrain(power, 0, 100);
}
```

```
void MotorController::run()
{
   this->ease();
   servo.writeMicroseconds(this->ms);
}

void MotorController::ease()
{
   int finalMs = map(power, 0, 100, 1500, 1600);
   if (finalMs < this->ms)
   {
      if (millis() - this->lastIncrementTime > 20)
      {
         this->ms -= 1;
         this->lastIncrementTime = millis();
      }
   }
   else if (finalMs > this->ms)
   {
      if (millis() - this->lastIncrementTime > 20)
      {
         this->ms += 1;
         this->lastIncrementTime = millis();
      }
   }
}

/**
 * RelayController
 */
class RelayController
{
private:
   int pin;
   bool enabled = false;
   bool active = true;
   void updatePin();

public:
   RelayController(int pin);
   ~RelayController();
   void setEnabled(bool enabled);
   bool getEnabled();
   void setActive(bool active);
   bool getActive();
};

RelayController::RelayController(int pin)
{
   this->pin = pin;
   pinMode(this->pin, OUTPUT);
   this->updatePin();
}

RelayController::~RelayController()
```

```
{
}

bool RelayController::getEnabled()
{
   return this->enabled;
}

void RelayController::setEnabled(bool enabled)
{
   this->enabled = enabled;
   this->updatePin();
   return;
}

void RelayController::updatePin()
{
   buttonsPressed.lastInterruptTime = millis();
   if (this->enabled && this->active)
   {
      digitalWrite(this->pin, HIGH);
   }
   else
   {
      digitalWrite(this->pin, LOW);
   }
   return;
}

void RelayController::setActive(bool active)
{
   this->active = active;
   this->updatePin();
   return;
}

bool RelayController::getActive()
{
   return this->active;
}

/**
 * TemperatureSensor
 */
class TemperatureSensor
{
private:
   int pin1;
   int pin2;
   int pin3;
   double currentTemp;

   double adcMax = 4095.0, Vs = 3.3;
   double R1 = 100000.0; // voltage divider resistor value
   double Beta = 3950.0; // Beta value
   double To = 298.15;   // Temperature in Kelvin for 25 degree Celsius
```

```
    double Ro = 100000.0; // Resistance of Thermistor at 25 degree Celsius

    double calculateTemp(int pin);

public:
    TemperatureSensor(int pin1, int pin2, int pin3);
    ~TemperatureSensor();
    double getCurrentTemp();
};

TemperatureSensor::TemperatureSensor(int pin1, int pin2, int pin3)
{
    this->pin1 = pin1;
    this->pin2 = pin2;
    this->pin3 = pin3;
}

TemperatureSensor::~TemperatureSensor()
{
}

double TemperatureSensor::calculateTemp(int pin)
{
    double Vout, Rt = 0;
    double T, Tc, Tf = 0;

    double temps[15];

    for (int i = 0; i < 15; i++)
    {
        Vout = analogRead(pin) * this->Vs / this->adcMax;
        Rt = this->R1 * Vout / (this->Vs - Vout);
        T = 1 / (1 / this->To - log(Rt / this->Ro) / this->Beta);
        temps[i] = T - 273.15;
    }

    Tc = (temps[0] + temps[1] + temps[2] + temps[3] + temps[4] + temps[5] + temps[6] + temps[7] + temps[8] +
temps[9] + temps[10] + temps[11] + temps[12] + temps[13] + temps[14]) / 15;
    return Tc;
}

double TemperatureSensor::getCurrentTemp()
{
    double temps[3];
    temps[0] = this->calculateTemp(this->pin1);
    temps[1] = this->calculateTemp(this->pin2);
    temps[2] = this->calculateTemp(this->pin3);
    this->currentTemp = (temps[0] + temps[1] + temps[2]) / 3;
    return this->currentTemp;
}

/**
 * TemperatureSensor2
 */
class TemperatureSensor2
{
```

```
private:
   int pin4;
   double currentTemp2;

   double adcMax = 4095.0, Vs = 3.3;
   double R1 = 100000.0; // voltage divider resistor value
   double Beta = 3950.0; // Beta value
   double To = 298.15;   // Temperature in Kelvin for 25 degree Celsius
   double Ro = 100000.0; // Resistance of Thermistor at 25 degree Celsius

   double calculateTemp2(int pin);

public:
   TemperatureSensor2(int pin4);
   ~TemperatureSensor2();
   double getCurrentTemp2();
};
TemperatureSensor2::TemperatureSensor2(int pin4)
{
   this->pin4 = pin4;
}

TemperatureSensor2::~TemperatureSensor2()
{
}

double TemperatureSensor2::calculateTemp2(int pin)
{
   double Vout, Rt = 0;
   double T, Tc, Tf = 0;

   double temps[15];

   for (int i = 0; i < 15; i++)
   {
      Vout = analogRead(pin) * this->Vs / this->adcMax;
      Rt = this->R1 * Vout / (this->Vs - Vout);
      T = 1 / (1 / this->To - log(Rt / this->Ro) / this->Beta);
      temps[i] = T - 273.15;
   }

   Tc = (temps[0] + temps[1] + temps[2] + temps[3] + temps[4] + temps[5] + temps[6] + temps[7] + temps[8] +
temps[9] + temps[10] + temps[11] + temps[12] + temps[13] + temps[14]) / 15;
   return Tc;
}

double TemperatureSensor2::getCurrentTemp2()
{
   double temps[3];
   temps[0] = this->calculateTemp2(this->pin4);
   this->currentTemp2 = temps[0];
   return this->currentTemp2;
}

/**
 * TemperatureSensor3
```

```
 */
class TemperatureSensor3
{
private:
   int pin5;
   double currentTemp3;

   double adcMax = 4095.0, Vs = 3.3;
   double R1 = 100000.0; // voltage divider resistor value
   double Beta = 3950.0; // Beta value
   double To = 298.15;   // Temperature in Kelvin for 25 degree Celsius
   double Ro = 100000.0; // Resistance of Thermistor at 25 degree Celsius

   double calculateTemp3(int pin);

public:
   TemperatureSensor3(int pin5);
   ~TemperatureSensor3();
   double getCurrentTemp3();
};
TemperatureSensor3::TemperatureSensor3(int pin5)
{
   this->pin5 = pin5;
}

TemperatureSensor3::~TemperatureSensor3()
{
}

double TemperatureSensor3::calculateTemp3(int pin)
{
   double Vout, Rt = 0;
   double T, Tc, Tf = 0;

   double temps[15];

   for (int i = 0; i < 15; i++)
   {
      Vout = analogRead(pin) * this->Vs / this->adcMax;
      Rt = this->R1 * Vout / (this->Vs - Vout);
      T = 1 / (1 / this->To - log(Rt / this->Ro) / this->Beta);
      temps[i] = T - 273.15;
   }

   Tc = (temps[0] + temps[1] + temps[2] + temps[3] + temps[4] + temps[5] + temps[6] + temps[7] + temps[8] +
temps[9] + temps[10] + temps[11] + temps[12] + temps[13] + temps[14]) / 15;
   return Tc;
}

double TemperatureSensor3::getCurrentTemp3()
{
   double temps[3];
   temps[0] = this->calculateTemp3(this->pin5);
   this->currentTemp3 = temps[0];
   return this->currentTemp3;
}
```

```
/**
 * TemperatureSensor4
 */
class TemperatureSensor4
{
private:
   int pin6;
   double currentTemp4;

   double adcMax = 4095.0, Vs = 3.3;
   double R1 = 100000.0; // voltage divider resistor value
   double Beta = 3950.0; // Beta value
   double To = 298.15;   // Temperature in Kelvin for 25 degree Celsius
   double Ro = 100000.0; // Resistance of Thermistor at 25 degree Celsius

   double calculateTemp4(int pin);

public:
   TemperatureSensor4(int pin6);
   ~TemperatureSensor4();
   double getCurrentTemp4();
};
TemperatureSensor4::TemperatureSensor4(int pin6)
{
   this->pin6 = pin6;
}

TemperatureSensor4::~TemperatureSensor4()
{
}

double TemperatureSensor4::calculateTemp4(int pin)
{
   double Vout, Rt = 0;
   double T, Tc, Tf = 0;

   double temps[15];

   for (int i = 0; i < 15; i++)
   {
      Vout = analogRead(pin) * this->Vs / this->adcMax;
      Rt = this->R1 * Vout / (this->Vs - Vout);
      T = 1 / (1 / this->To - log(Rt / this->Ro) / this->Beta);
      temps[i] = T - 273.15;
   }

   Tc = (temps[0] + temps[1] + temps[2] + temps[3] + temps[4] + temps[5] + temps[6] + temps[7] + temps[8] +
temps[9] + temps[10] + temps[11] + temps[12] + temps[13] + temps[14]) / 15;
   return Tc;
}

double TemperatureSensor4::getCurrentTemp4()
{
   double temps[3];
   temps[0] = this->calculateTemp4(this->pin6);
```

```
    this->currentTemp4 = temps[0];
    return this->currentTemp4;
}

/**
 * IO
 */
class IO
{
private:
    MotorController *motorController;
    RelayController *heaterController;
    RelayController *heaterController2;
    RelayController *ledArrayController;
    RelayController *heaterController3;
    RelayController *heaterController4;
    TemperatureSensor *temperatureSensor;
    TemperatureSensor2 *temperatureSensor2;
    TemperatureSensor3 *temperatureSensor3;
    TemperatureSensor4 *temperatureSensor4;

public:
    IO(int motorPin, int heaterPin, int heaterPin2, int ledArrayPin, int lidPin, int lidPin2, int tempPin1, int tempPin2,
int tempPin3, int tempPin4, int tempPin5, int tempPin6);
    ~IO();
    void setMotorPower(int power);
    int getMotorPower();
    int lastMotorPower = 95;
    void run();
    void setHeaterEnabled(bool enabled);
    bool getHeaterEnabled();
    bool getHeaterActive();
    void setHeaterEnabled2(bool enabled);
    bool getHeaterEnabled2();
    bool getHeaterActive2();
    void setHeaterEnabled3(bool enabled);
    bool getHeaterEnabled3();
    bool getHeaterActive3();
    void setHeaterEnabled4(bool enabled);
    bool getHeaterEnabled4();
    bool getHeaterActive4();
    void setLedArrayEnabled(bool enabled);
    bool getLedArrayEnabled();
    double getCurrentTemperature();
    double getCurrentTemperature2();
    double getCurrentTemperature3();
    double getCurrentTemperature4();
    String getJsonState();
    void updateIoState();
};

IO::IO(int motorPin, int heaterPin, int heaterPin2, int ledArrayPin, int lidPin, int lidPin2, int tempPin1, int tempPin2,
int tempPin3, int tempPin4, int tempPin5, int tempPin6)
{
    this->motorController = new MotorController(motorPin);
    this->heaterController = new RelayController(heaterPin);
```

```
    this->heaterController2 = new RelayController(heaterPin2);
    this->ledArrayController = new RelayController(ledArrayPin);
    this->heaterController3 = new RelayController(lidPin); //Lid Relay
    this->heaterController4 = new RelayController(lidPin2); //Lid Relay2
    this->temperatureSensor = new TemperatureSensor(tempPin1, tempPin2, tempPin3);
    this->temperatureSensor2 = new TemperatureSensor2(tempPin4);
    this->temperatureSensor3 = new TemperatureSensor3(tempPin5);
    this->temperatureSensor4 = new TemperatureSensor4(tempPin6);
    this->updateIoState();
}

IO::~IO()
{
}

void IO::setMotorPower(int power)
{
    motorController->setPower(power);
    if (power != 0)
    {
        if (timer.motorTimer == 0)
        {
            timer.motorTimer = timer.currentTime;
        }
        this->lastMotorPower = power;
    }
    else
    {
        timer.motorTimer = 0;
    }
    this->updateIoState();

    return;
}

int IO::getMotorPower()
{
    return motorController->getPower();
}

void IO::run()
{
    motorController->run();
    if (millis() - ioState.lastTempCheck > 2000) // original value 5000
    {
        if (temperatureSensor->getCurrentTemp() > 95.5 && heaterController->getEnabled())
        {
            heaterController->setActive(false);
        }
        else if (temperatureSensor->getCurrentTemp() < 94.5 && temperatureSensor->getCurrentTemp() > -15.0 &&
heaterController->getEnabled())
        {
            heaterController->setActive(true);
        }
        else if (temperatureSensor->getCurrentTemp() < -15.0)
        {
```

```
            heaterController->setActive(false);
        }
        ioState.lastTempCheck = millis();
    }
    if (millis() - timer.lastTimerTick > 1000)
    {
        timer.lastTimerTick = millis();
        timer.currentTime += 1;
    }

    if (millis() - ioState.lastTempCheck2 > 2000) // original value 5000
    {
        if (temperatureSensor2->getCurrentTemp2() > 53.0 && heaterController2->getEnabled())
        {
            heaterController2->setActive(false);
        }
        else if (temperatureSensor2->getCurrentTemp2() < 42.5 && temperatureSensor2->getCurrentTemp2() > -15.0
&& heaterController2->getEnabled())
        {
            heaterController2->setActive(true);
        }
        else if (temperatureSensor2->getCurrentTemp2() < -15.0)
        {
            heaterController2->setActive(false);
        }
        ioState.lastTempCheck2 = millis();
    }
    if (millis() - timer.lastTimerTick > 1000)
    {
        timer.lastTimerTick = millis();
        timer.currentTime += 1;
    }

    if (millis() - ioState.lastTempCheck3 > 2000) // original value 5000 // lid1
    {
        if (temperatureSensor3->getCurrentTemp3() > 105.0 && heaterController3->getEnabled())
        {
            heaterController3->setActive(false);
        }
        else if (temperatureSensor3->getCurrentTemp3() < 103.0 && temperatureSensor3->getCurrentTemp3() > -15.0
&& heaterController3->getEnabled())
        {
            heaterController3->setActive(true);
        }
        else if (temperatureSensor3->getCurrentTemp3() < -15.0)
        {
            heaterController3->setActive(false);
        }
        ioState.lastTempCheck3 = millis();
    }
    if (millis() - timer.lastTimerTick > 1000)
    {
        timer.lastTimerTick = millis();
        timer.currentTime += 1;
    }
```

```
   if (millis() - ioState.lastTempCheck4 > 2000) // original value 5000 //lid2
   {
      if (temperatureSensor4->getCurrentTemp4() > 83.0 && heaterController4->getEnabled())
      {
         heaterController4->setActive(false);
      }
      else if (temperatureSensor4->getCurrentTemp4() < 81.0 && temperatureSensor4->getCurrentTemp4() > -15.0
&& heaterController4->getEnabled())
      {
         heaterController4->setActive(true);
      }
      else if (temperatureSensor4->getCurrentTemp4() < -15.0)
      {
         heaterController4->setActive(false);
      }
      ioState.lastTempCheck4 = millis();
   }
   if (millis() - timer.lastTimerTick > 1000)
   {
      timer.lastTimerTick = millis();
      timer.currentTime += 1;
   }
   return;
}

void IO::setHeaterEnabled(bool enabled)
{
   heaterController->setEnabled(enabled);
   if (enabled && timer.heaterTimer == 0)
   {
      timer.heaterTimer = timer.currentTime;
   }
   else if (!enabled)
   {
      timer.heaterTimer = 0;
   }
   this->updateIoState();
   return;
}

void IO::setHeaterEnabled2(bool enabled)
{
   heaterController2->setEnabled(enabled);
   if (enabled && timer.heaterTimer2 == 0)
   {
      timer.heaterTimer2 = timer.currentTime;
   }
   else if (!enabled)
   {
      timer.heaterTimer2 = 0;
   }
   this->updateIoState();
   return;
}

void IO::setHeaterEnabled3(bool enabled)
```

```
{
   heaterController3->setEnabled(enabled);
   if (enabled && timer.heaterTimer3 == 0)
   {
      timer.heaterTimer3 = timer.currentTime;
   }
   else if (!enabled)
   {
      timer.heaterTimer3 = 0;
   }
   this->updateIoState();
   return;
}

void IO::setHeaterEnabled4(bool enabled)
{
   heaterController4->setEnabled(enabled);
   if (enabled && timer.heaterTimer4 == 0)
   {
      timer.heaterTimer4 = timer.currentTime;
   }
   else if (!enabled)
   {
      timer.heaterTimer4 = 0;
   }
   this->updateIoState();
   return;
}

bool IO::getHeaterEnabled()
{
   return heaterController->getEnabled();
}

bool IO::getHeaterEnabled2()
{
   return heaterController2->getEnabled();
}

bool IO::getHeaterEnabled3()
{
   return heaterController3->getEnabled();
}

bool IO::getHeaterEnabled4()
{
   return heaterController4->getEnabled();
}

bool IO::getHeaterActive()
{
   return this->heaterController->getActive();
}

bool IO::getHeaterActive2()
{
```

```
    return this->heaterController2->getActive();
}

bool IO::getHeaterActive3()
{
    return this->heaterController3->getActive();
}

bool IO::getHeaterActive4()
{
    return this->heaterController4->getActive();
}

void IO::setLedArrayEnabled(bool enabled)
{
    ledArrayController->setEnabled(enabled);
    if (enabled && timer.ledArrayTimer == 0)
    {
        timer.ledArrayTimer = timer.currentTime;
    }
    else if (!enabled)
    {
        timer.ledArrayTimer = 0;
    }
    this->updateIoState();
    return;
}

bool IO::getLedArrayEnabled()
{
    return ledArrayController->getEnabled();
}

double IO::getCurrentTemperature()
{
    return this->temperatureSensor->getCurrentTemp();
}

double IO::getCurrentTemperature2()
{
    return this->temperatureSensor2->getCurrentTemp2();
}

double IO::getCurrentTemperature3()
{
    return this->temperatureSensor3->getCurrentTemp3();
}

double IO::getCurrentTemperature4()
{
    return this->temperatureSensor4->getCurrentTemp4();
}

String IO::getJsonState()
{
    return (String) "{\"heaterEnabled\":" + (this->getHeaterEnabled() ? (String) "true," : (String) "false,")
```

```
    + (String) "{\"heaterEnabled2\":" + (this->getHeaterEnabled2() ? (String) "true," : (String) "false,")
    + (String) "{\"heaterEnabled3\":" + (this->getHeaterEnabled3() ? (String) "true," : (String) "false,")
    + (String) "{\"heaterEnabled4\":" + (this->getHeaterEnabled4() ? (String) "true," : (String) "false,")
    + (String) "\"motorPower\":" + this->getMotorPower()
    + (String) ",\"ledArrayEnabled\":" + (this->getLedArrayEnabled() ? (String) "true," : (String) "false,")
    + (String) "\"currentTemp\":" + (String)this->getCurrentTemperature()
    + (String) "\"currentTemp2\":" + (String)this->getCurrentTemperature2()
    + (String) "\"currentTemp3\":" + (String)this->getCurrentTemperature3()
    + (String) "\"currentTemp4\":" + (String)this->getCurrentTemperature4()
    + (String) ",\"motorTimer\":" + (String)(timer.currentTime - timer.motorTimer)
    + (String) ",\"ledArrayTimer\":" + (String)(timer.currentTime - timer.ledArrayTimer)
    + (String) ",\"heaterTimer\":" + (String)(timer.currentTime - timer.heaterTimer)
    + (String) ",\"heaterTimer2\":" + (String)(timer.currentTime - timer.heaterTimer2)
    + (String) ",\"heaterTimer3\":" + (String)(timer.currentTime - timer.heaterTimer3)
    + (String) ",\"heaterTimer4\":" + (String)(timer.currentTime - timer.heaterTimer4)
    + (String) "}";
}

void IO::updateIoState()
{
    ioState.currentTemp = this->getCurrentTemperature();
    ioState.currentTemp2 = this->getCurrentTemperature2();
    ioState.currentTemp3 = this->getCurrentTemperature3();
    ioState.currentTemp4 = this->getCurrentTemperature4();
    ioState.heaterActive = this->getHeaterActive();
    ioState.heaterEnabled = this->getHeaterEnabled();
    ioState.heaterActive2 = this->getHeaterActive2();
    ioState.heaterEnabled2 = this->getHeaterEnabled2();
    ioState.heaterActive3 = this->getHeaterActive3();
    ioState.heaterEnabled3 = this->getHeaterEnabled3();
    ioState.heaterActive4 = this->getHeaterActive4();
    ioState.heaterEnabled4 = this->getHeaterEnabled4();
    ioState.ledArrayEnabled = this->getLedArrayEnabled();
    ioState.motorPower = this->getMotorPower();
}

/**
 * TFT
 */
class TFT
{
private:
    Adafruit_ILI9341 *tft;
    IO *io;
    Controls currentSelection = Controls::Heater;
    String getTimerText(Controls controls);

public:
    TFT(int CS, int DC, IO *io);
    ~TFT();
    void clear();
    void text(String text);
    void text(String text, int x, int y);
    void text(String text, unsigned short color);
    void text(String text, int x, int y, unsigned short color);
    void run();
```

```
};

TFT::TFT(int CS, int DC, IO *io)
{
   this->tft = new Adafruit_ILI9341(CS, DC, -1);
   this->tft->begin();
   this->tft->setRotation(1);
   this->tft->fillScreen(ILI9341_BLACK);
   this->tft->setFont(&FreeSans9pt7b);
   this->io = io;
}

TFT::~TFT()
{
}

void TFT::clear()
{
   tft->fillScreen(ILI9341_BLACK);
}

void TFT::text(String text)
{
   this->text(text, 0, 0);
}

void TFT::text(String text, int x, int y)
{
   this->text(text, x, y, 0xFFFF);
}

void TFT::text(String text, unsigned short color)
{
   this->text(text, 0, 0, color);
}

void TFT::text(String text, int x, int y, unsigned short color)
{
   tft->setCursor(x, y);
   tft->setTextColor(color);
   tft->setTextWrap(true);
   tft->print(text);
}

void TFT::run()
{
   this->clear();

   if (buttonsPressed.wasDownPressed || buttonsPressed.wasOkPressed || buttonsPressed.wasUpPressed)
   {
      if (buttonsPressed.wasUpPressed)
      {
         switch (currentSelection)
         {
         case Controls::Heater2:
            currentSelection = Controls::Heater;
```

```
            break;

        case Controls::Heater3:
            currentSelection = Controls::Heater2;
            break;

        case Controls::Heater4:
            currentSelection = Controls::Heater3;
            break;

        case Controls::LedArray:
            currentSelection = Controls::Heater4;
            break;

        case Controls::Motor:
            currentSelection = Controls::LedArray;
            break;

        default:
            break;
        }
        buttonsPressed.wasUpPressed = false;
    }
    if (buttonsPressed.wasDownPressed)
    {
        switch (currentSelection)
        {
        case Controls::Heater:
            currentSelection = Controls::Heater2;
            break;

        case Controls::Heater2:
            currentSelection = Controls::Heater3;
            break;

        case Controls::Heater3:
            currentSelection = Controls::Heater4;
            break;

        case Controls::Heater4:
            currentSelection = Controls::LedArray;
            break;

        case Controls::LedArray:
            currentSelection = Controls::Motor;
            break;

        default:
            break;
        }
        buttonsPressed.wasDownPressed = false;
    }
    if (buttonsPressed.wasOkPressed)
    {
        switch (currentSelection)
        {
```

```
        case Controls::Heater:
        {
           io->getHeaterEnabled() ? io->setHeaterEnabled(false) : io->setHeaterEnabled(true);
           break;
        }

        case Controls::Heater2:
        {
           io->getHeaterEnabled2() ? io->setHeaterEnabled2(false) : io->setHeaterEnabled2(true);
           break;
        }

       case Controls::Heater3:
        {
           io->getHeaterEnabled3() ? io->setHeaterEnabled3(false) : io->setHeaterEnabled3(true);
           break;
        }

        case Controls::Heater4:
        {
           io->getHeaterEnabled4() ? io->setHeaterEnabled4(false) : io->setHeaterEnabled4(true);
           break;
        }

        case Controls::LedArray:
        {
           io->getLedArrayEnabled() ? io->setLedArrayEnabled(false) : io->setLedArrayEnabled(true);
           break;
        }

        case Controls::Motor:
        {
           int currentPower = io->getMotorPower();
           if (currentPower > 0)
           {
              io->setMotorPower(0);
           }
           else
           {
              io->setMotorPower(io->lastMotorPower);
           }
           break;
        }

        default:
           break;
        }
        buttonsPressed.wasOkPressed = false;
     }
  }

  // Base
  this->text(tftStatus.message, 0, 15, tftStatus.colour);
  this->text((String) "Block Temp: " + (String)(ioState.currentTemp), 0, 35, 0xFFFF);
  this->text((String) "LAMP Air Temp: " + (String)(ioState.currentTemp2+3), 0, 60, 0xFFFF);
```

```
   this->text((String) "LID1: " + (String)(ioState.currentTemp3) + "     LID2: " + (String)(ioState.currentTemp4-10),
0, 85, 0xFFFF);
   this->text((String) "Block (95 C): " + (String)(ioState.heaterEnabled ? "On" : "Off"), 0, 110, currentSelection ==
Controls::Heater ? 0xFF80 : 0xBDD7);
   this->text((String) "LAMP Air: " + (String)(ioState.heaterEnabled2 ? "On" : "Off"), 0, 135, currentSelection ==
Controls::Heater2 ? 0xFF80 : 0xBDD7);
   this->text((String) "Lid 1: " + (String)(ioState.heaterEnabled3 ? "On" : "Off"), 0, 160, currentSelection ==
Controls::Heater3 ? 0xFF80 : 0xBDD7);
   this->text((String) "Lid 2: " + (String)(ioState.heaterEnabled4 ? "On" : "Off"), 0, 185, currentSelection ==
Controls::Heater4 ? 0xFF80 : 0xBDD7);
   this->text((String) "LED Array: " + (String)(ioState.ledArrayEnabled ? "On" : "Off"), 0, 210, currentSelection ==
Controls::LedArray ? 0xFF80 : 0xBDD7);
   // this->text((String) "Motor Power: " + (String)ioState.motorPower + (String) "%", 0, 160, currentSelection ==
Controls::Motor ? 0xFF80 : 0xBDD7);
   this->text((String) "Press Up/Down/Ok to toggle state.", 0, 235, 0xDEDB);

   // Timers
   if (timer.heaterTimer > 0)
      this->text(this->getTimerText(Controls::Heater), 250, 110, 0x073F);
   if (timer.heaterTimer2 > 0)
      this->text(this->getTimerText(Controls::Heater2), 250, 135, 0x073F);
   if (timer.heaterTimer3 > 0)
      this->text(this->getTimerText(Controls::Heater3), 250, 160, 0x073F);
   if (timer.heaterTimer4 > 0)
      this->text(this->getTimerText(Controls::Heater4), 250, 185, 0x073F);
   if (timer.ledArrayTimer > 0)
      this->text(this->getTimerText(Controls::LedArray), 250, 210, 0x073F);
}

String TFT::getTimerText(Controls controls)
{
   unsigned long startTime;
   // String name;
   switch (controls)
   {
   case Controls::Heater:
      startTime = timer.heaterTimer;
      break;

   case Controls::Heater2:
      startTime = timer.heaterTimer2;
      break;

   case Controls::Heater3:
      startTime = timer.heaterTimer3;
      break;

   case Controls::Heater4:
      startTime = timer.heaterTimer4;
      break;

   case Controls::LedArray:
      startTime = timer.ledArrayTimer;
      break;

   case Controls::Motor:
```

```
        startTime = timer.motorTimer;
        break;

    default:
        break;
    }
    unsigned long elapsedSeconds = timer.currentTime - startTime;
    int seconds = elapsedSeconds % 60;
    int minutes = elapsedSeconds / 60;
    int hours = elapsedSeconds / 3600;
    String strMinutes;
    String strSeconds;
    String strHours;
    if (minutes >= 60)
        minutes = minutes - 60*hours;
    if (minutes / 10 == 0)
        strMinutes = (String) "0" + (String)minutes;
    else
        strMinutes = (String)minutes;
    if (seconds / 10 == 0)
        strSeconds = (String) "0" + (String)seconds;
    else
        strSeconds = (String)seconds;
    if (hours / 10 == 0)
        strHours = (String) "0" + (String)hours;
    else
        strHours = (String)hours;
    return strHours + (String) ":" + strMinutes + (String) ":" + strSeconds;
}

/**
 * WifiAP
 */
class WifiAP
{
private:
    WebServer *server = new WebServer(80);
    IO *io;
    TFT *tft;

public:
    WifiAP(const char *ssid, const char *password, IO *io, TFT *tft);
    ~WifiAP();
    void handleClient();
    bool handleRequest(String device, String newState);
};

WifiAP::WifiAP(const char *ssid, const char *password, IO *io, TFT *tft)
{
    WiFi.softAP(ssid, password);
    this->io = io;
    this->tft = tft;
    this->server->on("/", [this]() {
        this->server->send(200, "application/json", this->io->getJsonState());
    });
    this->server->on("/{}/{}", [this]() {
```

```
        if (this->handleRequest(this->server->pathArg(0), this->server->pathArg(1)))
        {
            this->server->send(200, "application/json", this->io->getJsonState());
            tftStatus.message = "Ready";
            tftStatus.colour = 0x17E0;
        }
        else
        {
            this->server->send(404, "text/plain", "Bad request");
            tftStatus.message = "Error: Bad Request";
            tftStatus.colour = 0xF800;
        }
        this->tft->run();
    });
    server->begin();
}

WifiAP::~WifiAP()
{
}

void WifiAP::handleClient()
{
    this->server->handleClient();
    return;
}

bool WifiAP::handleRequest(String device, String newState)
{
    if (device == "heater")
    {
        if (newState == "on")
        {
            this->io->setHeaterEnabled(true);
            return true;
        }
        else if (newState == "off")
        {
            this->io->setHeaterEnabled(false);
            return true;
        }
        else
        {
            return false;
        }
    }
    if (device == "heater2")
    {
        if (newState == "on")
        {
            this->io->setHeaterEnabled2(false);
            return true;
        }
        else if (newState == "off")
        {
            this->io->setHeaterEnabled2(true);
```

```
        return true;
    }
    else
    {
        return false;
    }
}
if (device == "heater3")
{
    if (newState == "on")
    {
        this->io->setHeaterEnabled3(false);
        return true;
    }
    else if (newState == "off")
    {
        this->io->setHeaterEnabled3(true);
        return true;
    }
    else
    {
        return false;
    }
}
if (device == "heater4")
{
    if (newState == "on")
    {
        this->io->setHeaterEnabled4(false);
        return true;
    }
    else if (newState == "off")
    {
        this->io->setHeaterEnabled4(true);
        return true;
    }
    else
    {
        return false;
    }
}
if (device == "ledArray")
{
    if (newState == "on")
    {
        this->io->setLedArrayEnabled(true);
        return true;
    }
    else if (newState == "off")
    {
        this->io->setLedArrayEnabled(false);
        return true;
    }
    else
    {
        return false;
```

```
        }
    }
    if (device == "motor")
    {
        this->io->setMotorPower(newState.toInt());
        return true;
    }
}

/**
 * Buttons
 */
class Buttons
{
private:
    int upPin;
    int downPin;
    int okPin;
    bool upPresssed;
    bool downPressed;
    bool okPressed;
    TFT *tft;

public:
    Buttons(int upPin, int downPin, int okPin, TFT *tft);
    ~Buttons();
    static void onUpPress();
    static void onDownPress();
    static void onOkPress();
};

Buttons::Buttons(int upPin, int downPin, int okPin, TFT *tft)
{
    this->upPin = upPin;
    this->downPin = downPin;
    this->okPin = okPin;
    pinMode(upPin, INPUT_PULLUP);
    pinMode(downPin, INPUT_PULLUP);
    pinMode(okPin, INPUT_PULLUP);
    attachInterrupt(upPin, this->onUpPress, RISING);
    attachInterrupt(downPin, this->onDownPress, RISING);
    attachInterrupt(okPin, this->onOkPress, RISING);
    this->tft = tft;
}

Buttons::~Buttons()
{
}

void Buttons::onUpPress()
{
    if (millis() - buttonsPressed.lastInterruptTime > 350)
    {
        buttonsPressed.wasUpPressed = true;
        Serial.println("upPressed");
    }
```

```
    buttonsPressed.lastInterruptTime = millis();
}

void Buttons::onDownPress()
{
    if (millis() - buttonsPressed.lastInterruptTime > 350)
    {
        buttonsPressed.wasDownPressed = true;
        Serial.println("downPressed");
    }
    buttonsPressed.lastInterruptTime = millis();
}

void Buttons::onOkPress()
{
    if (millis() - buttonsPressed.lastInterruptTime > 350)
    {
        buttonsPressed.wasOkPressed = true;
        Serial.println("okPressed");
    }
    buttonsPressed.lastInterruptTime = millis();
}

/**
 * Bluetooth (Noah)
 */

NState states;
BLE *ble;
IO *io;
TFT *tft;
WifiAP *wifiAP;
Buttons *buttons;

static NState processBLERequests() {
    if (!ble->justRequested()) return NState {};

    NState requests;

    requests.deserialize(ble->getRequestData());
    Serial.println("Receive: " + String(ble->getRequestData()));

    if (requests.heater1) {
        states.heater1 = !states.heater1;
    }
    if (requests.heater2) {
        states.heater2 = !states.heater2;
    }
    if (requests.led) {
        states.led = !states.led;
    }
    if (requests.up) {
        buttonsPressed.wasUpPressed = true;
    }
    if (requests.down) {
        buttonsPressed.wasDownPressed = true;
```

```
    }
    if (requests.ok) {
        buttonsPressed.wasOkPressed = true;
    }

    ble->setStateData(states.serialize32());

    return requests;
}

// Called when the state should be applied to the GPIO pins
static void applyState(NState requests) {
    if (requests.heater1) io->setHeaterEnabled(states.heater1);
    if (requests.heater2) io->setHeaterEnabled2(states.heater2);
    if (requests.led) io->setLedArrayEnabled(states.led);
}

/**
 * Converts a boolean value to either HIGH or LOW.
 * @param data the boolean value
 * @return HIGH if data = true, LOW otherwise
 */
int val(bool data) {
    if (data) return HIGH;
    return LOW;
}

void setup()
{
    Serial.begin(9600);
    io = new IO(SERVO_PIN, HEATER_PIN, HEATER_PIN2, LED_ARRAY_PIN, LID_PIN, LID_PIN2,
TEMP1_SENSOR_PIN, TEMP2_SENSOR_PIN, TEMP3_SENSOR_PIN, TEMP4_SENSOR_PIN,
TEMP5_SENSOR_PIN, TEMP6_SENSOR_PIN);
    tft = new TFT(TFT_CS, TFT_DC, io);
    tft->text("ABL Covid Test", 0, 15, 0xFCA0);
    tft->text("Initializing...\nPlease wait", 0, 35, 0xFFFF);
    delay(2000);
    tftStatus.message = "Ready";
    tftStatus.colour = 0x17E0;
    tft->run();
    buttons = new Buttons(UP_PIN, DOWN_PIN, OK_PIN, tft);
    ble = new BLE();
    ble->setup(N_BIOBOX);

}

/**
 * Loop
 */
void loop()
{
    ble->loop();
    NState requests = processBLERequests();
    applyState(requests);

    io->run();
```

```
  if (buttonsPressed.wasDownPressed || buttonsPressed.wasOkPressed || buttonsPressed.wasUpPressed)
  {
    tft->run();
  }

  if (millis() - screenRefresh > 5000)
  {
    io->updateIoState();
    tft->run();
    screenRefresh = millis();
  }
}
```

Tools Option:

Board : “ESP32 Dev Module”
Flash Mode: “QIO”
Partition Scheme: “Default 4MB with spiffs (1.2MB APP/1.5MB SPIFFS)”
Flash Frequency: “80MHz”
Upload Speed: “921600”
Core Debug Level: “None”

APPENDIX B. Arduino Code For ESP32-CAM

ESP32-CAM used for the convection-based device in Chapter 4 was executed with the following code from Arduino – File – Examples – ESP32 – Camera – CameraWebServer.

```
#include "esp_camera.h"
#include <WiFi.h>

// Select camera model
#define CAMERA_MODEL_AI_THINKER // Has PSRAM

#include "camera_pins.h"

const char* ssid = "yoonjung";
const char* password = "123456789";

void startCameraServer();

void setup() {
  Serial.begin(115200);
  Serial.setDebugOutput(true);
  Serial.println();

  camera_config_t config;
  config.ledc_channel = LEDC_CHANNEL_0;
  config.ledc_timer = LEDC_TIMER_0;
  config.pin_d0 = Y2_GPIO_NUM;
  config.pin_d1 = Y3_GPIO_NUM;
  config.pin_d2 = Y4_GPIO_NUM;
  config.pin_d3 = Y5_GPIO_NUM;
  config.pin_d4 = Y6_GPIO_NUM;
  config.pin_d5 = Y7_GPIO_NUM;
  config.pin_d6 = Y8_GPIO_NUM;
  config.pin_d7 = Y9_GPIO_NUM;
  config.pin_xclk = XCLK_GPIO_NUM;
  config.pin_pclk = PCLK_GPIO_NUM;
  config.pin_vsync = VSYNC_GPIO_NUM;
  config.pin_href = HREF_GPIO_NUM;
  config.pin_sscb_sda = SIOD_GPIO_NUM;
  config.pin_sscb_scl = SIOC_GPIO_NUM;
  config.pin_pwdn = PWDN_GPIO_NUM;
  config.pin_reset = RESET_GPIO_NUM;
  config.xclk_freq_hz = 20000000;
  config.pixel_format = PIXFORMAT_JPEG;

  // if PSRAM IC present, init with UXGA resolution and higher JPEG quality
  //                     for larger pre-allocated frame buffer.
  if(psramFound()){
    config.frame_size = FRAMESIZE_UXGA;
    config.jpeg_quality = 10;
```

```
    config.fb_count = 2;
  } else {
    config.frame_size = FRAMESIZE_SVGA;
    config.jpeg_quality = 12;
    config.fb_count = 1;
  }

#if defined(CAMERA_MODEL_ESP_EYE)
  pinMode(13, INPUT_PULLUP);
  pinMode(14, INPUT_PULLUP);
#endif

  // camera init
  esp_err_t err = esp_camera_init(&config);
  if (err != ESP_OK) {
    Serial.printf("Camera init failed with error 0x%x", err);
    return;
  }

  sensor_t * s = esp_camera_sensor_get();
  // initial sensors are flipped vertically and colors are a bit saturated
  if (s->id.PID == OV3660_PID) {
    s->set_vflip(s, 1); // flip it back
    s->set_brightness(s, 1); // up the brightness just a bit
    s->set_saturation(s, -2); // lower the saturation
  }
  // drop down frame size for higher initial frame rate
  s->set_framesize(s, FRAMESIZE_QVGA);

#if defined(CAMERA_MODEL_M5STACK_WIDE) || defined(CAMERA_MODEL_M5STACK_ESP32CAM)
  s->set_vflip(s, 1);
  s->set_hmirror(s, 1);
#endif

  WiFi.begin(ssid, password);

  while (WiFi.status() != WL_CONNECTED) {
    delay(500);
    Serial.print(".");
  }
  Serial.println("");
  Serial.println("WiFi connected");

  startCameraServer();

  Serial.print("Camera Ready! Use 'http://");
  Serial.print(WiFi.localIP());
  Serial.println("' to connect");
}

void loop() {
  // put your main code here, to run repeatedly:
  delay(10000);
}
```

Tools Option:
Board : “ESP32 Wrover Module”
Flash Mode: “QIO”
Partition Scheme: “Hue APP (3MB No OTA/1MB SPIFFS)”
Flash Frequency: “40MHz”
Upload Speed: “115200”
Core Debug Level: “None”

APPENDIX C. Schematic of PCB Board For Convection-based Device

Schematics and designs of the main, LCD and LED PCB board were made using EasyEDA and are shown as follows:

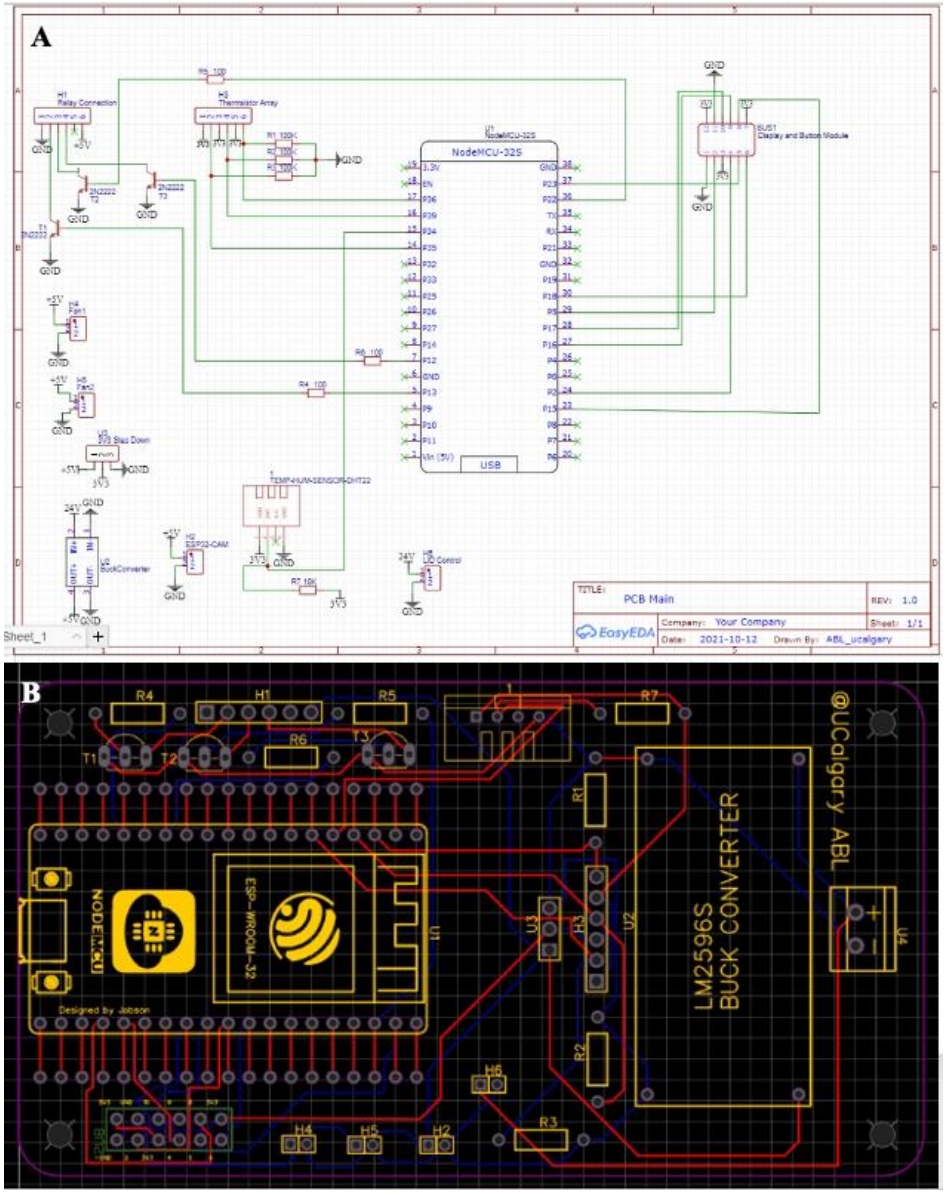

Figure A.1. (A) Schematic of main PCB board. (B) Design of main PCB board.

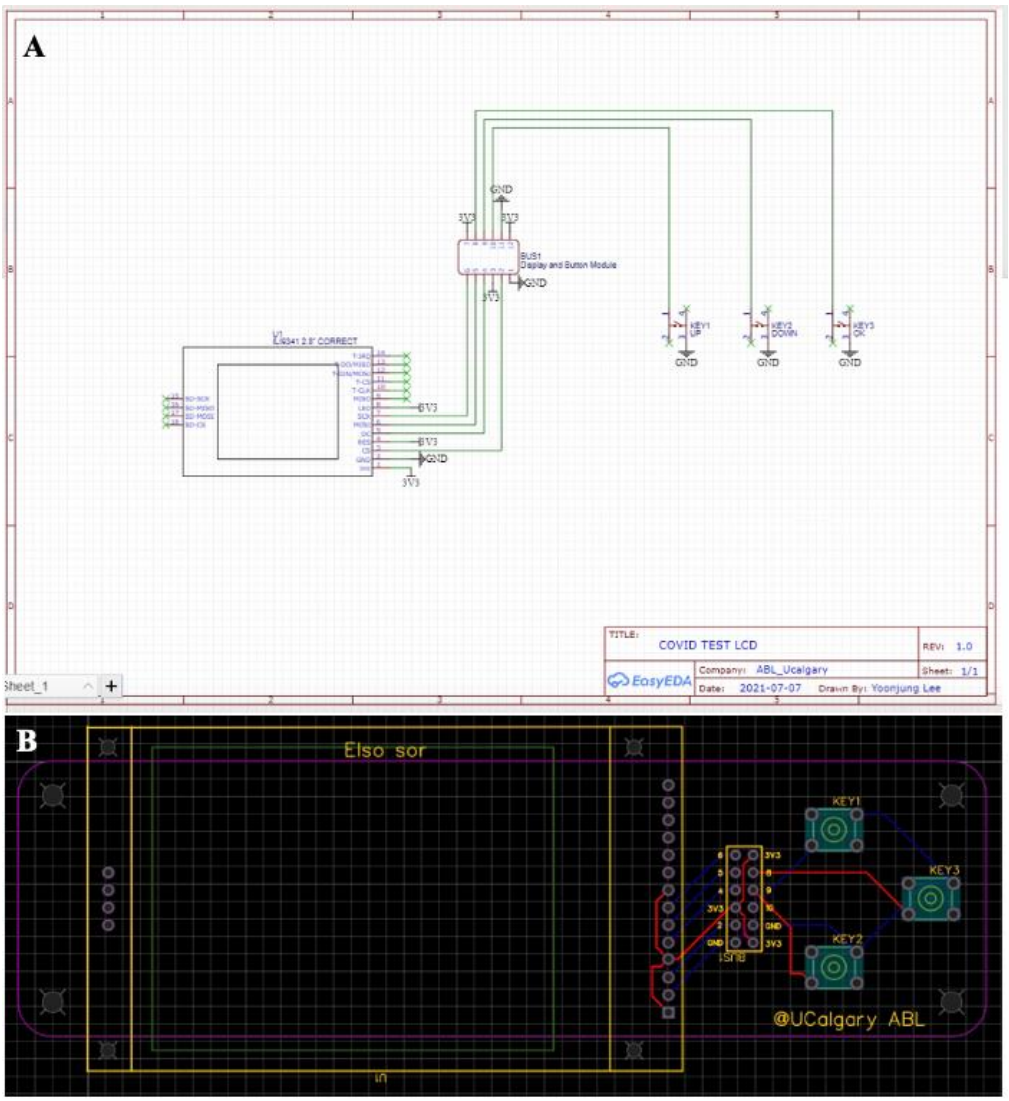

Figure A.2. (A) Schematic of LCD PCB board. (B) Design of LCD PCB board.

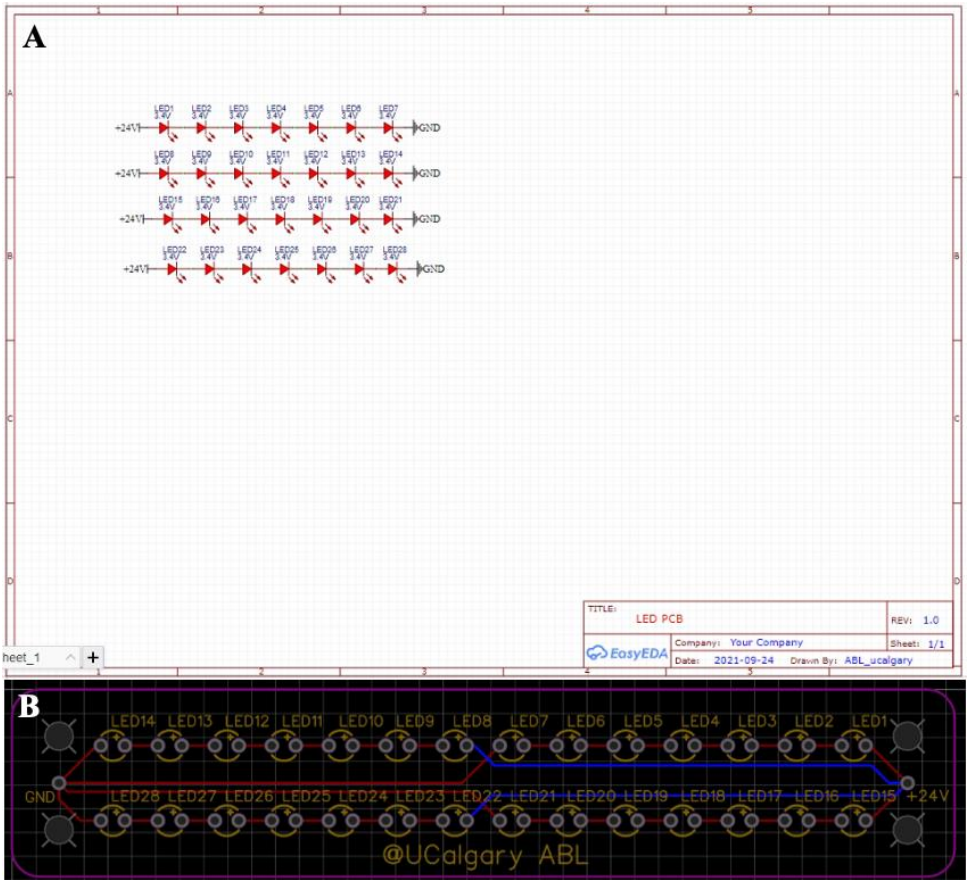

Figure A.3. (A) Schematic of LED PCB board. (B) Design of LED PCB board.